



Università degli Studi di Padova

DIPARTIMENTO DI INGEGNERIA CIVILE
EDILE ED AMBIENTALE

Master thesis:

HYDROLOGICAL MODEL
OF THE
MUSON DEI SASSI

SUPERVISOR: PROF. GIANLUCA BOTTER

CO-SUPERVISOR: PROF. ANDREA RINALDO

ASSISTANT SUPERVISOR: ING. PASSADORE GIULIA

STUDENT: DE MARCHI ELIA

PADOVA - APRILE 2014

Contents

Introduction	1
1 Description of the “Muson dei Sassi”	3
1.1 Geographical and morphological decription	3
1.2 Streamflow regime	4
2 Available data	9
2.1 Geometrical data	9
2.1.1 Stream network and sub-watersheds	19
2.2 Hydrologic data	19
2.2.1 Kriging	23
3 Mathematical models	33
3.1 Mass balance equation and effective rainfall generation	33
3.2 Evapotranspiration model	35
3.2.1 The FAO method	35
3.3 Geomorphological model	48
3.4 Runoff generation	58
3.5 Dispersion from channel bed	59
3.6 Model parameters	60
4 Results	63
4.1 Calibration	63
4.2 Validation	65
4.3 Reviews of the results	94
Conclusion	97
Bibliography	98

Introduction

The goal of this master thesis is the development of a rainfall-runoff model and its application to the “Muson dei Sassi” creek. The hydrological model developed will be part of a comprehensive model, required by the province of Padua, that shall also include an hydro-dynamic model able to compute the river discharge and stages all along the river network, as well as the flooded area during extreme events. Such models are very important supporting tools to address flood forecasting and hydraulic hazard assessment studies. To achieve this challenging objective, a continuous and spatially explicit rainfall-runoff model based on the geomorphological theory of the hydrologic response has been built and implemented.

The Muson dei Sassi creek has a small catchment located within the Veneto region; the river can be divided in two main parts: a northern part, closed at Castelfranco Veneto, where the runoff is produced and a transportation network (built and dammed by the Venetian Republic in the 1612) conveying stream discharges to the Brenta river, where no other significant contributions are introduced. The river is characterized by an erratic flow regime and frequently experiences floods that create problems and damages to populations. In the recent past the main events occurred in October 1998 and January 2009, in the area of Loreggia and Castelfranco, respectively.

With the climate changes that the world is facing, also North-Eastern Italy is facing a change in the statistical distribution of climate variables. More and more the rainfall events are characterized by higher intensities concentrated in shorter time spans. Moreover in the last decades an exponential increase of the urbanization has occurred in the whole Venetian plane, impacting significantly the hydrologic response of streams and rivers. The increasing urbanization reduces the infiltration capacity of land and increases the speed of runoff generation processes. The combined effect of these two processes can pose serious problem in terms of hydraulic safety of landscapes and cities. And this is especially true for the Muson catchment, that is a small catchment characterized by an erratic flow regime and a really fast hydrologic response.

In this perspective, the future development of a comprehensive hydrologic and hydraulic model properly combined with weather forecasting input data shall positively contribute to create a real-time alert system for flood forecast. Hence, the predictive power of the mathematical models of the type discussed in this thesis is extremely important to reduce the social and economic drawbacks created by floods in urbanized areas.

Chapter 1

Description of the “Muson dei Sassi”

1.1 Geographical and morphological description

The “Muson dei Sassi” creek is a small river located in the Veneto region, North-Eastern Italy, among the provinces of Treviso, Vicenza and Padua.

The river can be divided in two parts: the northern part, up to the closure section in Castelfranco Veneto and the southern part, from Castelfranco down to the confluence with the Brenta river in Ponte Vigodarzere, that is embanked. The northern portion of the catchment is characterized by an area of around 310 km^2 and an elevation comprised between 1775 m at Cima Grappa and 40 m at Castelfranco Veneto.

The headwaters are located on the hills of Asolo mainly in the municipality of Maser, Monfumo and Castalcucco. At Spineda the river collects the water of its main tributary, the Lastego stream, and then at Castello di Godego it receives the tributary stream Brentone-Pighenzo. The catchment can be considered closed after the city of Castelfranco Veneto, where the stream Avenale, which collects the water of the eastern area of the basin, flows into the Muson. The main branch of the Muson in this section has a length of around 20 km . However this study is limited at Castelfranco Veneto, before the injection of the Avenale stream.

The river used to flow in the Venice Lagoon until the 1612, when the Venetian Republic decided to divert the river to make it flow into the Brenta river creating the canal Muson dei Sassi. The old channel, the Muson Vecchio, which flows into the lagoon still exists and the two rivers intersect in Camposampiero with a canal-bridge.

The stretch of river that goes from Castelfranco to the Brenta river has a length of around 25 km and in addition to the Muson Vecchio it overpass also the stream Tergola and Vandura and it receives waters only from a small catchment, of around 32 km^2 , where the water is mechanically pumped. This dammed part of the catchment is the most prone to flood events, embankment erosion and breaks. The main events in the recent past occurred in October 7, 1998 and January 21, 2009, in the area of Castelfranco and Loreggia (Figure 1.2 and 1.3).

Within the catchment other critical situations have recently occurred (e.g. the event oc-

curred on November 11, 2012, Figure 1.4) and in fact some detention basins are in the process of designing and building. The main one of these basins will be located at Spineda at the junction of the Muson with the stream Lastego and will be characterized by a volume of 1000000 m^3 .



Figure 1.1: *Muson river basin*

1.2 Streamflow regime

The river Muson dei Sassi is characterized by an erratic flow regime, which is featured by a pronounced variability of river flows. For this reason it creates problems in terms of floods almost every year. It has an average discharge $Q_{ave} = 2,2\text{ m}^3/s$ but it can reach relatively high values of discharge during intense rainfall events. For a return period T_r of 100 years the hypothetical maximum discharges Q_{max} ([D’Alpaos, 2003]) are:

- $140\text{ m}^3/s$ for the Muson at Castelfranco Veneto;
- $30\text{ m}^3/s$ for the Avenale at Castelfranco Veneto;
- $37\text{ m}^3/s$ for the Lastego at Spineda;



Figure 1.2: *Flood occurred at Castelfranco on October 7, 1998.*



Figure 1.3: *Embankment break at Loreggia on January 21, 2009.*



Figure 1.4: *Overflow of the embankment at Spineda on November 11, 2012.*

- $34\text{ m}^3/\text{s}$ for the Brentone at Castello di Godego

providing a maximum discharge downstream Castelfranco Veneto of around $170\text{ m}^3/\text{s}$. The maximum discharge capacity within the embankment is around $140\text{ m}^3/\text{s}$ and so an event like the one characterized by a return period of 100 years would cause many floods in the all the area, upstream and downstream Castelfranco. Actually, even for events characterized by an estimated return period of the rainfall depth around 50 years (as measured during the event of November 11, 2012) many problems and floods were caused all over the contributing catchment (mainly in the area of Castelfranco Veneto and Castello di Godego) and a maximum discharge at Castelfranco of about $110\text{ m}^3/\text{s}$ was generated. In Figure 1.5 it is reported the hourly measures of discharge for the year 2004 and in Figure 1.6 the duration curve for the considered period. The duration curve has been obtained for the spanning period from 2004 to 2013. The characteristic shape of erratic flow regimes (with pronounced slopes for low duration and a concave shape) can be clearly recognized.

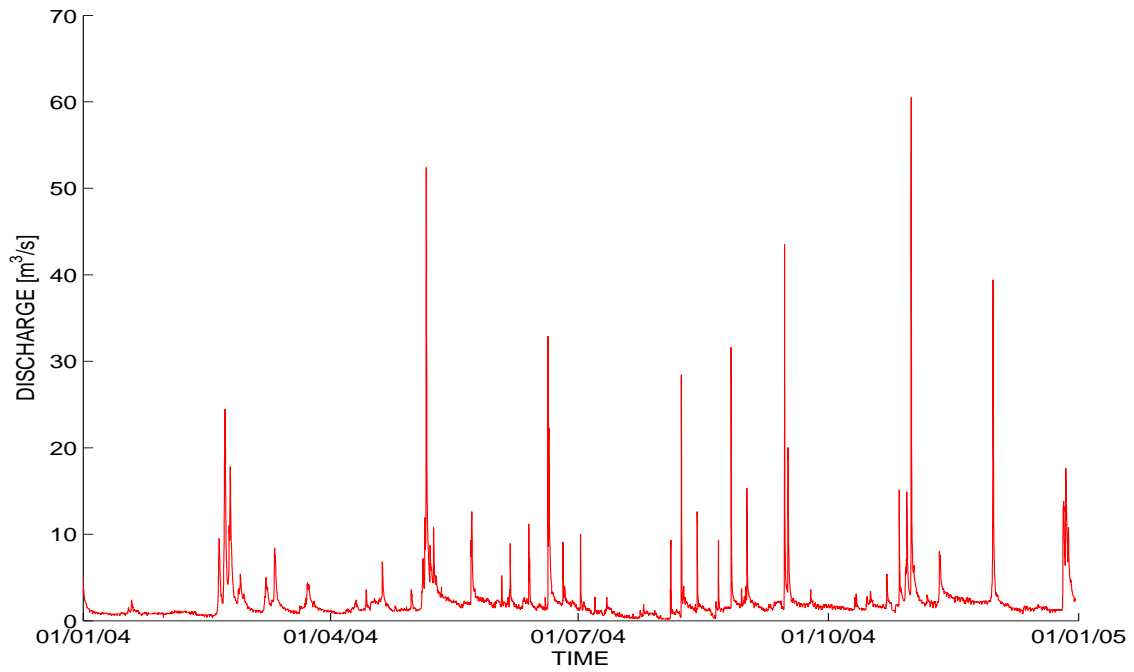


Figure 1.5: *Measured discharge at Castelfranco Veneto for the year 2004*

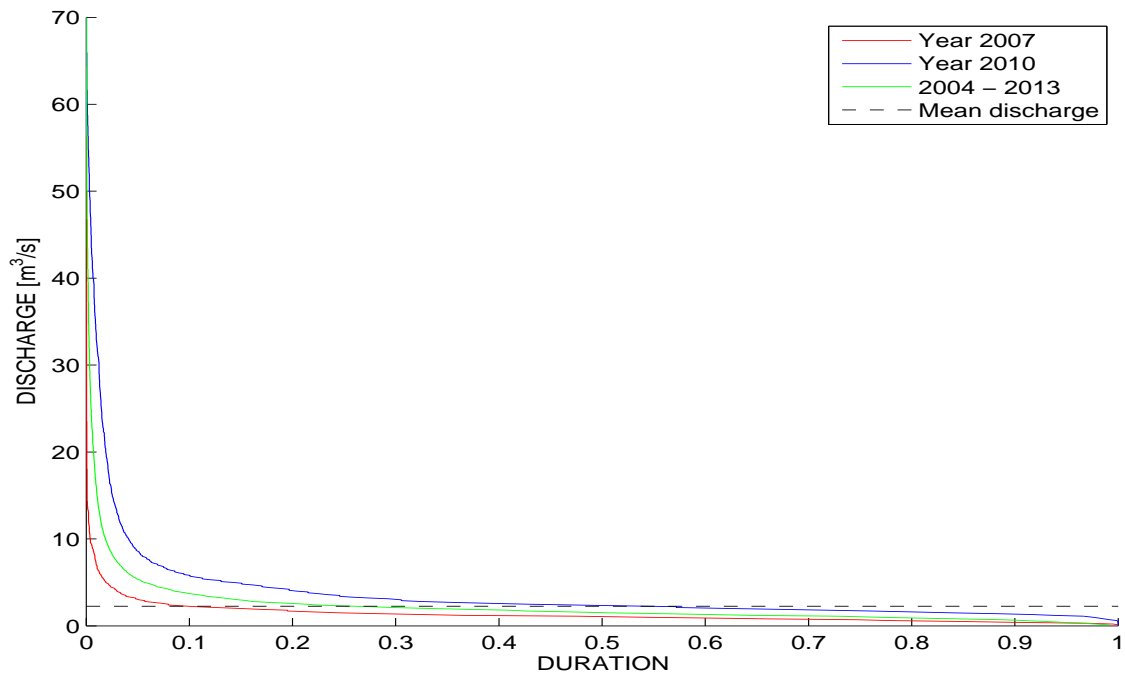


Figure 1.6: *Duration curve of the Muson river measured at Castelfranco Veneto for the period 2004-2013*

Chapter 2

Available data

To build an hydrological model, many data are required, both geometrical and meteorological. In this chapter a list of all the available data is reported. Moreover the geometrical data are used in order to extract the stream network and the sub-watersheds and the meteorological data are spatially distributed with the Kriging interpolator to create the hydrological forcing for the model.

2.1 Geometrical data

The geometrical data for the Muson dei Sassi catchment area have been downloaded from the online data catalog of the Veneto region. These data are listed below:

Hydrographic network

The hydrographic network includes all the rivers, streams and irrigation canals of any order. It can be noticed (Figure 2.1) that the catchment is characterized by a really high drainage density, making difficult the selection of the main network.

DEM

The DEM or Digital Elevation Model gives the information on the elevation of the area of interest. It consists in a grid of squares with 5 *m* side with the mean elevation for each square and it has been created starting from the contour lines of the technical map of the area. In the case of the Muson river catchment the elevation goes from the 1775 *m* at Cima Grappa to the 40 *m* at Castelfranco Veneto, but, with the exception of the south side of the Monte Grappa and the hills around Asolo, most of the basin is located in a plane region. The mean elevation of the catchment is 184 *m*.

Geo-pedology

The geo-pedology gives information on the soil of the area of interest, on their characteristics and their permeability. From the granulometric composition of the soil depends the infiltration of the rainfall in the soil and s the hydrologic response of the catchment. The classification has been obtained from the soil provinces of the “Carta dei suoli”, the map of the kind of soil, of the Veneto region ([ARPAV, 2005]. The type of soil of the

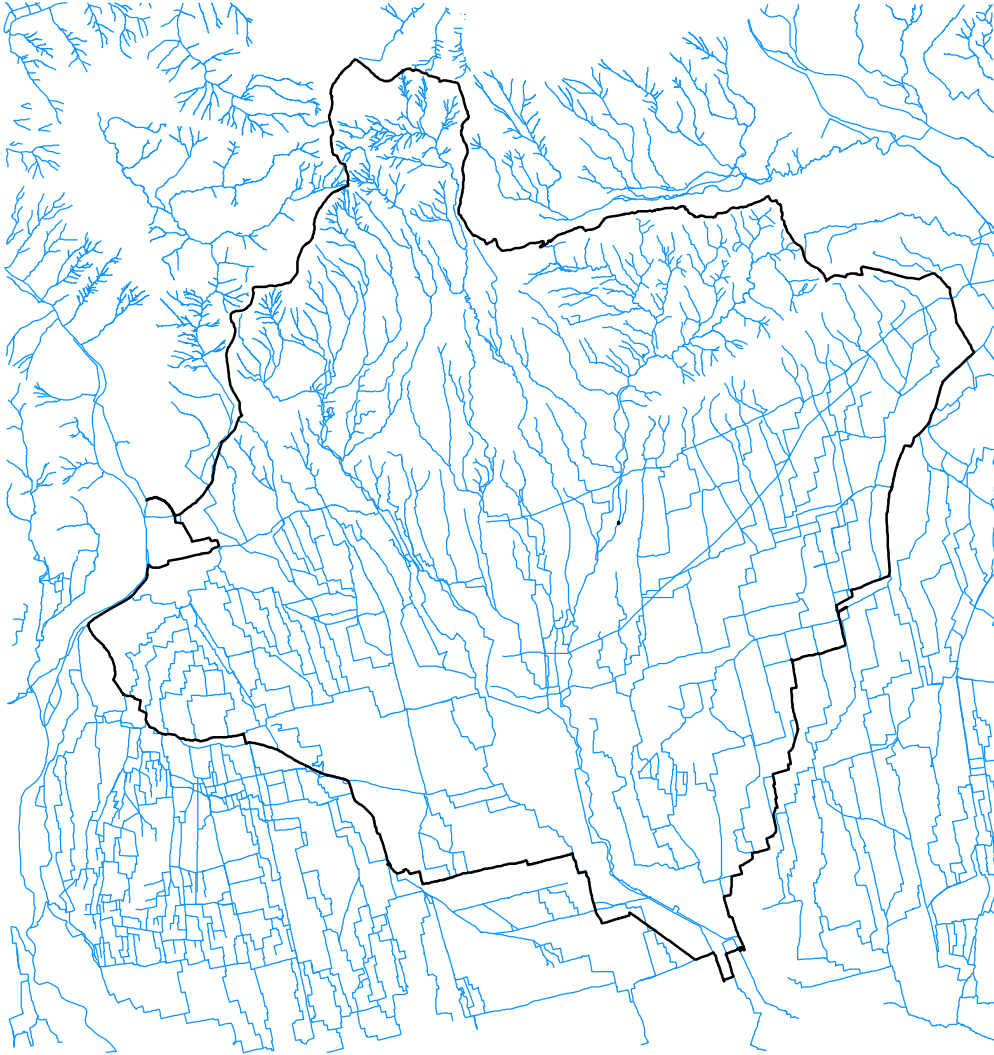


Figure 2.1: *Hydrographic network*

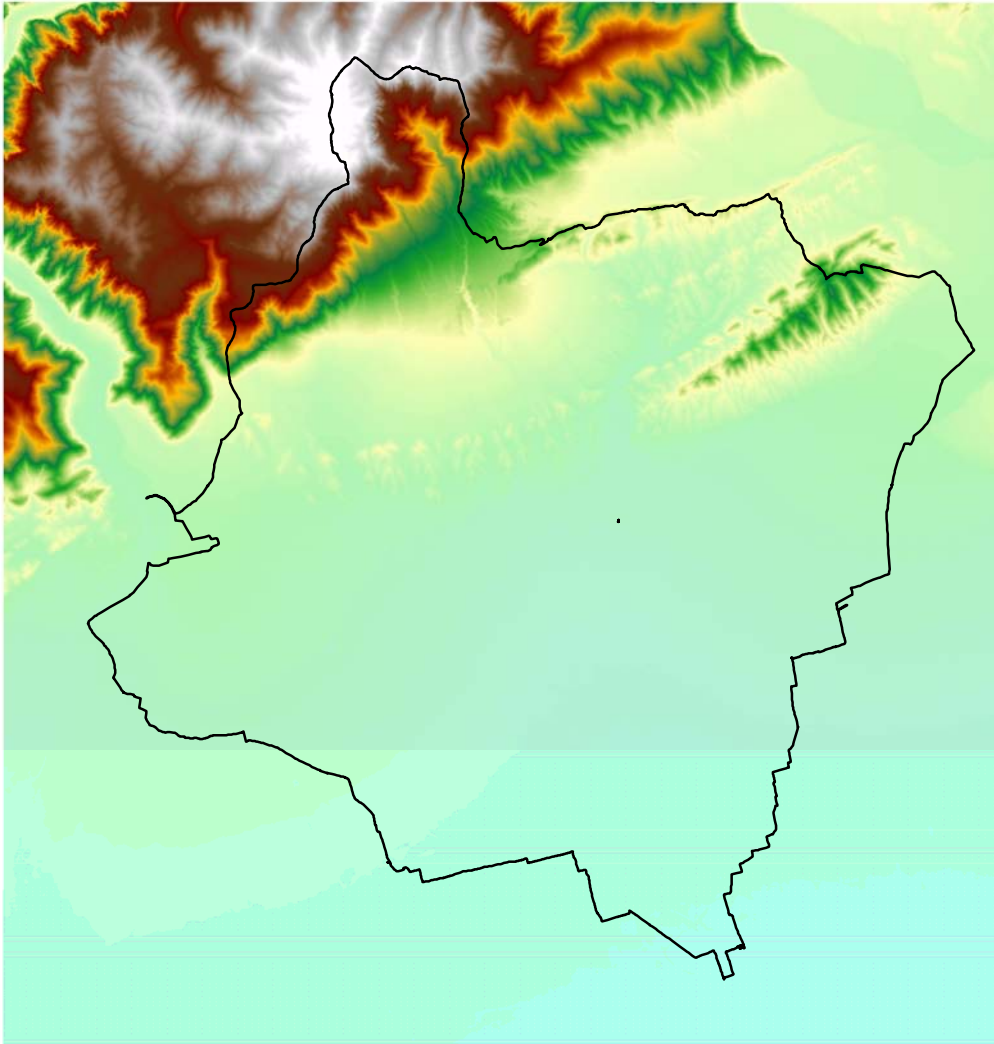


Figure 2.2: *DEM*

area of the Muson catchment are reported in the following Table 2.1 and shown in the Figure 2.3. From an analysis of the geo-pedologic scheme it is clear that the plane area is characterized by an high value of permeability, being the soil composed for most of it of gravel deposits.

Soil province code	Description	Permeability K (m/s)
Plane AA	Ancient upper plane, glaciofluvial conoids composed by limestone gravels	$8 \cdot 10^{-4}$
Plane AR	Recent upper plane, alpine fluvial conoids composed by limestone gravels and silts	$8 \cdot 10^{-4}$
Plane BA	Ancient lower plane, plane below the spring line composed by limestone sands	$5 \cdot 10^{-4}$
Hills RC	Pre-Alpine hills, narrow and elongated ridges composed by marly limestones	10^{-4}
Mountains SA	Pre-Alps with wavy peaks composed by hard and stratified limestones	10^{-5}
Mountains SI	Canyon in the pre-Alps composed by dolomite rocks and hard limestones	10^{-5}

Table 2.1: Soil province classification

Land use

The definition of land use is important for two aspects in this project: the classification of the total area in urban and non-urban area for runoff generation modeling and the classification of different crops for the evapotranspiration model. The urban area is considered impervious while the non-urban area allows to infiltrate aal the rainfall. Starting from the classification downloaded from the region catalog, the catchment area has been re-classified in twelve different classes as reported in the Table 2.2 and shown in Figure 2.4. This classification was obtained by remote sensing and refers to the year 2009 but in this project it is considered constant for the entire period of study (2004-2013).

Wastewater treatment plants

An important issue for the model is the leak of water also from the urban runoff component. This fact can be justified by the location of the wastewater treatment plant. The main plants of the area are indeed located out of our catchment area and so the rainfall water collected from the sewage system and treated in these plants does not contribute to the formation of the discharge of the Muson river. Even in case of big rainfall event the water by-passing the plants exits from the river basin. The list of the wastewater treatment plants is reported on the Table 2.3 and shown on the Figure 2.6.

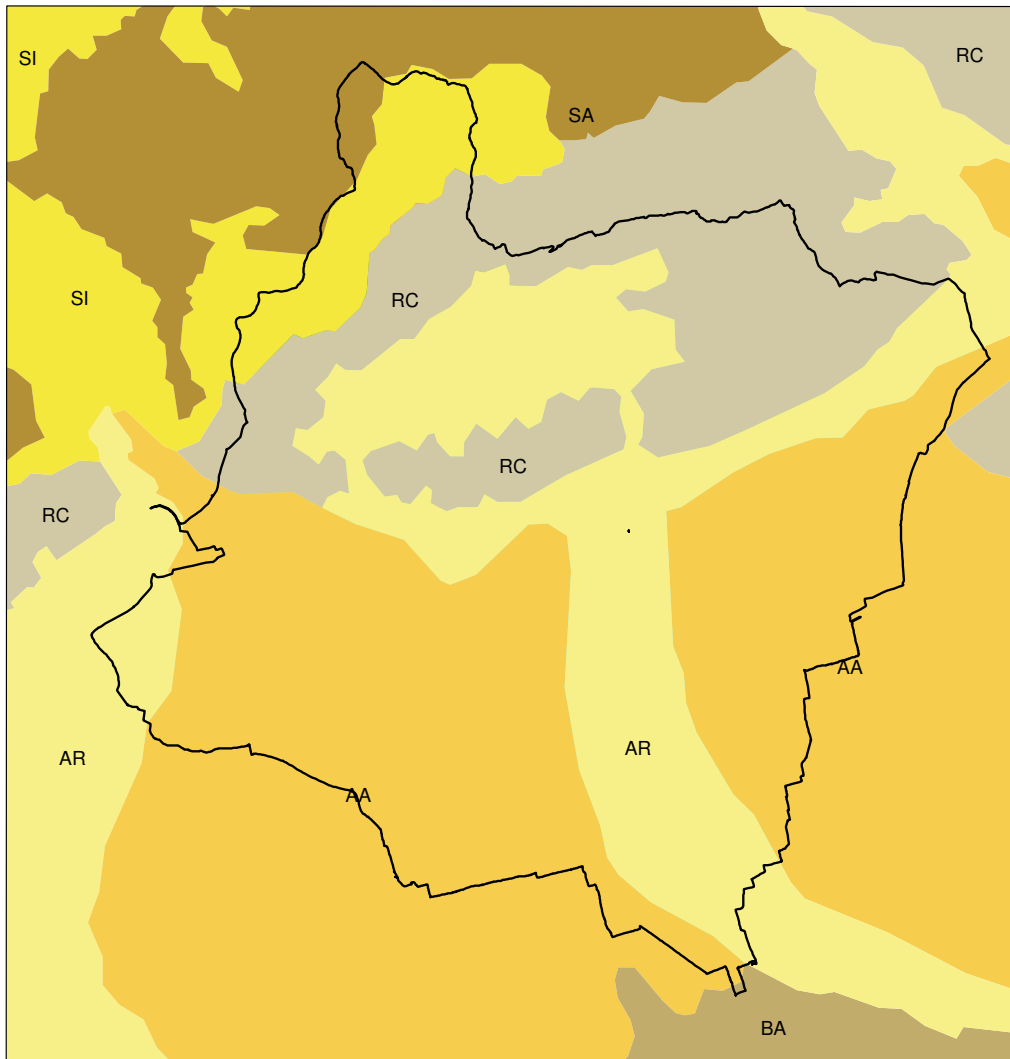


Figure 2.3: *Soil provinces classification as reported in Table (2.1)*













Land use class	Area percentage (%)	Colour
Urban area	21,01	
Water bodies	0,05	
Bare soil	9,18	
Soybean	0,43	
Corn	28,03	
Sunflower	0,01	
Wood	20,38	
Vineyard	2,17	
Olive grove	0,33	
Fruit plants	0,31	
Pasture	15,18	
Cereal	2,94	

Table 2.2: Land use classification

Municipality	Classification	P.E.	Location
Tezze sul Brenta	1 st cat. > 13000 p.e.	100000	out
Bassano del Grappa	1 st cat. > 13000 p.e.	96000	out
Castelfranco Veneto	1 st cat. > 13000 p.e.	67500	out
Cittadella	1 st cat. > 13000 p.e.	60000	out
Castelfranco Veneto	1 st cat. > 13000 p.e.	40000	out
Mussolente	2 nd cat. type A 1000-12999 p.e.	12000	in
Asolo	2 nd cat. type A 1000-12999 p.e.	7500	in
Maser	2 nd cat. type A 1000-12999 p.e.	4990	in
Crespano del Grappa	2 nd cat. type A 1000-12999 p.e.	3500	in
Cornuda	2 nd cat. type A 1000-12999 p.e.	2500	in
Fonte	2 nd cat. type A 1000-12999 p.e.	2000	in
Montebelluna	2 nd cat. type A 1000-12999 p.e.	1500	out
San Zenone degli Ezzelini	2 nd cat. type A 1000-12999 p.e.	1000	in
Cornuda	2 nd cat. type C < 1000 p.e.	980	out
Montebelluna	2 nd cat. type C < 1000 p.e.	600	out
San Zenone degli Ezzelini	2 nd cat. type C < 1000 p.e.	600	in
Castelfranco Veneto	2 nd cat. type C < 1000 p.e.	400	out

Table 2.3: Wastewater treatment plants

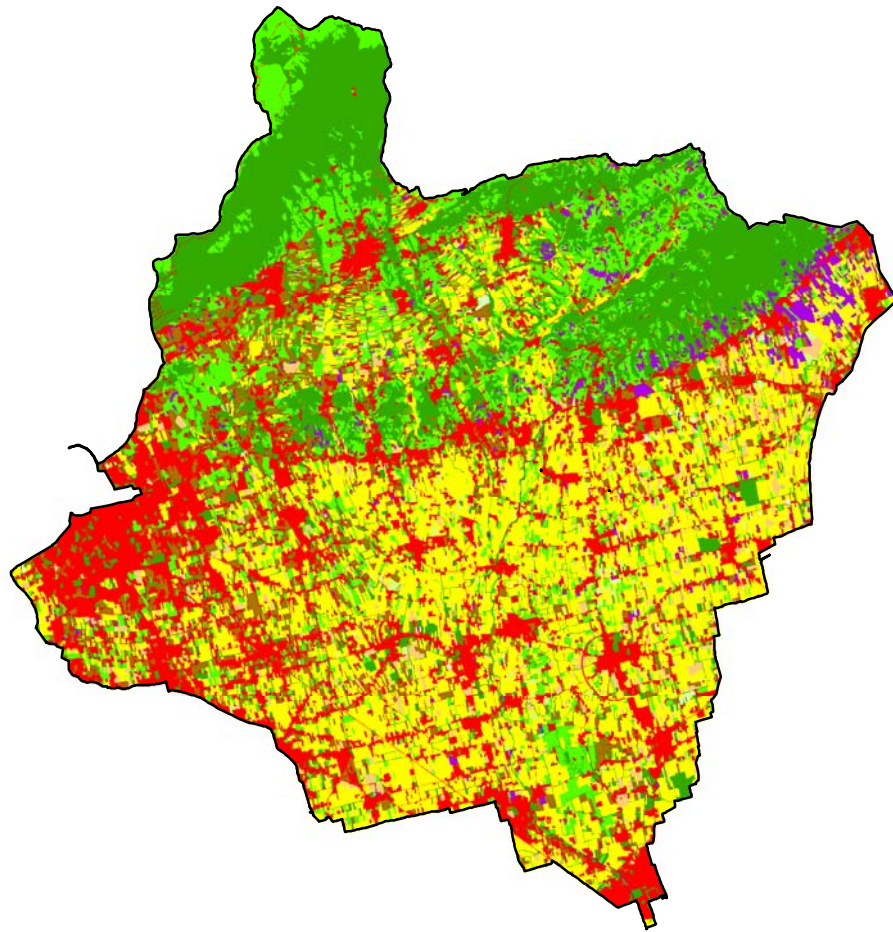


Figure 2.4: *Land use classification as reported in Table 2.2*

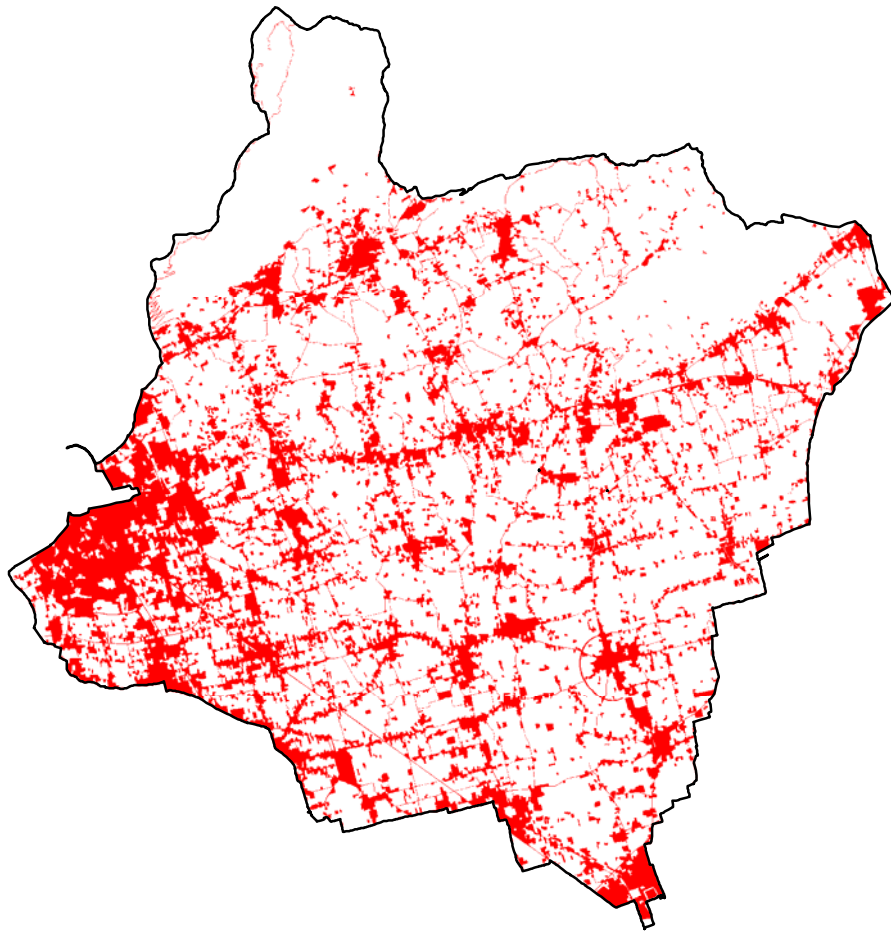


Figure 2.5: *Urban area*

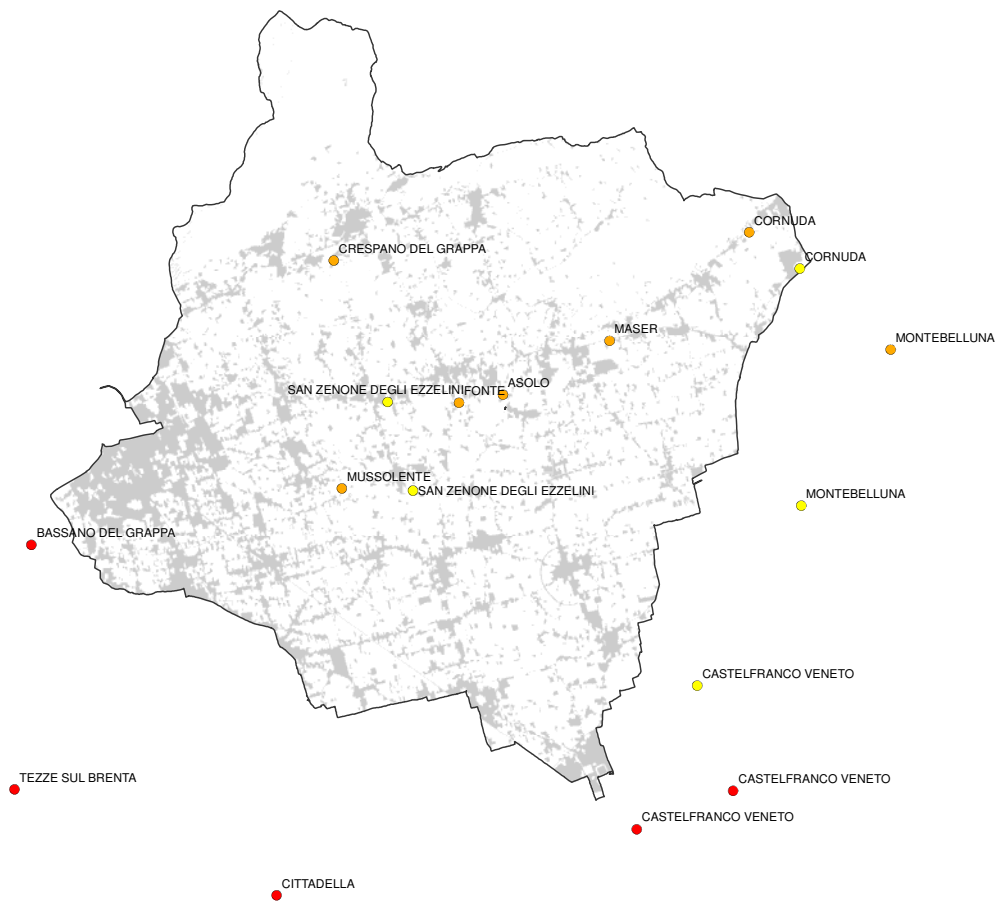


Figure 2.6: Waste water treatment plant classified as 1st category for more than 13000 population equivalent (red dots), 2nd cat. for p.e. between 1000 and 12999 (orange dots) and 2nd cat. for less than 1000 p.e. (yellow dots). In gray is shown the urban area.

Karst area

A factor that can influence the leaching term of the model and can not be precisely considered is the carsism of the area. Due to carsism, indeed, a relevant amount of water can leaks in the ground. In the Figure 2.7 are reported the area of the catchment that are considered to be karst by the Veneto region.



Figure 2.7: *Karst area*

2.1.1 Stream network and sub-watersheds

Starting from the hydrographic network (Figure 2.1), with an high density of irrigation canals, and the Digital Elevation Map (Figure 2.2), the catchment area has been divided manually in 59 sub-basins with an average size of $5,25 \text{ km}^2$. The process was not easy being the catchment, for most of it, located in plane. This fact does not allow the use of automatic extraction processes for the sub-basins (e.g. the algorithms D_8 or D_{inf}). These methods, starting from the digital terrain map, evaluate the drainage direction of each pixel of the grid, which can be single (D_8) or multiple (D_{inf}), and, imposing a threshold on the contributing area of a single pixel, define the channel network and the sub-basins. In the case of the Muson river the slope of the catchment is too gentle and the hydrographic network too anthropic to allow the automatic extraction to give a correct result. Figure 2.8 shows the characterization of the stream network obtained and the subdivision of the catchment in sub-basins, essential components for the hydrological model. Since there is only one hydrometric ARPAV station for the measure of the discharge and it is located in the Muson river at Castelfranco Veneto, before the interception with the Avenale stream, which collects the water of the eastern part of the basin, for the calibration of the model it has been used only the western part of the catchment, reducing the sub-basins from 59 to 49 and the area from 310 km^2 to 208 km^2 .

2.2 Hydrologic data

The accurate description of the spatio-temporal distribution of rainfall and other meteorological data has a huge importance in the modeling of the hydrologic response of the Muson river. The meteorological data used for the model and the calibration are the following:

- h , hourly measurements of rainfall in the stations in or near the basin [mm];
- $Tmax$ and $Tmin$, daily measurements of the maximum and minimum temperature in the stations in or near the basin [$^{\circ}C$];
- $RHmax$ and $RHmin$, daily measurements of the maximum and minimum relative humidity of the air in the stations in or near the basin;
- wv , daily average wind velocity in the stations in or near the basin [$m \text{ s}^{-1}$];
- R , daily average solar radiation in the stations in or near the basin [$MJ \text{ m}^{-2} \text{ s}^{-1}$];
- Q , hourly measures of discharge in the hydrometric station of Castelfranco Veneto [m^3/s];

Data from the twelve meteorological gauges reported in Figure 2.10 and listed in Table 2.4 have been considered. These are located within or nearby the basin. One hydrometric station, situated in Castelfranco, provided discharge data between 2000 and 2013. All the available data are provided by ARPAV, the regional agency for the environment and their temporal-spatial distribution have been interpolated using the Kriging tool (Section 2.2.1).

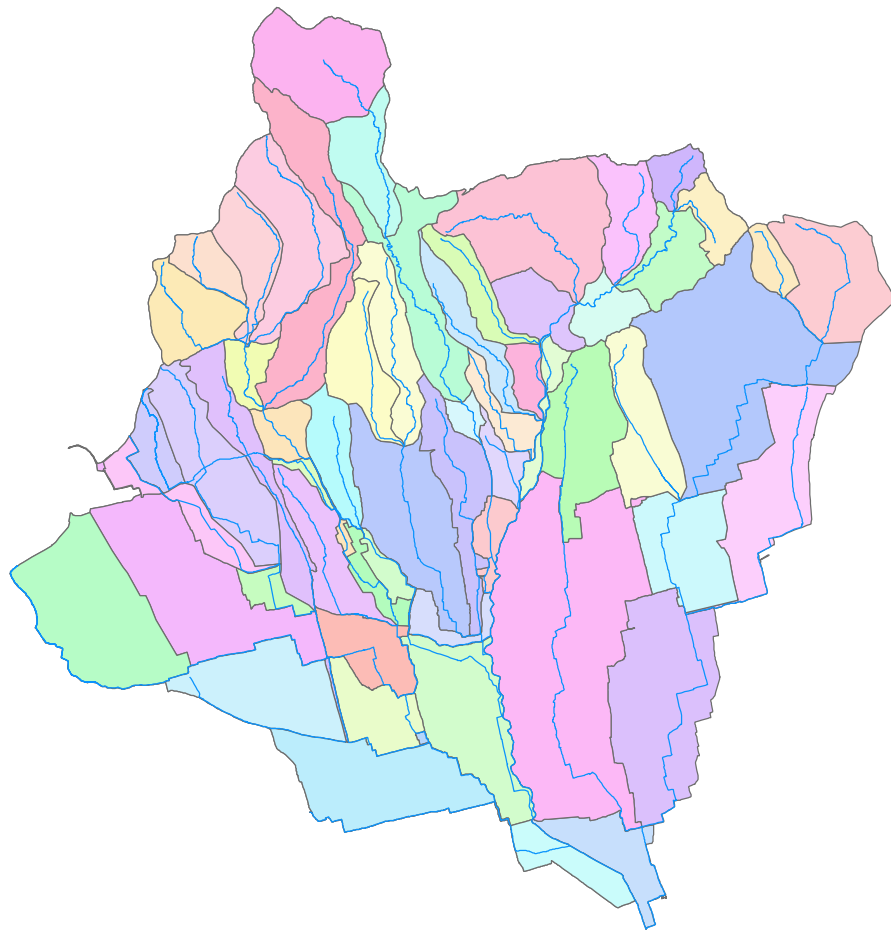


Figure 2.8: *Geometry of the basin with main hydrography and sub-basins*

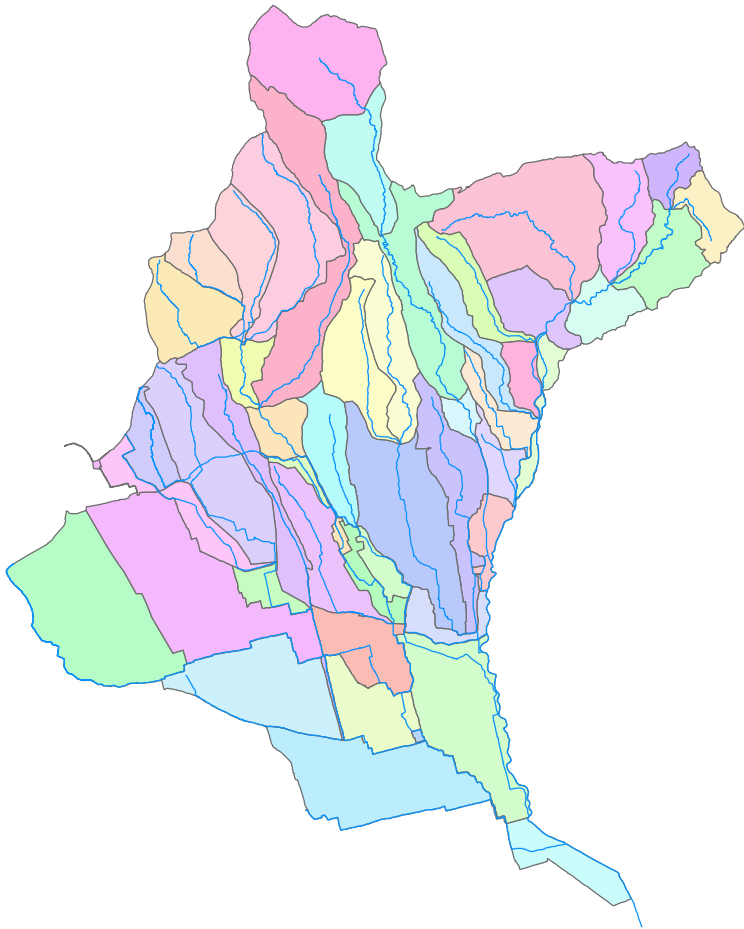


Figure 2.9: *Western part of the basin*

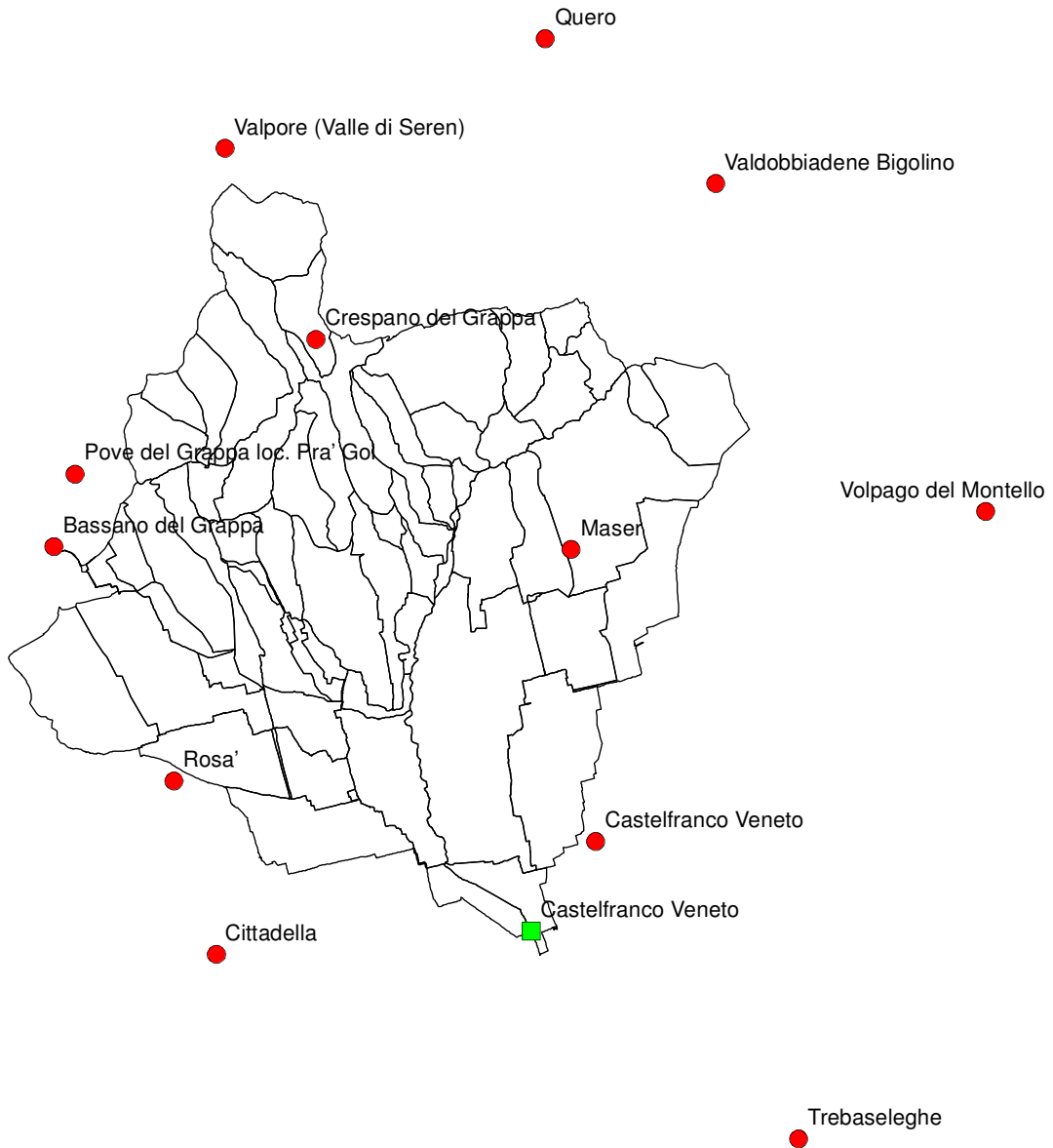


Figure 2.10: Meteorological stations used (red dots). The green square is the hydrometric station in Castelfranco

Meteorological station	Gauss-Boaga coordinates		Elevation (m a.s.l)	Year of activation
	X	Y		
Bassano del Grappa	1712258	5073804	128	2000
Castelfranco Veneto	1729544	5064403	50	1989
Cittadella	1717437	5060795	56	1991
Crespano del Grappa	1720610	5080406	401	2002
Maser	1728768	5073708	101	1992
Pove del Grappa	1712940	5076113	675	1985
Quero	1727948	5089994	249	2002
Rosá	1716095	5066330	85	1991
Trebaseleghe	1736015	5054913	23	1995
Valdobbiadene	1733368	5054913	222	1992
Valpore	1717709	5086487	1275	2004
Volpago	1742000	5074920	125	1992

Table 2.4: List of the meteorological stations present in the area of study.

2.2.1 Kriging

Rainfall is a natural phenomenon characterized by high spatial and temporal variability. In rainfall-runoff models it is necessary to describe with a desired precision rainfall fields starting from data measured in a set of meteorological gauges available in the area of study. If the area of the catchment is comparable with the typical size of convective rain cells it is possible to assume uniform rainfall; otherwise, when the catchment's size is larger than the integral scale of rainfall events, the hypothesis of homogeneous rainfall is no longer valid. The Kriging is a statistical interpolator, useful for meteorological data, that allows linear and optimal estimates of spatially distributed random fields. Starting from a series of data measured in different stations the method allows one to calculate the most probable value of rainfall in any arbitrary point or the region. Repeating the calculation for all the cells over a regular grid, it is possible to determine the spatial distribution of the rainfall.

Assuming the rainfall, $z(\bar{x})$, to be a function of the spatial coordinate \bar{x} , such function is unknown for all the points of the region. Nevertheless it can be reconstructed starting from the available measures and from other considerations related to the nature of the physical phenomena involved. For this reason the distribution of rainfall is considered a spatial random variable $z(\bar{x})$, with respect to which the observed distributions $Z(\bar{x})$ are supposed to be just some of the infinite equiprobable realizations $Z(\bar{x})_1, Z(\bar{x})_2, \dots, Z(\bar{x})_k$. To describe in a complete way the continuous random function z , its moments are used, that gives some information on the statistical properties of the stochastic field. The moments involved in the computation are:

- the *mean*

$$\mu = E(z) = \int_{-\infty}^{+\infty} z \cdot f(z) \cdot dz \quad (2.1)$$

- the *variance*

$$\sigma_z^2 = \int_{-\infty}^{+\infty} (z - \mu)^2 \cdot f(z) \cdot dz \quad (2.2)$$

- the *variogram*

$$\begin{aligned} \gamma(\bar{x}, \bar{h}) &= 1/2 \sigma^2 [Z(\bar{x} + \bar{h}) - Z(\bar{h})] = \\ &= 1/2 E \left\{ [Z(\bar{x} + \bar{h}) - Z(\bar{x})] - E[Z(\bar{x} + \bar{h}) - Z(\bar{x})] \right\}^2 \end{aligned} \quad (2.3)$$

where \bar{x} represents the coordinates' vector of a generic point in space and $\bar{x} + \bar{h}$ the coordinates' vector of a point far \bar{h} from \bar{x} ;

- the *autocovariance*

$$C(\bar{x}, \bar{h}) = E\{[Z(\bar{x} + \bar{h}) - \mu] \cdot [Z(\bar{x}) - \mu]\}. \quad (2.4)$$

The last two moments can be related by the following equation:

$$2\gamma(\bar{x}, \bar{h}) = \sigma^2(\bar{x}, \bar{h}) + \sigma^2(\bar{x}) - 2C(\bar{x}, \bar{h}) \quad (2.5)$$

To solve the interpolation problem, two statistical properties need to be introduced:

- *homogeneity* (or *stationarity*), that allows to introduce, to the whole field $z(\bar{x})$, the statistical properties obtained from the available measures. In a stationary field the statistical properties does not vary in space;
- *ergodicity*, that means that the available observations are representative of the whole population under examination. Given a stochastic process, indicated with $m(x)$ the mean, calculated on a single realization of N elements, the process is ergodic on the mean if, for N going to infinity, $m(x)$ goes to the same result $\mu(x)$ for every realization. In particular the second order stationarity implies the following properties:

$$\begin{aligned} E[z(\bar{x})] &= \mu \\ C(\bar{x}, \bar{h}) &= C(\bar{h}) \\ \gamma(\bar{x}, \bar{h}) &= \gamma(\bar{h}) \end{aligned}$$

In case of homogeneous field equation (2.5) can be rewritten as:

$$\gamma(\bar{h}) = \sigma^2(z) - C_z(h) \quad (2.6)$$

For h going to infinity the covariance goes to zero, and so the variogram tends to the variance σ^2 ; On the other hand, for $h \rightarrow 0$ the variogram goes to zero as well. Hence, the less the distance between two generic points of the space, the closer the value of the random variables assumed in those points. The variogram gives a measure of the correlation degree of the random field: when the field is strong correlated, the variogram goes very quickly

to its maximum value (the variance). In case of rainfall fields it is possible to approximate the behavior of the variogram for increasing distance through the following exponential law:

$$\gamma_h(r) = \sigma_h^2[1 - e^{-Z}] \quad Z = \sqrt{\left(\frac{r_x}{I}\right)^2 + \left(\frac{r_y}{I}\right)^2} \quad (2.7)$$

where r_x and r_y represent the components of a radial vector related to the axis coordinated by the distance between the two points respect which the variogram is calculated, $\sigma^2(h)$ is the variance of the random variable h , I is the *integral scale* of h and represents the distance at which the stochastic field cease to be correlated.

Kriging in an homogeneous field

A good estimation of $\hat{z}(x_0, y_0)$, that identifies a random variable belonging to an homogeneous field in a generic point (x_0, y_0) , must fulfill the following conditions: i) absence of a systematic error (i.e. mean error equal to zero) and ii) minimum variance of the errors:

$$\begin{aligned} E(\hat{z}_0 - z_0) &= 0 \\ var(\hat{z}_0 - z_0) &= min \end{aligned} \quad (2.8)$$

If $z_i(x_i, y_i)$ are the values of z measured in n points of the space, an optimal estimation $\hat{z}(x_0, y_0)$ is given by the linear combination of the observations $z_i(x_i, y_i)$:

$$\hat{z} = \sum \lambda_{i0} \cdot z_i \quad (2.9)$$

Substituting the equation (2.9) in the first of the conditions (2.8) and exploiting the linearity of the mean, it is possible to verify the first condition for the optimal estimation:

$$E[\hat{z}_0 - z_0] = E\left[\sum \lambda_{i0} z_i - z_0\right] = \mu - \mu = 0 \quad (2.10)$$

The second condition, introducing the definition of the variance and exploiting the relation (2.10), becomes:

$$var(\hat{z}_0 - z_0) = E[(\hat{z}_0 - z_0) - E(\hat{z}_0 - z_0)]^2 = E[(\hat{z}_0 - z_0)^2] = min \quad (2.11)$$

To simplify the discussion it is possible to transform the original field in a zero mean field, introducing the variable $Y(x, y)$: $[Y(x, y) = z(x, y) - \mu]$, reducing the problem to a linear estimation:

$$\hat{Y}_0 = \sum \lambda_i \cdot Y_i \quad (2.12)$$

Equation (2.11) becomes:

$$var(\hat{z}_0 - z_0) = var(\hat{Y}_0 - Y_0) = E[(\hat{Y}_0 - Y_0)^2] \quad (2.13)$$

Developing the square and exploiting the linearity property of the mean, it is obtained:

$$E[(\widehat{Y}_0 - Y_0)^2] = \sum_i \sum_j \lambda_{0i} \lambda_{0j} E[Y_i Y_j] + \sigma_Y^2 - 2 \sum_i \lambda_{0i} E[Y_0 Y_i] \quad (2.14)$$

where $E[(Y_i Y_k)]$ is the covariance of the random variable $Y(x, y)$, evaluated in the points (x_i, y_i) and (x_k, y_k) :

$$E[(Y_i Y_k)] = C[(x_i, y_i) - (x_k, y_k)] = C(\bar{r}_{ik}) \quad (2.15)$$

imposing $\sum \lambda_{0i} C(\bar{r}_{ik}) = C(\bar{r}_{0k})$ e $\bar{r}_{ik} = (x_i - x_k)$, $\bar{r}_{0k} = (x_0 - x_k)$. Substituting the equation (2.15) in the (2.14) it is possible to obtain the final expression for the objective function:

$$var(\widehat{Y}_0 - Y_0) = \sum_i \sum_j \lambda_{0i} \lambda_{0j} C(\bar{r}_{ij}) + \sigma_Y^2 - 2 \sum_i \lambda_{0i} C(\bar{r}_{0i}) \quad (2.16)$$

To determine the values of the parameter λ that minimize this function:

$$\frac{\partial [var(\widehat{Y}_0 - Y_0)]}{\partial \lambda_{k0}} = 0 \quad k = 1, 2, \dots, n \quad (2.17)$$

The solution of the (2.17) is given by the following linear system, in a matrix form:

$$\widetilde{C} \bar{\lambda} = \bar{C}_0 \quad (2.18)$$

from which there can be calculated the values of the parameter $\bar{\lambda} = \widetilde{C}^{-1} \cdot \bar{C}_0$, where

- \widetilde{C} is the covariance matrix, in which the generic element \widetilde{C}_{ij} represents the autocovariance of the random variable between the points that are distant each other r_{ij} , i.e. $C(\bar{r}_{ij})$:

$$\widetilde{C} = \begin{bmatrix} C_{11} & C_{12} & \dots & C_{1n} \\ C_{21} & C_{22} & \dots & C_{2n} \\ \dots & \dots & \dots & \dots \\ C_{n1} & \dots & \dots & C_{nn} \end{bmatrix}$$

- \bar{C}_0 is the vector whose generic element C_{0i} represents the autocovariance of the random variable evaluated in the point (x_0, y_0) fo the all n observations.

Solving the linear system given by the equation (2.18) one can derive the weights λ_{0i} that are there inserted in equation (2.9) to calculate \widehat{z}_0 . In correspondence of the solution of the linear system, the objective function (eq. 2.14) has a minimum:

$$\sum \lambda_{0i} C(\bar{r}_{ik}) = C(\bar{r}_{0k})$$

And so:

$$[var(\widehat{Y}_0 - Y_0)]_{MIN} = \sigma_Y^2 - \sum \lambda_i C(\bar{r}_{0i}) \quad (2.19)$$

from which it is deduced that the variance of the error is smaller than the variance of the variable. The more the field is correlated, the bigger is $C(\bar{r}_{0i})$ and the smaller is the error in the estimate procedure.

Kriging in a non-homogeneous field

Considering a spatial domain, which is assumed to be squared with side L for simplicity, one can define the following variable:

$$m_z = \frac{1}{L^2} \int_{L \times L} z(\bar{x}) d\bar{x} \quad (2.20)$$

$$s^2(z) = \frac{1}{L^2} \int_{L \times L} [z(\bar{x}) - m_z]^2 d\bar{x} \quad (2.21)$$

While, in general, for L going to infinity m tends to the mean, it is not true that for all the random variables' fields, for L going to infinity, $s^2(z)$ tends asymptotically to a defined values (equal to the variance). In some cases, indeed, some heterogeneities take place and $s^2(z)$ goes to infinity. This implies the non-existence of the variance. Hence, in non-homogeneous fields it is necessary to use a more general tool (i.e. the covariance). To apply the Kriging for the interpolation of measured data, an *intrinsic hypothesis* is introduced, assuming homogeneous increments in the field:

$$\begin{aligned} E[z(\bar{x} + \bar{h}) - z(\bar{x})] &= \mu_{\Delta}(\bar{h}) \\ var[z(\bar{x} + \bar{h}) - z(\bar{x})] &= 2\gamma(\bar{x}, \bar{h}) = 2\gamma(\bar{h}) \end{aligned}$$

The variogram function γ generalize the variance function: it indeed exists also when the variance does not exist. The Kriging formulation results to be similar to the one of the homogeneous case:

$$\begin{aligned} E(\hat{z}_0) &= \mu \\ var(\hat{z}_0 - z_0) &= \min \end{aligned} \quad (2.22)$$

Developing the first of the conditions (2.22), it is obtained:

$$E \left(\sum_i^n \lambda_{i0} z_i \right) = \sum_i^n \lambda_{i0} E(z_i) = \mu \sum_i^n \lambda_{i0} \quad (2.23)$$

from which

$$\sum_i^n \lambda_{i0} = 1 \quad (2.24)$$

This way, it is obtained a more restrictive bond respect to the stationary case, that can be use to determine the solution. From the second of the conditions (2.22), it is obtained

$$E \left[\sum_i^n (\lambda_{i0} z_i - z_0)^2 \right] = \min \quad (2.25)$$

The variogram gives information on the spatial correlation between different points of the field. Assuming that the variance σ_z^2 exists, the relation between the covariance and variogram can be determined as:

$$\gamma(\bar{r}) = \frac{1}{2}E[z^2(\bar{x} + \bar{r}) + z^2(\bar{x}) - 2z(\bar{x} + \bar{r})z(\bar{x})] \quad (2.26)$$

In case of second order stationarity $E[z(\bar{x})] = \mu = \text{const}$, and exploiting the linearity property of the mean, it is possible to write the following equation:

$$\sigma_z^2 = E[(z(\bar{x} + \bar{r}) - \mu)^2] = E[z^2(\bar{x} + \bar{r})] - \mu^2 \quad (2.27)$$

Substituting equation (2.27) in (2.26), one finally obtains:

$$\gamma(\bar{r}) = (\sigma_z^2 + \mu^2) - E[z(\bar{x} + \bar{r}) \cdot z(\bar{x})]; \quad (2.28)$$

Meanwhile, recalling the definition of covariance:

$$C(\bar{r}) = E[z(\bar{x} + \bar{r}) \cdot z(\bar{x})] - \mu^2 \quad (2.29)$$

and calculating the product at the r.h. side of the equation (2.29), after using the linearity property of the mean, the following expression is obtained:

$$\gamma(\bar{r}) = \sigma_z^2 - C(\bar{r}) \quad (2.30)$$

Eq. (2.30) shows that the variogram contains information on the correlation of the field, even in case of non-existing variance, and that σ_z^2 and $C(\bar{r})$ lose their meaning. In a non-stationary case, where the variogram is not asymptotic to a finite value, the problem can be equally solved recalling the intrinsic hypothesis:

$$\begin{aligned} E[z(\bar{x})] &= \mu \\ \gamma(\bar{r}) &= 1/2E[(z(\bar{x} + \bar{r}) - z(\bar{x}))^2] \end{aligned} \quad (2.31)$$

It is now necessary to minimize the equation (2.25). Calculating the square as the multiplication of two sums it is obtained:

$$E[(\hat{z}_0 - z_0)^2] = E\left[\left(\sum_i \lambda_{0i}(z_i - z_0)\right) \cdot \left(\sum_j \lambda_{0j}(z_j - z_0)\right)\right] \quad (2.32)$$

Adding and subtracting z_0 in the equation (2.26) it is obtained:

$$\gamma(\bar{r}_{ij}) = \frac{1}{2}E[(z_i - z_j)^2] = \frac{1}{2}E[((z_i - z_0) - (z_j - z_0))^2] \quad (2.33)$$

Calculating this square elevation, substituting in the (2.32) and applying the bond expressed by the equation (2.24) it is obtained:

$$E[(\hat{z}_0 - z_0)^2] = 2 \sum_i \lambda_{i0} \gamma(\bar{r}_{i0}) - \sum_i \sum_j \lambda_{i0} \lambda_{0j} \gamma(\bar{r}_{ij}) \quad (2.34)$$

The obtained expression has a shape similar to the one obtained for the homogeneous case (i.e. equation (2.14)), with the difference that in this one there is a case of *bonded minimization*. For determining the solution, the Lagrange multiplication method it is used and a new objective function it is built. The problem is now expressed by the condition:

$$\min \left\{ \frac{1}{2} E [(\hat{z}_0 - z_0)^2] - \alpha \left(\sum \lambda_{i0} - 1 \right) \right\} \quad (2.35)$$

where the following bond it is used:

$$\sum_i^n \lambda_{i0} = 1.$$

Deriving the equation (2.35), respect to λ_{i0} and α , the following conditions are obtained:

$$\begin{cases} \frac{\partial f}{\partial \lambda_{0k}} = \gamma(\bar{r}_{0k}) - \sum \lambda_{i0} \gamma(\bar{r}_{ik}) - \alpha = 0 & k = 1, 2, \dots, n \\ \frac{\partial f}{\partial \alpha} = \sum \lambda_i - 1 = 0 \end{cases} \quad (2.36)$$

The solution of the problem then becomes

$$\begin{cases} \gamma(\bar{r}_{k0}) = \sum \lambda_{0i} \gamma(\bar{r}_{ik}) + \alpha = 0 \\ \sum \lambda_i = 1 \end{cases}$$

And writing the system in a compact form:

$$\begin{cases} \bar{\gamma}_0 = \tilde{\Gamma} \bar{\lambda} + \alpha \\ \sum \lambda_i = 1 \end{cases}$$

where

$$\bar{\lambda} = [\lambda_1, \lambda_2, \dots, \lambda_n, \alpha] \quad \bar{\gamma}_0 = [\gamma_{10}, \gamma_{20}, \dots, \gamma_{n0}, \alpha] \quad \tilde{\Gamma} = \begin{bmatrix} \gamma(r_{11}) & \dots & \gamma(r_{1n}) & 1 \\ \gamma(r_{21}) & \dots & \gamma(r_{2n}) & 1 \\ \dots & \dots & \dots & \dots \\ 1 & \dots & 1 & 0 \end{bmatrix}$$

Eq. (2.2.1) provide a representation of the general solution of the spatial interpolation problem of the measured data in stochastic fields, valid also in case of homogeneous field.

Spatial and temporal distribution of the meteorological data

For all the data available pointwise, the corresponding spatial and temporal distributions have been estimated starting from point measures in different gauges. These operations have been performed in two separate phases:

1. calculation of the experimental variogram and of the statistical properties of the field of study (variance and integral scale);
2. determination of the spatial distribution of the meteorological data trough the interpolator Kriging of the measures.

The variogram it has been evaluated as the mean of the variograms calculated for all the time intervals considered. The experimental variogram it has been interpolated with the following exponential law:

$$\gamma_h(r) = \sigma_h^2[1 - e^{-Z}] \quad Z = \sqrt{\left(\frac{r_x}{I}\right)^2 + \left(\frac{r_y}{I}\right)^2} \quad (2.37)$$

where r_x and r_y represent the components related to the axis coordinated by the distance between the two points respect which the variogram is calculated, $\sigma^2(h)$ is the variance of the random variable h , I is the *integral scale* of h and represents the distance at which the stochastic field cease to be correlated. This operational method implies a priori a spatial and temporal hypothesis of the characteristics of the data. The estimation of the parameters $\sigma^2(h)$ and I it has been obtained with the least square method. Under the stationarity hypothesis, the macroscale I depends only on the distance r_i between the two points respect which the variogram is calculated. Denoting as $\gamma_i(r_i)$ the series of experimental variograms, equation (2.37) can be written as:

$$\gamma_i(r_i) = \sigma^2[1 - e^{-r_i/I}] \quad (2.38)$$

The parameters that approximate at best the experimental series makes minimum the square error Φ , defined as:

$$\Phi = \sum_{i=1}^n [\gamma_i(r_i) - \sigma^2[1 - e^{-r_i/I}]]^2 \quad (2.39)$$

where n is the number of the experimental data. Imposing the condition of minimum:

$$\frac{\partial \Phi}{\partial \sigma^2} = \frac{\partial \Phi}{\partial I} = 0 \quad (2.40)$$

one obtains the following system of equations:

$$\begin{aligned} \sigma^2 &= \frac{\sum_{i=1}^n \gamma_i(r_i)(1 - e^{-r_i/I})}{\sum_{i=1}^n (1 - e^{-r_i/I})^2} \\ \sum_{i=1}^n \gamma_i(r_i)r_i e^{-r_i/I} - \sigma^2 \sum_{i=1}^n (r_i)e^{-r_i/I}(1 - e^{-r_i/I}) &= 0 \end{aligned} \quad (2.41)$$

By solving the second equation of the system (2.41) (e.g. with the bisection method), the integral scale I is obtained and, after the substitution it in the first equation, it allows σ^2 to be determined.

Once the statistical properties of the observed fields are estimated, starting from the point measurements in the available meteorological stations, the spatial distribution of the data is calculated with the geostatistical interpolator Kriging, for a grid with a resolution of 100 m covering the entire area where the catchment is located.

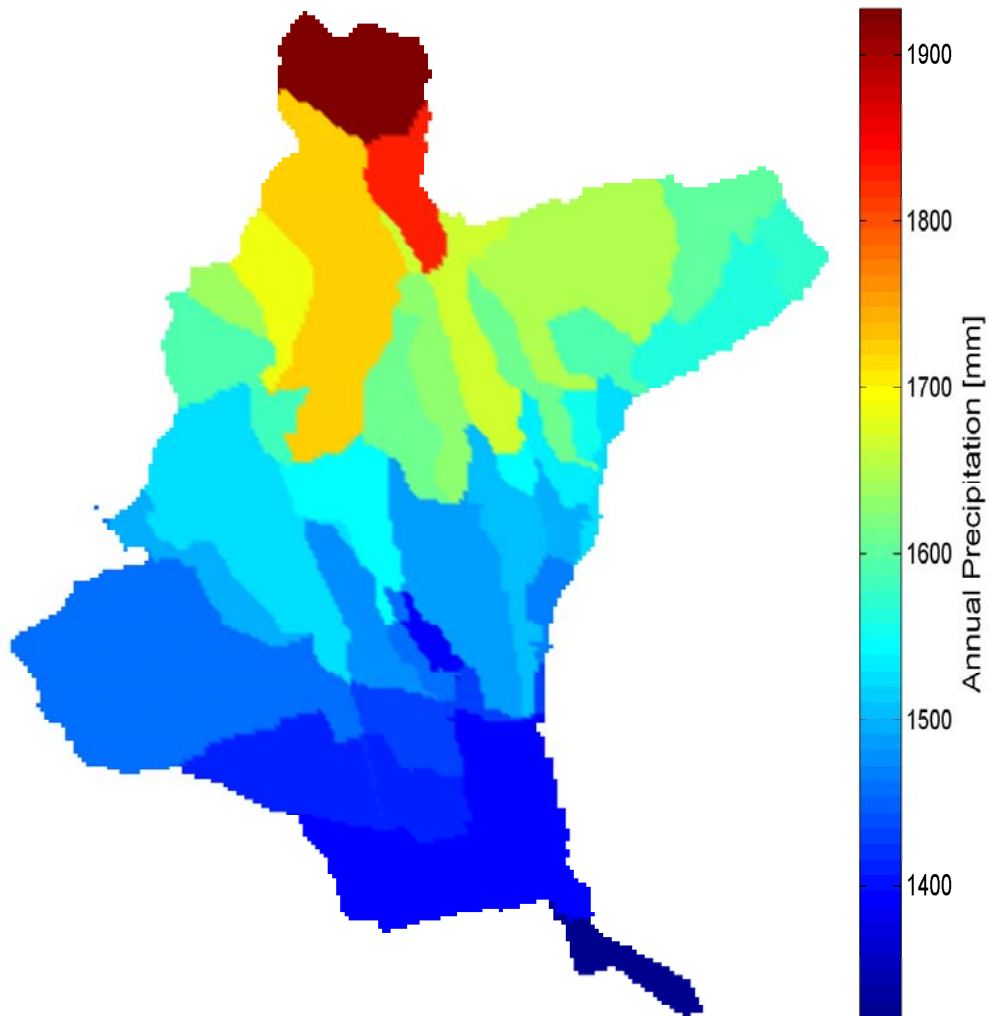


Figure 2.11: *Spatial distribution of the cumulative precipitation for the year 2004*

Chapter 3

Mathematical models

The hydrologic response of a catchment is the result of complex climatic, ecologic and hydrologic processes. All these processes have to be evaluated at the catchment scale. The phenomena that determine the hydrologic response of a catchment can be summarized as follows:

1. runoff is generated from the contributing area of a basin as the result of the interactions between rainfall and soil moisture dynamics;
2. the different components of the runoff moves within the soil of a given area (or over it) until they reach the channel network;
3. transport inside the canals of the network and the interaction between the hydrologic components generated by the different portions of the catchment are driven by the topology of the network itself.

The model used in this project is concentrated in the parameters but distributed in the description of the processes, since it uses information obtained from terrain digital model, geostatistical interpolation of pointwise measures of rainfalls and other climatic data, as well as maps of the pedology and soil use. The mechanisms of infiltration and separation of the flows that generate the total discharge are described by an approach based on TOPMODEL [Beven, 2001], that describes with a simple model based on the topographic characteristics of the catchment the partitioning of the outflows between rapid (or subsurface) runoff and deep runoff. The transport processes, described in the following sections, are instead described using a stochastic Lagrangian approach based on the distribution of the water residence time within a catchment control volume. This method is founded on the geomorphological theory of the hydrological response which relates the distributions of the residence times in the different paths inside the basin to the instantaneous unit hydrograph (e.g. [Rodriguez-Iturbe and Rinaldo, 1997]).

3.1 Mass balance equation and effective rainfall generation

In the model, suitable mass balance equations are used to identify the effective rainfall, which is the fraction of rainfall that actively contributes to streamflows. Considering a

well defined control volume that represents an entire catchment (or a given subcatchment), the mass balance equation of water can be written as:

$$\frac{dV}{dt} = P - R - O - Q_{cs} - ET - Q_{disp} \quad (3.1)$$

where: $V = V_{rz} + V_{urb} + V_{rap} + V_{slow}$ is the total volume of water stored within the considered system; V_{rz} , V_{urb} , V_{rap} and V_{slow} are, respectively, the volumes of water related to root zone, urban, rapid (i.e. shallow) and slow (i.e. deep) compartments; P is the total precipitation; R is the flux of deep percolation (i.e. the groundwater recharge), O is the outflow from urban areas, Q_{cs} is the total flow that leave the system at the closure section; ET is the evapotranspiration and Q_{disp} is the water leaking from the bottom of the river. A schematic representation of the control volume used in this project is represented in Figure 3.1.

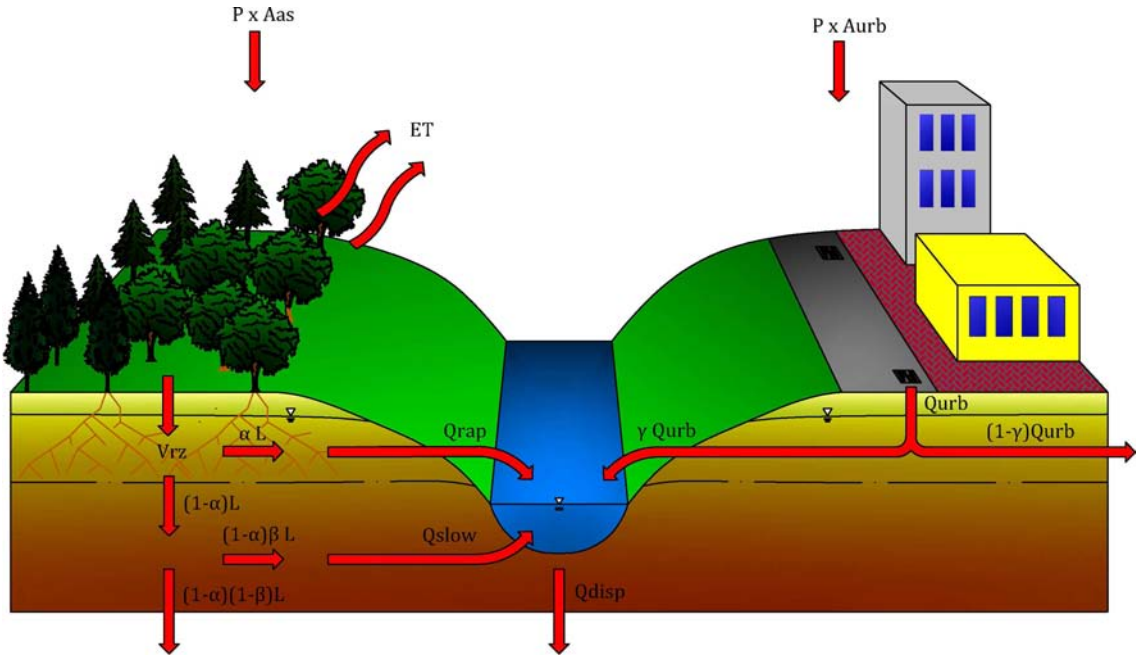


Figure 3.1: Control volume scheme used for the generation of the different runoff contributions.

The total area of the catchment is divided in two compartments: the urban area, A_{urb} , where the rainfall is not able to infiltrate, and the active surface, $A_{as} = A_{tot} - A_{urb}$, where the rainfall infiltrate and takes part to the root zone water balance. Vertically, the active surface is identified by two serial storages: the root-zone and a deeper aquifer. The rain falling on the active surface $P \cdot A_{as}$ totally infiltrates in the soil entering the root zone layer. The water balance of the root zone is the following:

$$\frac{dV_{rz}}{dt} = P \cdot A_{as} - L - ET \quad (3.2)$$

where ET is the evapotranspiration (Section 3.2) and L , the leaching component leaving the root-zone via deep percolation is given by:

$$L = K_0 \cdot s^c \quad (3.3)$$

In eq. (3.3), K_0 represent the saturated hydraulic conductivity determined by the maps of the use of the soil of the Muson basin and c is the Clapp and Hornberger coefficient [Clapp and Hornberger, 1978]. Meanwhile, the term s in eq. (3.3) represents the mean water content in the root zone, expressed as:

$$s = \frac{V_{rz}}{n \cdot Z_r \cdot A_{as}} \quad (3.4)$$

where n is the soil porosity and Z_r is the root zone depth. The leaching term L is then split, through a coefficient α , in two different contributions. αL constitutes the effective rainfall from rapid subsurface components, while, $(1 - \alpha)L$ leaches deeper in the ground. The coefficient β identifies the part of the deep leaching $(1 - \alpha)L$ that contributes to the streamflows, while $(1 - \beta)(1 - \alpha)L$ identifies the contribution to the recharge of the groundwater. The rain falling on the urban area $P \cdot A_{urb}$ constitutes the effective rainfall from urban areas.

The distinction between the three components of runoff is useful in the description of the hydrologic response of the catchment since they characterized by different timescales. For this reason a correct partition of the effective rainfall in this three flows is really important to enhance the model ability to reproduce the hydrologic response of the study catchment.

3.2 Evapotranspiration model

The calculation of the evapotranspiration is performed with the FAO-Penman-Montieth method ([Allen et al., 1998]), based on an energy conservation equation for the layer of soil interacting with the atmosphere. The meteorological input are obtained from the spatial interpolation by the Kriging (Section 2.2.1). The approach used for the estimation of the evapotranspiration take into account also the effective spatial distribution of the different cultures (obtained by the map of use of the soil) and the limitation due to the soil water content, calculated by the interaction between the continuity equation and the energy conservation equation.

3.2.1 The FAO method

The evaporation is the process through which the surface water changes in the gaseous phase and is transferred in the atmosphere. If the water evaporates from a water body or directly from the soil the process is called evaporation. If the evaporation occurs through the stomata, tiny opening on the leaf surface, the process is called transpiration. Three important conditions are required to the evapotranspiration (the combined process of evaporation and transpiration) to take place:

1. there must be water surface availability;

2. there must be availability of enough energy for the liquid-gaseous phase change;
3. there must be a transport mechanism that ensure the removal of the water vapour from the considered zone. Without this mechanism the atmosphere reaches progressively a saturation condition that does not allow further evaporation.

Meteorological factors affecting the evapotranspiration

The evapotranspiration flux is determined by the energy conservation equation on the soil surface. To set up that equation it is assumed a control volume delimited at the top by the soil surface and at the bottom by a surface deep enough to assume negligible the flux of energy that pass trough it at the considered temporal scale. In this way, for an unitary area, the energy balance can be writted as:

$$C \frac{dT_s}{dt} = R_h^\downarrow (1 - \alpha) + R_a^\downarrow - R_s^\uparrow - H - \lambda E \quad (3.5)$$

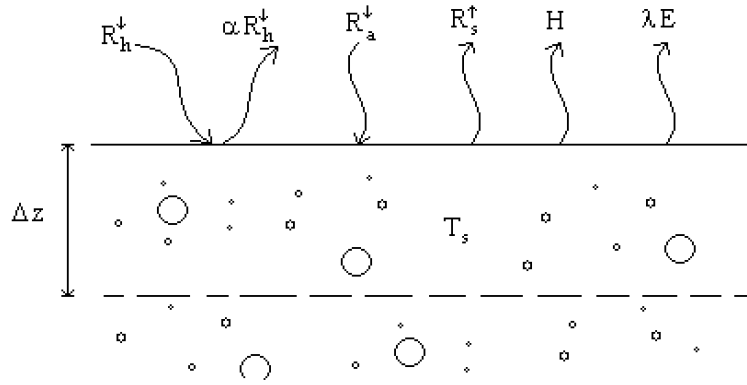


Figure 3.2: *The energy balance of the soil.*

where: C is the thermal capacity of the soil that can interact with the atmosphere;
 R_h^\downarrow is the solar radiation flux on the surface;
 α is the albedo of the system, that is the fraction of the solar radiation reflected;
 R_a^\downarrow is the radiation flux emitted from the atmosphere to the surface;
 R_s^\uparrow is the radiation flux emitted from the surface;
 H is the sensible heat;
 E is the evapotranspiration;
 λ is the latent heat of vaporization ($\lambda = 2.25 \cdot 10^6 \text{ Jkg}^{-1}$ for 10°C , but slightly dependent on the temperature).

It is possible to notice that the evapotranspiration term is present both in the mass conservation equation (hydrologic balance) and in the energy conservation mass. They are strongly coupled and it is not possible to solve one equation without solving the other, at least when the evapotranspiration component is not negligible.

The energy conservation equation, with the equations that describe the state of the atmosphere and the vapour transport, can be used to determine the evapotranspiration flux in an explicit way, obtaining the Penman-Monteith equation.

Penman-Monteith equation

The evaporation flux can be expressed in the following way:

$$E = \frac{\rho}{r} (q_s - q_a) \quad (3.6)$$

where $1/r$ take into account the conditions of stability of the atmosphere and the turbulent transport, q_s is the specific air humidity near the surface and q_a its value at an higher layer. The parameter r is the resistance of the atmosphere to the vapor transport. In the evapotranspiration evaluation it is necessary to considerate additional resistance terms, due to the vegetation and the surface tension in partially saturated soils. The surface resistance, r_s , describes the resistance of vapour flow through stomata openings, total leaf area and soil surface. The aerodynamic resistance, r_a , describes the resistance from the vegetation upward and involves friction from air flowing over vegetative surfaces.

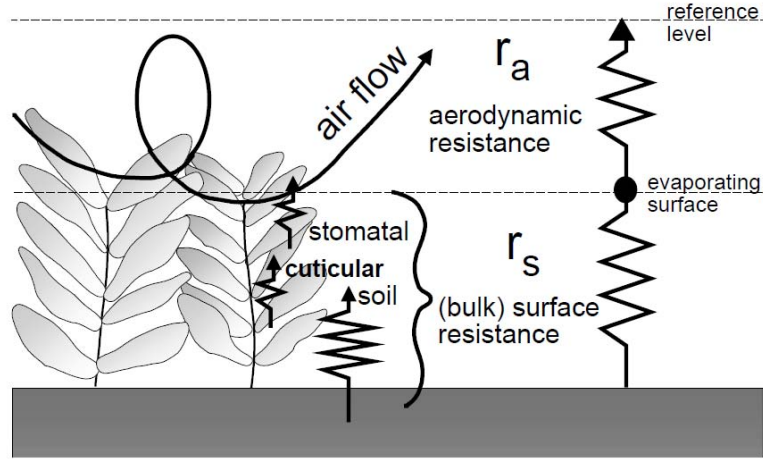


Figure 3.3: *Simplified representation of the surface and aerodynamic resistances for water vapour flow.*

The evapotranspiration can be expressed as:

$$ET = \frac{\rho}{r_a + r_s} (q^*(T_s) - q_a) \quad (3.7)$$

where it has been introduced the assumption that the water vapour in the soil pores and in the stomata is under saturation condition at the surface temperature T_s , i.e. $q_s = q^*(T_s)$.

With a similar meaning, the heat flux H can be expressed in the following way:

$$H = \frac{\rho c_p}{r_a} (T_s - T_a) \quad (3.8)$$

where the only atmospheric resistance is present.

The (3.7) and (3.8) need, for the estimation of the fluxes, measures at two different level (q_s, T_s e q_a, T_a). Since the energy balance equation for the surface is an independent

equation that contain ET it is possible to remove the two level measurements. The energy conservation equation (3.5) can be expressed as:

$$H = R_n - G - \lambda ET \quad (3.9)$$

where R_n is the net solar radiation on the surface, G is the soil heat flux (the term CdT_s/dt in the (3.5)).

To combine the two equations it is necessary to linearize the expression (3.7) for the evapotranspiration around the value of the air temperature:

$$ET = \frac{\rho}{r_a + r_s} \left(q^*(T_a) + \left. \frac{dq^*}{dT} \right|_{T_a} (T_s - T_a) - q_a \right) \quad (3.10)$$

Assuming

$$\left. \frac{dq^*}{dT} \right|_{T_a} = \frac{\epsilon}{p} \frac{de^*}{dT} = \frac{\epsilon}{p} \Delta$$

and removing $(T_s - T_a)$ between the (3.8) and the (3.10) is obtained:

$$ET = \frac{\rho}{r_a + r_s} \left(q^*(T_a) + \frac{\epsilon}{\rho c_p p} r_a H \Delta - q_a \right)$$

Defining now

$$\gamma = \frac{c_p p}{\epsilon \lambda}$$

and using eq. (3.9) to express H , the evapotranspiration term can be expressed as:

$$\lambda ET = \frac{\frac{\Delta}{\gamma} (R_n - G) + \frac{\rho \lambda}{r_a} [q^*(T_a) - q_a]}{1 + \frac{\Delta}{\gamma} + \frac{r_s}{r_a}} \quad (3.11)$$

This is the Penman-Montieth equation that says that the latent heat flux is given by the composition of the available energy $R_n - G$ and the atmospheric evaporation demand $(\rho \lambda)/r_a [q^*(T_a) - q_a]$.

The transfer of heat and water vapour from the evaporating surface into the air above the canopy is determined by the aerodynamic resistance:

$$r_a = \frac{\ln \left[\frac{z_m - d}{z_{om}} \right] \ln \left[\frac{z_h - d}{z_{oh}} \right]}{k^2 (u_z)} \quad (3.12)$$

where z_m is the height of wind measurements, z_{om} is the roughness length governing momentum transfer, z_h is the height of humidity measurements, z_{oh} is the roughness length governing transfer of heat and vapour, d is the zero plane displacement height, u_z is the wind speed at height z_m and k is the von Karman's constant.

The 'bulk' surface resistance describes the resistance of vapour flow through the transpiring crop and evaporating soil surface. An acceptable approximation to a much more complex relation of the surface resistance of dense full cover vegetation is:

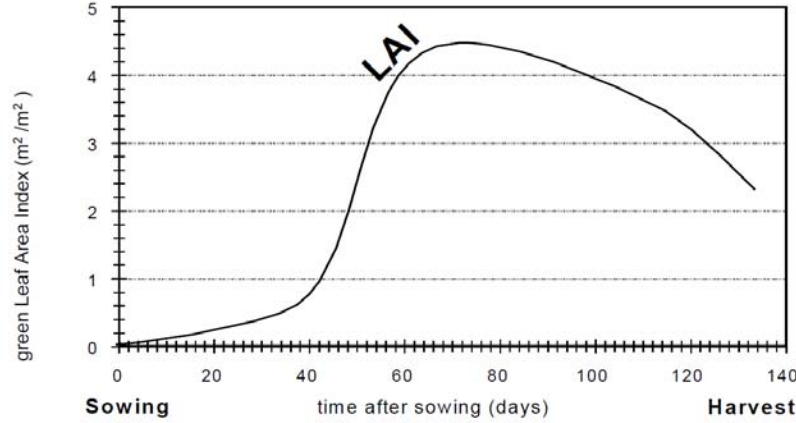


Figure 3.4: Typical presentation of the variation in the active (green) Leaf Area Index over the growing season for a maize crop.

$$r_s = \frac{r_l}{LAI_{active}} \quad (3.13)$$

where r_l is the bulk stomatal resistance of the well-illuminated leaf. The LAI_{active} is the active Leaf Area Index, it is the index of the leaf area that actively contributes to the surface heat and vapour transfer. It is generally the upper, sunlit portion of a dense canopy. For a given crop, LAI_{active} changes throughout the season and normally reaches its maximum before or at flowering (3.4). LAI_{active} further depends on the plant density and the crop variety. A general equation for LAI_{active} is:

$$LAI_a = 0,5 LAI \quad (3.14)$$

which takes into consideration the fact that generally only the upper half of dense clipped grass is actively contributing to the surface heat and vapour transfer.

Calculation procedure

Atmospheric pressure

$$P = 101,3 \left(\frac{293 - 0,0065 z}{293} \right)^{5,26}$$

Gives values in kPa depending on the elevation z respect to the m.s.l..

Latent heat of vaporization

The latent heat of vaporization, λ , expresses the energy required to change a unit mass of water from liquid to water vapour in a constant pressure and constant temperature process. As λ varies only slightly over normal temperature ranges a single value of $2,45 M J k g^{-1}$ is taken in the simplification of the FAO Penman-Monteith equation. This

is the latent heat for an air temperature of about $20^\circ C$.

Psychrometric constant

The psychrometric constant is given by:

$$\gamma = \frac{c_p P}{\epsilon \lambda}$$

where $c_p = 1,013 \cdot 10^3 J kg^{-1} \circ K^{-1}$ and $\epsilon = 0,622$.

Mean saturation vapour pressure

As saturation vapour pressure is related to air temperature, it can be calculated from the air temperature. The relationship is expressed by:

$$e^0(T) = 0,6108 \cdot e^{\frac{17,27T}{T+237,3}} \quad (3.15)$$

where $e^0(T)$ represent the saturation vapour pressure at the air temperature $T[kPa]$. Due to the non-linearity of the above equation, the mean saturation vapour pressure for a day, week, decade or month should be computed as the mean between the saturation vapour pressure at the mean daily maximum and minimum air temperatures for that period:

$$e_s = \frac{e^0(T_{max}) + e^0(T_{min})}{2}$$

Slope of saturation vapour pressure curve

$$\Delta = \frac{4098 \cdot \left[0,6108 \cdot e^{\frac{17,27T}{T+237,3}} \right]}{(T + 237,3)^2} \quad (3.16)$$

where Δ is the slope of saturation vapour pressure curve at air temperature $T [kPa^\circ C^{-1}]$ and T the air temperature $[\circ C]$.

Actual vapour pressure

If there are no available measures of e_a , the actual vapour pressure can be calculated from the maximum and minimum relative humidity as follows:

$$e_a = \frac{e^0(T_{max})RH_{min}/100 + e^0(T_{min})RH_{max}/100}{2}$$

with $e^0(T_{max})$ and $e^0(T_{min})$ respectively the saturation vapour pressure at daily maximum and minimum temperature $[kPa]$, RH_{max} and RH_{min} the maximum and minimum

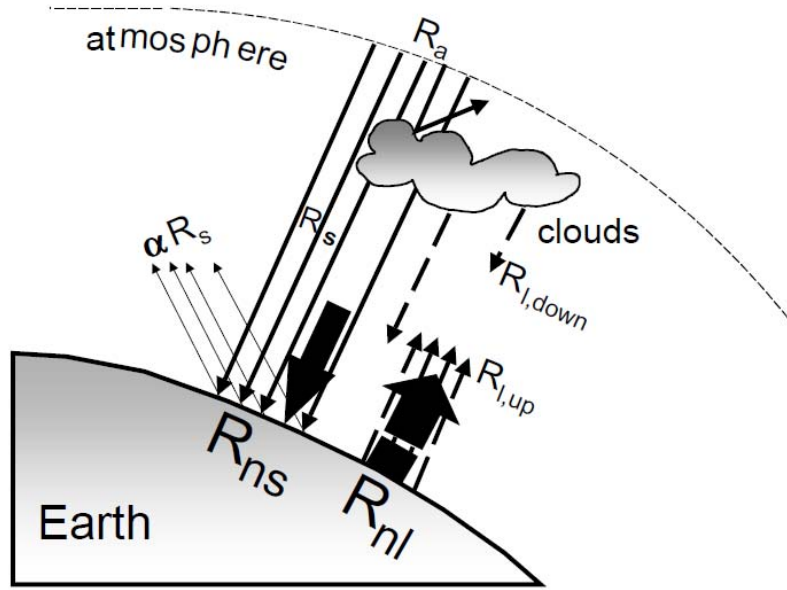


Figure 3.5: Various components of radiation

relative humidity [%].

Extraterrestrial radiation

$$R_a = \frac{24(60)}{\pi} G_{sc} d_r [\omega_s \sin(\varphi) \sin(\delta) + \cos(\varphi) \cos(\delta) \sin(\omega_s)] \quad (3.17)$$

where the extraterrestrial radiation R_a represents solar radiation received at the top of the earth's atmosphere on a horizontal surface [$MJm^{-2}day^{-1}$], G_{sc} is the solar constant = $0.0820MJm^{-2}min^{-1}$, d_r is the inverse relative distance Earth-Sun, φ the latitude [rad] and δ the solar declination and ω_s is the sunset angle.

$$d_r = 1 + 0,033 \cos\left(\frac{2\pi J}{365}\right) \quad (3.18)$$

$$\delta = 0,409 \sin\left(\frac{2\pi}{365} J - 1,39\right) \quad (3.19)$$

where J is the number of the day in the year between 1 (1 January) and 365 or 366 (31 December).

$$\omega_s = \arccos[-tg(\phi)tg(\delta)] \quad (3.20)$$

Net solar or net shortwave radiation

The net shortwave radiation resulting from the balance between incoming and reflected solar radiation is given by:

$$R_{ns} = (1 - \alpha) \cdot R_s \quad (3.21)$$

where R_s is the incoming solar radiation [$MJm^{-2}day^{-1}$] and α is the albedo.

Net longwave radiation

The rate of longwave energy emission is proportional to the absolute temperature of the surface raised to the fourth power. This relation is expressed quantitatively by the Stefan-Boltzmann law. As humidity and cloudiness play an important role, the Stefan-Boltzmann law is corrected by these two factors when estimating the net outgoing flux of longwave radiation.

$$R_{nl} = \sigma \left[\frac{T_{max,K}^4 + T_{min,K}^4}{2} \right] (0,34 - 0,14\sqrt{e_a}) \left(1,35 \frac{R_s}{R_{s0}} - 0,35 \right) \quad (3.22)$$

where $T_{max,K}$ and $T_{min,K}$ are the maximum and minimum absolute temperature during the 24-hour period, e_a is the actual vapour pressure, R_s is the measured or calculated solar radiation, R_{s0} is the clear-sky radiation and σ is the Stefan-Boltzmann constant [$= 4,903 \cdot 10^{-9} MJ K^{-4} m^{-2} day^{-1}$]. The net outgoing longwave energy R_{nl} is expressed in [$MJ m^{-2} day^{-1}$]. The clear-sky radiation is:

$$R_{s0} = (0,75 + 2 \cdot 10^{-5} z) R_a \quad (3.23)$$

where z is the station elevation a.s.l. [m].

Net radiation

The net radiation is the difference between the incoming net shortwave radiation and the outgoing net longwave radiation:

$$R_n = R_{ns} - R_{nl} \quad (3.24)$$

Soil heat flux

Complex models are available to describe soil heat flux. Because soil heat flux is small compared to R_n , particularly when the surface is covered by vegetation and calculation time steps are 24 hours or longer, it may be ignored and thus:

$$G_{day} \approx 0 \quad (3.25)$$

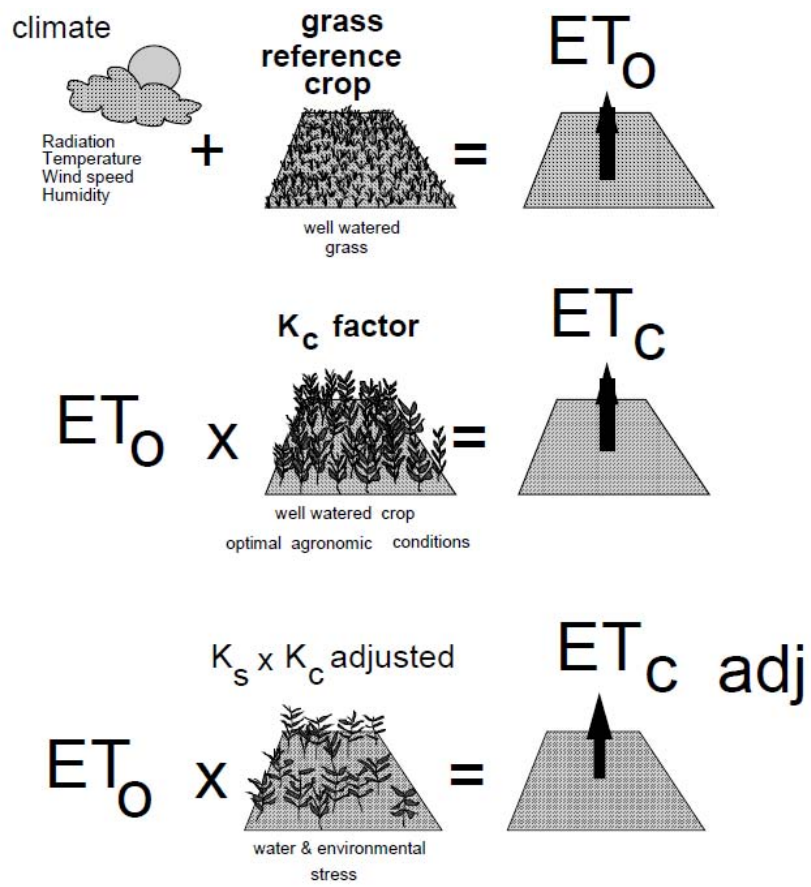


Figure 3.6: Reference (ET_0), crop evapotranspiration under standard (ET_c) and non-standard conditions ($ET_{c\ adj}$)

The FAO-Penman-Montieth model

In the FAO-Penman-Montieth model a distinction is made among reference crop evapotranspiration (ET_0), crop evapotranspiration under standard conditions (ET_c) and evapotranspiration under non-standard conditions ($ET_{c,adj}$). The reference crop evapotranspiration (ET_0), called also reference potential evapotranspiration, is the evaporation rate that a reference crop would produce during its growing season in the absence of limitations induced by water stress, under the actual climate conditions. The reference crop is an hypothetical colture with an height of $12cm$, a fixed soil-vegetation resistance of $70s/m$, and an albedo of 0.23; in practice an active grassland during the growing season, with unlimited water availability. The only factors affecting ET_0 are climatic parameters. Consequently, ET_0 is a climatic parameter and can be computed from weather data. The evaporation rate ET_0 can be expressed by the Penman-Montieth equation as follow:

$$\lambda ET_0 = \frac{\Delta(R_n - G) + \frac{\epsilon\lambda}{208R_d} \frac{\gamma u_2}{T} [e^0 - e_a]}{\gamma(1 + 0,34 u_2) + \Delta} \quad (3.26)$$

The crop evapotranspiration under standard conditions (ET_c), or potential evapotranspiration, is the evaporation rate from disease-free, well-fertilized crops, grown in large fields, under optimum soil water conditions, and achieving full production under the given climatic conditions. It can be calculated for any different coltures as follow:

$$ET_c = k_c \cdot ET_0 \quad (3.27)$$

where k_c is a crop coefficient, different for any colture. The crop evapotranspiration under non-standard conditions ($ET_{c,adj}$), or actual evapotranspiration ET , is the evaporation rate from crops grown under management and environmental conditions that differ from the standard conditions. $ET_{c,adj}$ is calculated by using a water stress coefficient k_s and/or by adjusting k_c for all kinds of other stresses and environmental constraints on crop evapotranspiration.

$$ET_{c,adj} = k_s(s(t)) \cdot ET_c \quad (3.28)$$

where $s(t)$ is the soil moisture at time t (equation 3.4).

ET_c - Dual crop coefficient

The FAO proposes different approaches for the evaluation of k_c . Differences in evaporation and transpiration between field crops and the reference grass surface can be integrated in a single crop coefficient (K_c) or separated into two coefficients: a basal crop (K_{cb}) and a soil evaporation coefficient (K_e). In this project it has been used the second approach taking into account in a different way the contributes from the evaporation from the soil and the transpiration from the plants. The sum of the two parts can not exceed a maximum vale determined by the availability of energy. The calculation of k_e need also to consider actual water availability in the soil trough a daily water balance in the root zone. The potential evapotranspiration becomes:

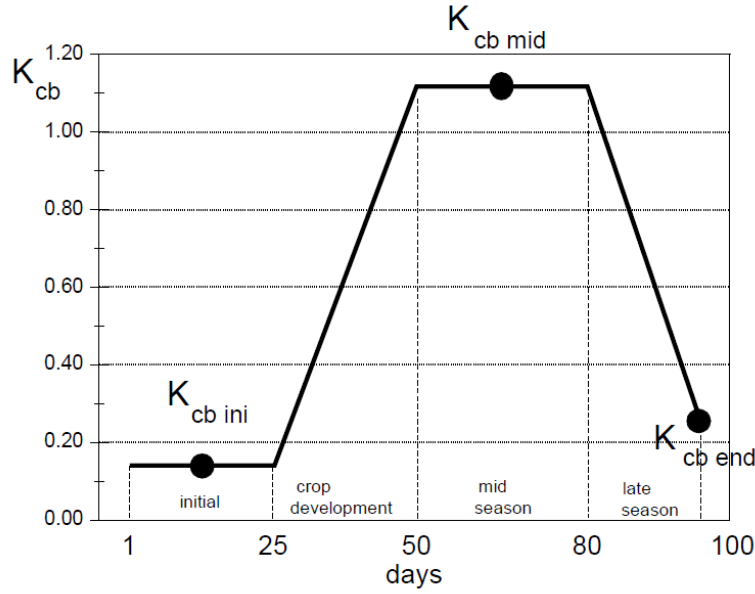


Figure 3.7: Constructed basal crop coefficient (K_{cb}) curve for a dry bean crop using growth stage lengths of 25, 25, 30 and 20 days.

$$ET_c = (k_{cb} + k_e)ET_0 \quad (3.29)$$

Transpiration component

Recommended values of k_{cb} are listed in [Allen et al., 1998] during the different periods of the year through which it is possible to build the k_{cb} curve, as showed in the Figure 3.7. From this curve, depending on the day of the year, it is possible to determine the coefficient k_{cb} .

For specific adjustment in climates where RH_{min} differs from 45% or where the wind speed is larger or smaller than $2m/s$, the $K_{cb_{mid}}$ and $K_{cb_{end}}$ values larger than 0,45 must be adjusted using the following equation:

$$k_{cb} = k_{cb(Tab)} + [0,04(u_2 - 2) - 0,004(RH_{min} - 45)]\left(\frac{h}{3}\right)^{0,3} \quad (3.30)$$

where u_2 is the mean value for daily wind speed at $2m$ height over grass [$m s^{-1}$], RH_{min} is the mean value for daily minimum relative humidity [%] and h is the mean plant height.

Evaporation component

The soil evaporation coefficient, K_e , describes the evaporation component of ET_c . Where the topsoil is wet, following rain or irrigation, K_e is maximal. Where the soil surface is dry, K_e is small and even zero when no water remains near the soil surface for evaporation.

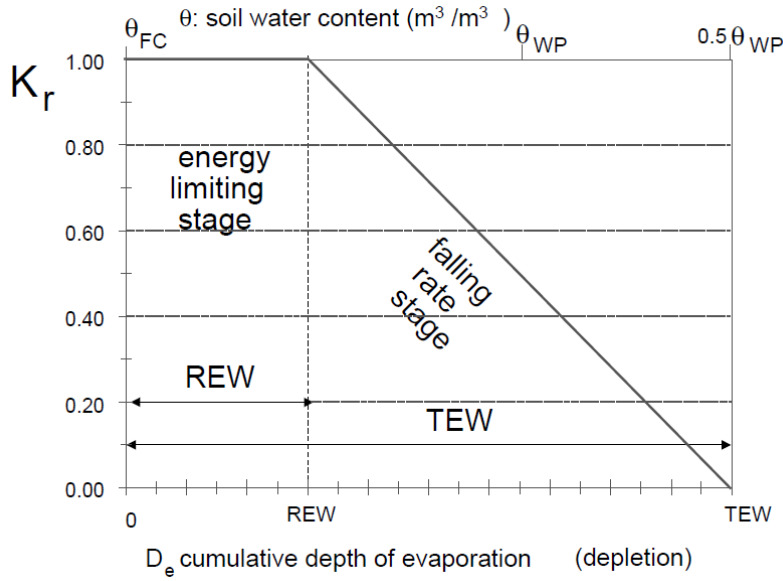


Figure 3.8: Soil evaporation reduction coefficient k_r .

$$k_e = k_r(k_{cmax} - k_{cb}) \leq (f_{ew}k_{cmax}) \quad (3.31)$$

dove k_e is the soil evaporation coefficient, k_{cb} is the basal crop coefficient, k_{cmax} is the maximum value of k_c following rain or irrigation, k_r is the dimensionless evaporation reduction coefficient dependent on the cumulative depth of water depleted (evaporated) from the topsoil, f_{ew} is the fraction of the soil that is both exposed and wetted, i.e., the fraction of soil surface from which most evaporation occurs.

$$k_{cmax} = \max(\{1, 2 + [0,04(u_2 - 2) - 0,004(RH_{min} - 45)](\frac{h}{3})^{0,3}\}, \{k_{cb} + 0,05\}) \quad (3.32)$$

where h is the mean maximum plant height during the period of calculation [m]. Soil evaporation from the exposed soil can be assumed to take place in two stages: an energy limiting stage, and a falling rate stage. When the soil surface is wet, K_r is 1. When the water content in the upper soil becomes limiting, K_r decreases and becomes zero when the total amount of water that can be evaporated from the topsoil is depleted. The amount of water that can be depleted by evaporation, or total evaporable water TEW expressed in mm , during a complete drying cycle can be estimated as:

$$TEW = 1000(\theta_{FC} - 0,5\theta_{WP})Z_e \quad (3.33)$$

where θ_{FC} is the soil water content at field capacity, θ_{WP} is the soil water content at wilting point and Z_e is the depth of the surface soil layer that is subject to drying by way of evaporation.

The fraction of soil surface from which most evaporation occurs, f_{ew} , is essentially defined as:

$$f_{ew} = 1 - f_c \quad (3.34)$$

where f_c is the average exposed soil fraction covered by vegetation.

Water stress coefficient

Forces acting on the soil water decrease its potential energy and make it less available for plant root extraction. When the soil is wet, the water has a high potential energy, is relatively free to move and is easily taken up by the plant roots. In dry soils, the water has a low potential energy and is strongly bound by capillary and absorptive forces to the soil matrix, and is less easily extracted by the crop. When the potential energy of the soil water drops below a threshold value, the crop is said to be water stressed. As the water content above field capacity cannot be held against the forces of gravity and will drain and as the water content below wilting point cannot be extracted by plant roots, the total available water TAW in the root zone is the difference between the water content at field capacity and wilting point:

$$TAW = 1000(\theta_{FC} - \theta_{WP})Z_e \quad (3.35)$$

where θ_{FC} is the water content at field capacity, θ_{WP} is the water content at wilting point and Z_r is the rooting depth. The effects of soil water stress on crop ET are described by reducing the value for the crop coefficient. This is accomplished by multiplying the crop coefficient by the water stress coefficient K_s as showed in the Figure 3.9. The threshold θ_t is defined as:

$$\theta_t = \theta_{FC} - (\theta_{FC} - 0,5\theta_{WP})\frac{RAW}{TAW} \quad (3.36)$$

where RAW is the readily available water.

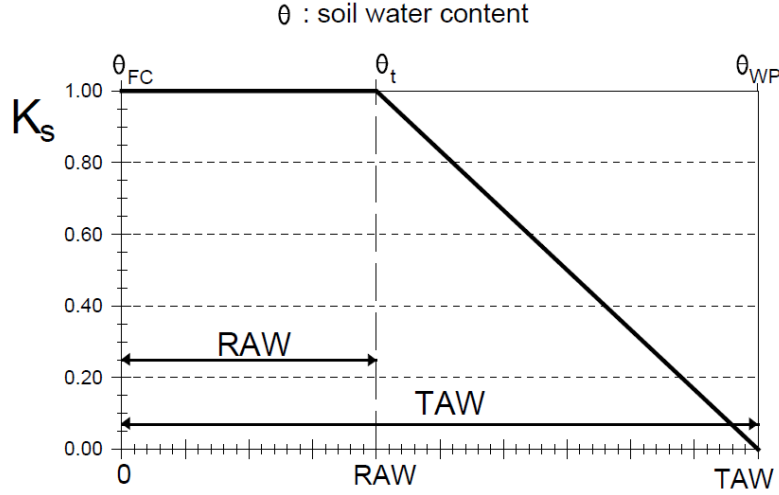


Figure 3.9: *Water stress coefficient k_s .*

3.3 Geomorphological model

The flow model used in this project is the geomorphological model: this model determines the response hydrologic of the basin starting from its morphological characteristics. The model is based on the consideration that the time that a drop of water, injected in a certain point of the catchment, need to reach the closure section, is related to the path taken and so on the morphology of the drainage network. The multiplicity of the situations that characterized the journey of the drop within the basin makes improbable a deterministic approach of the problem and requires a probabilistic approach. The probabilistic variables associated to each possible path has to be specified trough the study of the morphology of the basin. The spatial scale used has a relevant influence on this characteristics. For this reason the spatial scale has to be chosen considering the dimension of the contributing area, requiring a more precise definition of the network and watersheds for smaller catchment.

The study of the residence time distributions is a suitable tool to deal with the complex processes involved in the hydrologic response at the catchment scale. This complexity derives from the physical media in which the rainfall-runoff processes take part (heterogeneous natural formations). Based on this heterogeneity, it is accepted that the deterministic models are too rough to describe the hydrologic processes involved (e.g. [Rinaldo and Rodriguez-Iturbe, 1996]).

Consider a particle of water moving in a control volume, subjected to an hydrologic convective motion, it has a trajectory that, at the moment $t \neq 0$, is partially known, only with a certain probability.

Being $m(\mathbf{x}_0, t_0)$ the initial mass of a water particle injected at the time t_0 in the initial position $\mathbf{X}_0(t_0) = \mathbf{x}_0$ (Figure 3.10); every trajectory is defined by the Lagrangian coordinates:

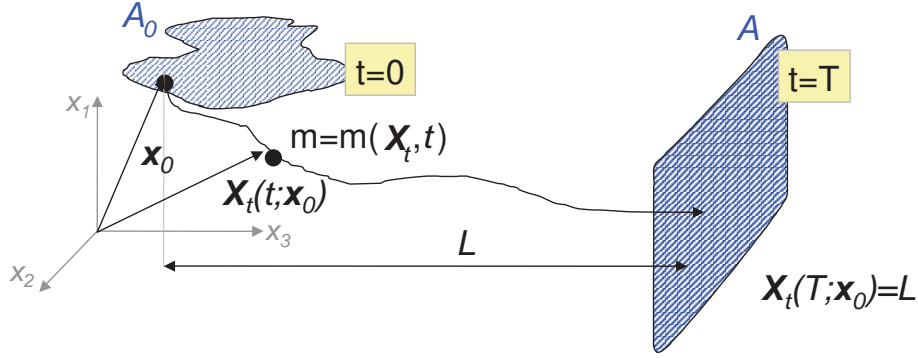


Figure 3.10: *Scheme of the trajectory of a particle with mass m .*

$$\mathbf{X}(t) = \mathbf{X}(t; \mathbf{x}_0, t_0) = \mathbf{x}_0 + \int_0^t \mathbf{u}(\mathbf{X}(\tau), \tau) d\tau \quad (3.37)$$

where $\mathbf{u}(\mathbf{X}, t)$ represents the velocity vector. It is possible to see how the notation (cf. equation 3.37) emphasizes the Lagrangian character of the analysis in which all the properties depend on the trajectory of the particle. The spatial distribution of the concentration in the control volume ν is given by (Taylor, 1921):

$$C(\mathbf{x}, t; \mathbf{x}_0, t_0) = \frac{m}{\phi} \cdot \delta(\mathbf{x} - \mathbf{X}(t; \mathbf{x}_0, t_0)) \quad (3.38)$$

where:

- i) ϕ is the porosity of the soil, the active portion of the transport volume;
- ii) $\int_{\nu} C \phi d\mathbf{x} = m$;
- iii) $\delta()$ is the Dirac's Delta function.

The distribution δ is defined by two integral properties:

$$\int_{-\infty}^{\infty} d\mathbf{x} \delta(\mathbf{x}) = 1 \quad (3.39)$$

$$\int_{-\infty}^{\infty} f(\mathbf{x}) \delta(\mathbf{x} - \mathbf{x}_0) d\mathbf{x} = f(\mathbf{x}_0) \quad (3.40)$$

The equation (3.38) suggests that the concentration is different from zero only in the point in which the particle is located (i.e. in its trajectory). It can be noticed how the system described above has to be generalized to be applied to the hydrologic response theory, that is typically characterized by vast areas of injection and large temporal variability.

The hydrological processes define the evolution in time and space of the particle's trajectory, $\mathbf{X}(t; \mathbf{x}_0, t_0)$, that is treated as a random variable, characterized by the probability distributions of the movements $g(\mathbf{x}, t)$; so $g(\mathbf{x}, t) d\mathbf{X}$ is the probability of the particle to be located, at the time t , in a neighborhood of a generic point \mathbf{x} . The mean of the n

possible achievements (i.e. the particle's paths), different due to the non-repetitive nature of natural systems, gives the following relation (e.g. Dagan, 1989; Taylor, 1921):

$$\langle C(\mathbf{x}, t) \rangle = \int_{-\infty}^{\infty} \frac{m(\mathbf{X}, t)}{\phi} \cdot \delta(\mathbf{x} - \mathbf{X}) g(\mathbf{X}, t) d\mathbf{X} \quad (3.41)$$

The particular case of a passive solute, whose mass is preserved in time and space, it is significant for the study of the transport processes related to the hydrologic response at the basin spatial scale. Being the solute passive it is possible to set $m(\mathbf{x}, t) \approx m$, and assume that the transported material does not influence the flow field. The integration of the equation (3.41) (e.g. Taylor, 1921) gives:

$$\langle C(\mathbf{x}, t) \rangle = \frac{m}{\phi} g(\mathbf{x}, t) \quad (3.42)$$

where the mean of the concentration is proportional to the probability density of the particle movements.

An important connection between the Lagrangian method described above and an Eulerian approach consists in the determination of a relation between the probability density of the particles movements, $g(\mathbf{x}, t)$, and the distribution of the residence time in control section corresponding to the closure section of the catchment. This relation is represented as an absorbing barrier trough which every particles injected in the control volume, ν , must pass in a finite time, τ , with a probability equal to one. The time of the first passage, τ , or residence time, is defined as the time interval between the injection of the particle and its passage trough the control section.

The uncertainty in the definition of the trajectory \mathbf{X} implies that the arrival time τ is a random variable characterized by a non-exceeding probability $P(\tau < t) = P(t; \mathbf{x}_0, t_0)$. The link between the Eulerian approach and the Lagrangian approach is given by the following relation:

$$P(\tau < t) = 1 - P(\tau > t) = 1 - \int_{\nu} g(\mathbf{x}, t; \mathbf{x}_0, t_0) d\mathbf{x} \quad (3.43)$$

$\int_{\nu} g(\mathbf{x}, t; \mathbf{x}_0, t_0) d\mathbf{x}$ represent the probability of the particle to be within the control volume at time t , i.e. the residence time is higher than t .

Substituting the relation (3.42) in the equation (3.43), it is obtained the fundamental relation:

$$P(\tau > t) = \frac{\phi}{m} \int_{\nu} \langle C(\mathbf{x}, t) \rangle d\mathbf{x} = \frac{\langle M(t) \rangle}{m}$$

where $\langle M(t) \rangle$ is the mean of the mass present in the control volume at time t , while m represent the total mass injected. Deriving both sides of the equation and reminding that $f(t)$ is the probability density of the residence time, it is possible to obtain, for a unitary injection:

$$f(t) = \frac{dP(\tau < t)}{dt} = -\frac{dP(\tau > t)}{dt} = -\frac{1}{m} \frac{d \langle M(t) \rangle}{dt} \quad (3.44)$$

After the injection, the mass balance in the control volume can be written as:

$$\frac{d \langle M \rangle}{dt} = -Q(t) \quad (3.45)$$

where $Q(t)$ is the mass discharge exiting the control volume ν . From this remark and from the equation (3.44), it is obtained:

$$f(t) = \frac{Q(t)}{m} \quad (3.46)$$

The probability density of the residence times coincide with the mass discharge exiting the control volume after an instantaneous injection of an unitary mass m . The physical meaning is clear: in surface hydrology, when the input is the flow producing rainfall, the probability density of the residence times is the instantaneous unit hydrograph. The determination of $f(t)$ corresponds to identify the probability distribution of the different path for the particles that fall on the catchment. To do this, some states are identified inside the basin and from their composition it is possible to obtain all the different path that the water particles can pass through. Calling Ω the order of the basin, it is defined as c_i , $1 \leq i \leq \Omega$ the state *hillslope* of the catchment that drain into the canal i . Assumes that, at the beginning ([Rodriguez-Iturbe e Valdes, 1979]), all the water particles are located in the *hillslope* state. This particles, initially placed in a region h_i , they have to comply with the following rules:

- a) the only transition permitted from a state h_i is $h_i \rightarrow c_i$, $1 \leq i \leq \Omega$;
- b) the only transition permitted from a state c_i is $c_i \rightarrow c_j$ with $j > i$, $i = 1, 2, \dots, \Omega$;
- c) the state $c_{\Omega+1}$ defines the closure section of the hydrographic catchment (i.e. the absorbing barrier).

Those rules define a set, Γ , of ways, γ , that a drop could follow in its path up to the closure section (e.g. 3.11). Every water particle spend a certain time, T_x , in every states that pass through; this time is a random variable characterized by a probability density $f_x(t)$. Assuming the statistic independence of the residence times inside two different states, it is obtained that the overall residence time within a generic path γ_i , is:

$$T_\gamma = T_{x_1} + T_{x_2} + \dots + T_{x_k} \quad (3.47)$$

with $x_1, \dots, x_k \in (h_1, \dots, h_\Omega, c_1, \dots, c_\Omega)$. From the statistic independence of the random variable T_{x_i} results that the probability density of the sum of the residence times, T_γ , is the convolution of the individual probability density:

$$f_\gamma(t) = f_{x_1} * \dots * f_{x_k} \quad (3.48)$$

where the asterisk stay for the convolution operator.

The density distribution of the residence times $f(t)$ at the closure section of a system, which initial mass is distributed on the entire domain (e.g. [Rodriguez-Iturbe e Valdes, 1979]; [Gupta et al., 1980]), is given by:

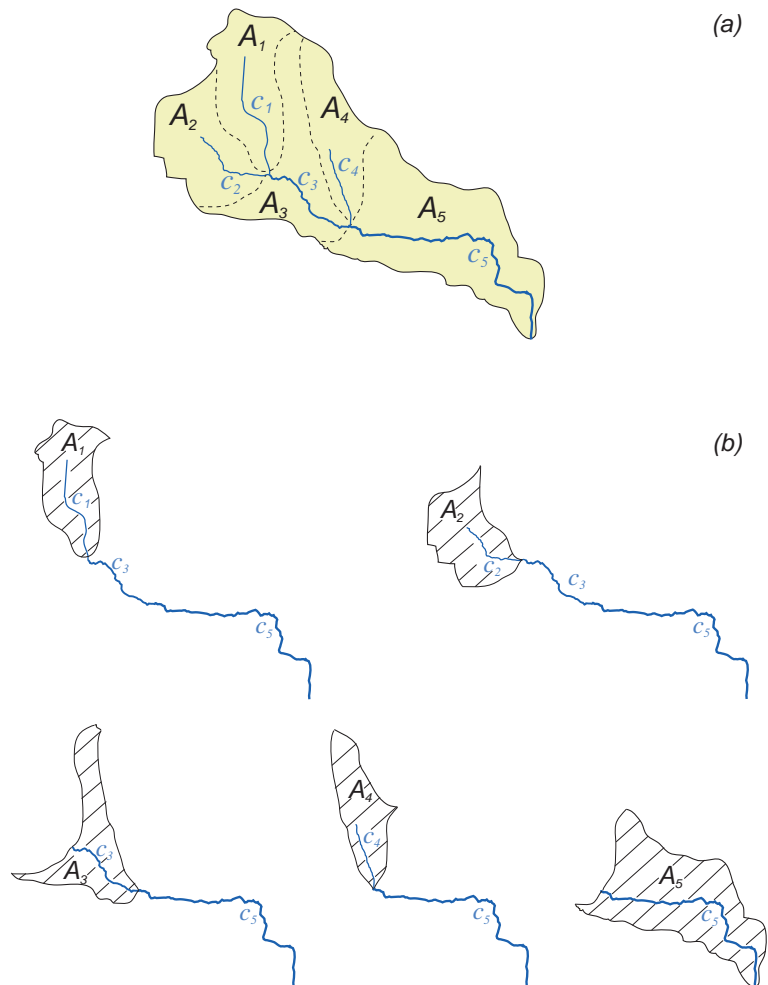


Figure 3.11: Identification of the possible path for a water particle in a generic hydrographic catchment.

$$f(t) = \sum_{\gamma \in \Gamma} p(\gamma) f_{\gamma}(t) \quad (3.49)$$

where $p(\gamma)$ is the probability of a particle to be in a generic path $\gamma = \{x_1, \dots, x_k\}$; this probability, in case of uniform rainfall, is given by the ratio between the contributing area to the path γ and the total area. The equation (3.49) shows how, during the transport process, the pulse of rainfall undergoes to a dispersion due to the heterogeneity of the possible particle's paths (i.e. geomorphologic dispersion, e.g. [Rinaldo and Rodriguez-Iturbe, 1996]). The issue of the residence time in the *hillslope* state requires some considerations related to the transport processes within the uplands. In particular, it should be recognized that the velocity of the particles increases of at least of one order of magnitude once that the water reaches *channel* states. To determine the residence times outside the network, an exponential probability density function is introduced:

$$f_{h_i}(t) = k_{h_i} e^{-k_{h_i} t} \quad (3.50)$$

where h_i is the i -th *hillslope* state outside the network, that can be *urban*, *rapid* and *slow*, depending on the flow component at hand. The parameter k_{h_i} of such distribution defines the timescale of the hydrologic response for the considered flow component. Different values of k_h are then used to define the response from urban areas, the fast flow from the root zone and the slow flow response from shallow groundwater:

$$k_{urb_i} = \frac{1}{t_{urb} \cdot (A_{urb}(i)/A_{urb\ mean})^{0,5}} \quad (3.51)$$

$$k_{rap_i} = \frac{1}{t_{rap} \cdot (A_{as}(i)/A_{as\ mean})^{0,5}} \quad (3.52)$$

$$k_{slow_i} = \frac{1}{t_{slow} \cdot (A_{tot}(i)/A_{mean})^{0,5}} \quad (3.53)$$

where t_{urb} , t_{rap} and t_{slow} are respectively the mean residence times in the urban area, in the rapid subsurface portion and in the slow subsurface portion expressed in seconds; $A_{urb}(i)$ and $A_{urb\ mean}$ are the urban area of the i -th sub-basin and the mean urban area; $A_{as}(i)$ and $A_{as\ mean}$ are the active surface area of the i -th sub-basin and the mean active surface area; $A_{tot}(i)$ and A_{mean} are the total area of the i -th sub-basin and the mean area of the sub-basins. The dependence on the area of each sub-catchment is introduced to express the fact that larger sub-catchments will be featured by a slower hydrologic response.

Mass transport with dispersion in channel reaches

The geomorphologic component originated from the heterogeneity of flow paths (eq. (3.49)) is not the only source of dispersion present in the system. There exists, indeed, an hydrodynamic dispersive component acting in the single parts of the stream related to the turbulent fluctuation of the velocity in rivers. To take into account these phenomena and quantifying them, consider the fluid movement in a generic part of the watercourse

with length L . The flow field $\mathbf{u}(\mathbf{x}, t)$ within this part at time t can be broken down in two terms: an average component $\langle \mathbf{u} \rangle = E[\mathbf{u}(\mathbf{x}, t)]$ and a fluctuating component $\mathbf{u}'(\mathbf{x}, t)$:

$$\mathbf{u}(\mathbf{x}, t) = \langle \mathbf{u} \rangle + \mathbf{u}'(\mathbf{x}, t) \quad (3.54)$$

Integrating equation (3.54) it is possible to express the position $\mathbf{x}(t)$ of the particle at time t as:

$$\mathbf{X}(t) = \langle \mathbf{X} \rangle + \mathbf{X}'(t; \mathbf{X}_0, t_0) + \mathbf{X}_B(t)$$

where

$$\langle \mathbf{X} \rangle = \langle \mathbf{u} \rangle t$$

$$\mathbf{X}'(t) = \int_0^t \mathbf{u}'(\mathbf{x}(\tau), \tau) d\tau$$

and \mathbf{x}_0 is the position of the particle at time $t = 0$; the term $\mathbf{X}_B(t)$ defines an isotropic and Brownian component of the flow, which is mathematically defined by $\langle \mathbf{X}_B \rangle = 0$, zero mean, and variance equal to $\langle \mathbf{X}_B^2 \rangle = 2D_B t$, with D_B diffusion coefficient.

To characterize the probability density of the movement $g(\mathbf{x}, t)$, it is used the Fokker-Planck model:

$$\frac{\partial g(\mathbf{x}, t)}{\partial t} + \sum_i \langle u \rangle_i \frac{\partial g(\mathbf{x}, t)}{\partial x_i} = \sum_i \sum_j D_{ij}(t) \frac{\partial^2 g(\mathbf{x}, t)}{\partial x_i \partial x_j} \quad (3.55)$$

where $D_{ij}(t)$ is the dispersion tensor. The function $g(\mathbf{x}, t)$ characterizes the probability that the trajectory of a particle to be \mathbf{x} , at time t ; the maximum probability is given by the average trajectory $\langle X \rangle_i = \langle u \rangle_i t$. The term $\sum_i \langle u \rangle_i \frac{\partial g(\mathbf{x}, t)}{\partial x_i}$ tends to move the maximum probability along the average trajectory, while the r.h. side of the equation considers the probability to have movement from the average trajectory, due to turbulent fluctuation of the velocity. It is to be noted that, mathematically, the diffusive terms usually is anisotropic and time-dependent but space-independent (e.g. [Rodriguez-Iturbe and Rinaldo, 1997]), different from the Fickian models.

The hydrodynamic equations that describe the spatial and temporal dependence of the depth $y(x, t)$ of the motion are now converted in equations that determine the shape of the probability density $g(x, t)$. Consider the De Saint-Venant equation:

$$\frac{\partial E}{\partial x} = \frac{\partial}{\partial x} \left(\alpha \frac{v^2}{2g} + \frac{P}{\gamma} + h \right) = -\frac{\beta}{g} \frac{\partial V}{\partial t} - j \quad (3.56)$$

where v is the mean velocity of the section, P is the pressure in a generic point and h the elevation of that point related to a datum plane. It is possible to notice that:

$$\frac{P}{\gamma} + h = y + z$$

where y is the depth of the motion, while z is the elevation of the bottom relative to the datum plane. Imposing $\alpha = 1$, the Coriolis coefficient, as usual for river problems (e.g. Rodriguez-Iturbe e Rinaldo, 1997), the equation (3.56) becomes:

$$\frac{1}{g}V\frac{\partial V}{\partial x} + \frac{\partial y}{\partial x} + \frac{\partial z}{\partial x} = -\frac{1}{g}\frac{\partial V}{\partial t} - j \quad (3.57)$$

that means:

$$\frac{1}{g}V\frac{\partial V}{\partial x} + \frac{\partial y}{\partial x} = -\frac{1}{g}\frac{\partial V}{\partial t} + i_f - j \quad (3.58)$$

where $i_f = -\partial z/\partial x$ is the bottom slope.

Adding the continuity equation for a linear current:

$$\frac{\partial Q}{\partial x} + \frac{\partial A}{\partial t} = 0 \quad (3.59)$$

The system of equations given by (3.58) and (3.59) allows to solve the flood wave propagation. Assuming a sequence of permanent flows ($\partial V/\partial t = 0$) and, neglecting the local acceleration ($\partial V/\partial x = 0$), the parabolic wave model is obtained:

$$j = i_f - \frac{\partial y}{\partial x} \quad (3.60)$$

$$\frac{\partial Q}{\partial x} + \frac{\partial A}{\partial t} = 0 \quad (3.61)$$

This is a good approximation when the waves are not too steep and so it is suitable for the study of the flood wave propagation in streams.

Suppose now, for sake of simplicity, that the channel is rectangular, that means that $A = By$. The equation governing the flow are:

$$j = i_f - \frac{\partial y}{\partial x} \quad (3.62)$$

$$\frac{\partial Q}{\partial x} + B\frac{\partial y}{\partial t} = 0 \quad (3.63)$$

Assuming valid the equations of the steady flow you get:

$$Q = CA^\gamma j^{1/2} = CA^\gamma \left(i_f - \frac{\partial y}{\partial x} \right) \quad (3.64)$$

where $\gamma = 3/2$. The spatial derivative of the discharge is:

$$\frac{\partial Q}{\partial x} = \frac{\partial Q}{\partial A} \frac{\partial A}{\partial x} + \frac{\partial Q}{\partial j} \frac{\partial j}{\partial x} = \frac{\partial Q}{\partial A} B \frac{\partial y}{\partial x} - \frac{\partial Q}{\partial j} \frac{\partial^2 y}{\partial x^2} \quad (3.65)$$

where to express the spatial derivative of j it has been used the equation (3.62). Using eq. (3.65), eq. (3.63) can be redraft:

$$\frac{\partial y}{\partial t} + \frac{\partial Q}{\partial A} \frac{\partial y}{\partial x} = \frac{1}{B} \frac{\partial Q}{\partial j} \frac{\partial^2 y}{\partial x^2} \quad (3.66)$$

Using now eq. (3.64) to express the derivative of Q respect to A and j :

$$\begin{aligned}\frac{\partial Q}{\partial A} &= C\gamma A^{\gamma-1}j^{1/2} = \frac{3}{2}V = a \\ \frac{1}{B} \frac{\partial Q}{\partial j} &= \frac{A}{B\gamma j} C\gamma A^{\gamma-1} \frac{1}{2}j^{1/2} = \frac{ay}{3\sqrt{i_f - \frac{\partial y}{\partial x}}} \cong \frac{ay_0}{3i_f} = D_H\end{aligned}\quad (3.67)$$

The parameter s is defined as celerity of the flood wave propagation, while D_H represent the hydrodynamic dispersion coefficient. Equation (3.66) becomes:

$$\frac{\partial y}{\partial t} + a \frac{\partial y}{\partial x} = D_H \frac{\partial^2 y}{\partial x^2} \quad (3.68)$$

that is a dispersion-diffusion equation (hydrodynamic dispersion D_H) with a convective component (celerity of propagation a); this equation is such as the (3.55). In fact it can be demonstrated that, with the described hypotheses, the proportionality $y(x, t) \propto g(x, t)$ is valid ¹.

Introducing the new independent variable $s = x - at$, eq. (3.68) can be simplified in:

$$\frac{\partial y}{\partial t} = D_H \frac{\partial^2 y}{\partial s^2} \quad (3.69)$$

Multiplying eq. (3.69) for s^2 and integrating between $-\infty$ and $+\infty$, it is obtained:

$$\int_{-\infty}^{+\infty} s^2 \frac{\partial y}{\partial t} ds = \int_{-\infty}^{+\infty} D_H s^2 \frac{\partial^2 y}{\partial s^2} ds = D_H \left[s^2 \frac{\partial y}{\partial s} - 2sy \right] + 2D_H \int_{-\infty}^{+\infty} y ds \quad (3.70)$$

If:

$$\lim_{s \rightarrow \pm\infty} s^2 \frac{\partial y}{\partial s} = 0$$

and:

$$\lim_{s \rightarrow \pm\infty} sy = 0$$

eq. (3.70) can be rewritten:

$$\frac{\partial}{\partial t} \int_{-\infty}^{+\infty} s^2 y ds = 2D_H \int_{-\infty}^{+\infty} y ds \quad (3.71)$$

¹ x represents the intrinsic coordinate, parallel in every section to the mean velocity $\langle \mathbf{u} \rangle$, and $g(x, t)$ is the probability of a particle, released in x_0 at $t = 0$, to be in $(x, x + dx)$ at time t . The probability that at time t the particle is still located within the considered reach is $P[T \geq t] = \int_0^L g(x, t) dx$, that means $P[T \leq t] = 1 - \int_0^L g(x, t) dx$. The probability density of the residence time in the considered reach is $f(t) = -\frac{d}{dt} \int_0^L g(x, t) dx$, and recalling that $f(t) = u(t) = -\frac{dV}{dt}$, is obtained $\frac{dV}{dt} = \frac{d}{dt} \int_0^L g(x, t) dx$, that is $V = \int_0^L g(x, t) dx$. If the channel is prismatic you get $V = \int_0^L y(x, t) dx$, da cui $y(x, t) \propto g(x, t)$

It should be noted that, assuming the barycenter $y(s)$ as datum for the spatial coordinates, the variance $y(s)$ is defined as:

$$\sigma^2(t) = \frac{\int_{-\infty}^{+\infty} s^2 y ds}{\int_{-\infty}^{+\infty} y ds} \quad (3.72)$$

The variance constitutes a measure of how 'dispersed' is the mass respect to the barycenter of the distribution. Eq. (3.71) gives:

$$\frac{d\sigma^2}{dt} = 2D_H \quad (3.73)$$

in which it has been taken into account the fact that

$$\frac{\partial}{\partial t} \int_{-\infty}^{+\infty} y ds = \frac{\partial M}{\partial t} = 0$$

since the total mass M must be preserved.

Eq. (3.73) gives:

$$\sigma^2(t) \propto 2D_H t \quad (3.74)$$

This relation indicates that the variance $y(s)$ increases linearly in time and proportionally to the dispersion coefficient. This is one of the general property of the dispersion equation (3.68).

Gheomorphological instantaneous unit hydrograph

From the relation $f(t) = -d/dt \int_{\nu} g(\mathbf{x}, t) d\mathbf{x}$ and solving eq. (3.55) with the appropriate boundary conditions, the probability density of the residence times in a channel reach can be obtained. The suitable boundary conditions are:

i) reflecting barrier for $x = 0$:

$$\left| \langle u \rangle g(x, t) - D_L \frac{\partial g}{\partial x} \right|_{x=0} = \delta(t) \quad (3.75)$$

ii) absorbing barrier for $x = L$, and so $g(L, t) = 0$.

To obtain a close solution it is useful to introduce the Laplace transform:

$$\hat{f}(s) = \int_0^{\infty} f(t) e^{-st} dt \quad (3.76)$$

Eq. (3.76) can be anti transformed to give:

$$f(t) = \int_0^{\infty} \hat{f}(s) e^{st} ds$$

The Laplace transform has the following property:

$$(f \hat{*} g)(s) = \hat{f}(s) \hat{g}(s)$$

that allows one to derive the following solution:

$$f_c(t) = \frac{L(\gamma)}{(4\pi D_H t^3)^{1/2}} \exp\left(-\frac{(L - at)^2}{4 D_H t}\right) \quad (3.77)$$

where $L(\gamma)$ is the length of the path γ .

Recalling the expression used for the probability density function of the mean residence times for the *hillslope* state h (eq. (3.50)), and assuming constant D_h values and wave celerities a along the channel network, the geomorphological instantaneous unit hydrograph can be written as:

$$f_h^i(t) = k_{h_i} \exp(-k_{h_i} t) * \frac{L(\gamma_i)}{(4\pi D_H)^{1/2}} t^{-3/2} \exp\left(-\frac{(L(\gamma_i) - at)^2}{4 D_H t}\right) \quad (3.78)$$

where k_{h_i} can be referred to *urban*, *fast* and *slow* flow components. In this project the path probabilities are included in the formulation of the effective rainfall described in Section 3.1. Hence, the outflow produced by the different components of discharge at the outlet of the entire catchment (originated from the various sub-catchments) is written as:

$$Q_h(t) = \sum_{i=1 \rightarrow N_{sub}} \int_0^t j_{eff,h}^i(\tau) f_h^i(t - \tau) d\tau, \quad (3.79)$$

where $j_{eff,h}^i$ is the effective rainfall pertaining to the considered flow component in the i -th sub-catchment.

3.4 Runoff generation

Starting from the effective rainfall rates calculated in Section 3.1, the rapid contribution αL , the slow contribution $\beta(1 - \alpha)L$ and the urban contribution $P \cdot A_{urb}$, the three runoff components at the closure section of the catchment can be calculated through the geomorphological instantaneous unit hydrographs as reported in eq. (3.79):

$$Q_{rap}(t) = \sum_{i=1 \rightarrow N_{sub}} \int_0^t \alpha L(\tau) f_{rap}^i(t - \tau) d\tau, \quad (3.80)$$

$$Q_{slow}(t) = \sum_{i=1 \rightarrow N_{sub}} \int_0^t \beta(1 - \alpha) L(\tau) f_{slow}^i(t - \tau) d\tau, \quad (3.81)$$

$$Q_{urb}(t) = \sum_{i=1 \rightarrow N_{sub}} \int_0^t P(\tau) A_{urb} f_{urb}^i(t - \tau) d\tau, \quad (3.82)$$

where i refers to the i -th sub-basin.

Only a portion of Q_{urb} , given by the coefficient γ , contributes to the runoff formation, while the $(1 - \gamma)$ portion exits from the system. The assumption of a leak of water from

the urban area can be justified by the fact that the main water treatment plants of the area are located outside of the catchment (Figure 2.6). Hence, most of the water collected by the sewage system does not contribute to the formation of the discharge of the Muson river. Moreover evaporation processes occur also on the urban area and they are not explicitly considered in the mass balance in urban areas and in the overall ET term. The total discharge is given by the following equation:

$$Q_{fin}(t) = \gamma Q_{urb}(t) + Q_{rap}(t) + Q_{slow}(t). \quad (3.83)$$

3.5 Dispersion from channel bed

The TRUST project (Tool for Regional scale assessment of groUndwater Storage improvement in adaptation of climate change) was co-financed by the European Community Environmental Program and the Italian Ministry of Environment and developed a wide range of tool to assess the implication of climate change on the hydrology and hydrogeology of the Veneto and Friuli high plain's unsaturated aquifer. The Muson catchment is located within the area of study of the project.

According to this studies many data, related to the unsaturated aquifer, have been taken and many aspects of the processes that occur into the soil have been considered. One of this processes is the dispersion from the channel bed.

For the main river of the area of study (i.e. Piave, Brenta, Astico, Tagliamento and Isonzo) a big campaign of measures was performed to better understand the curves correlating discharge and dispersion from the channel bed. The data used are: precipitation, discharge and water table level. The results of this studies showed that the dispersion from the bottom of the river are relevant, due to the presence of a thick layer composed by gravel deposits in the area, and the curves correlating discharge and dispersion have an exponential shape.

According to the results of the study [Cimolino et al., 2011], from the total discharge Q_{fin} (computed in the eq. (3.83)) it should be subtracted the quantity Q_{disp} that leaks from the bottom of the river and goes to recharge the groundwater during periods when the water table is below the river stage. This process would be distributed along the entire river stream but here, for sake of simplicity, it is considered to be concentrated at the closure section. According to the shape of the curves that define Q_{disp} calculated for the other rivers of the region ([Cimolino et al., 2011]), it has been chosen an exponential relation as follow:

$$Q_{disp}(t) = Q_d^* \cdot (1 - e^{-k \cdot Q_{fin}(t)}) \quad (3.84)$$

where Q_d^* is the maximum discharge that can leaks and k is a parameter to be calibrated. The behavior of the curve is represented in the Figure 3.12. Hence, the total discharge exiting the closure section is:

$$Q_{cs}(t) = Q_{fin}(t) - Q_{disp}(Q_{fin}(t)) \quad (3.85)$$

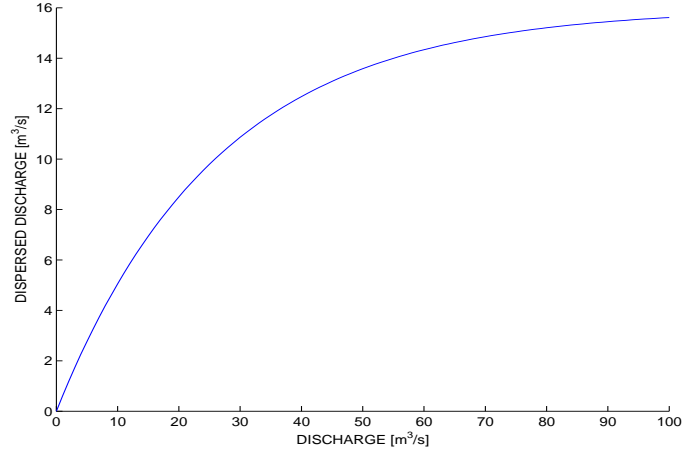


Figure 3.12: *Curve correlating discharge and dispersion from the channel bed.*

3.6 Model parameters

The parameters of the model developed are considered to be constant for each sub-basin, that is also assumed to be homogeneous. Hence, the model uses a spatial distributed description of the characteristics of the area specifying, at sub-basin scale, the following parameters:

1. parameters for the runoff production module:
 - saturated hydraulic conductivity of the soil K_0 [mm/s];
 - coefficient α which determines the partitioning of the water that infiltrates in the soil between the rapid and slow component of the runoff;
 - root zone depth Z_r [mm];
 - Clapp-Hornberger coefficient c , which allows to calculate the infiltration rate depending on the soil water content;
 - coefficient β which determines the part of the deep leaching that contributes to the formation of the slow runoff and the part that recharges the groundwater;
 - coefficient γ which determines the portion of the urban runoff that contributes to the discharge and the portion that exits the system;
 - porosity n ;
 - maximum discharge dispersed from the bottom of the river Q_d^* ;
 - coefficient that defines the dependence of the discharge leaked from channels, k ;
2. dynamical parameters:
 - flood-wave celerity a [m/s];
 - dispersion coefficient D_h [m^2/s];

- mean residence time of the water of the urban runoff component t_{urb} ;
- mean residence time of the water of the rapid runoff component t_{rap} ;
- mean residence time of the water of the slow runoff component t_{slow} .

3. parameters for the evaluation of evapotranspiration flux:

- water content at field capacity θ_{FC} ;
- water content at wilting point θ_{WP} ;

Some considerations have to be done for the saturated hydraulic conductivity K_0 , being it related to the geo-pedological characteristics of the soil. For reduce the number of parameters to be calibrated, it is maintained constant the ratio between the value of K of the different sub-basins. This ratio is calculated on the basis of the geo-pedology (Figure 2.1), and then, for each sub-basin, the value of K it is multiplied by a coefficient K_c , which is constant for the all catchment and needs to be calibrated, obtaining K_0 .

Chapter 4

Results

Each run of the hydrological model developed is made up by two consecutive phases:

1. calculation of the spatio-temporal distribution of the meteorological forcing starting from the point data available;
2. run of the rainfall-runoff model that evaluates the evapotranspiration flux, separates the different runoff components and computes the convolution of the obtained components with the appropriate instantaneous unit hydrographs.

In the first phase no parameters are needed since the only input are the meteorological data. For the second phase the parameters described in the Section 3.6 are needed to obtain a satisfying result for the model. In this chapter are reported the calibration and validation of the hydrological model described in the Chapter 3.

4.1 Calibration

A well-known problem of hydrology is related to the fact that many possible sets of parameters can produce similar performances. For this reason, for the calibration of the Muson hydrologic model, it has been used a Markov chain Monte Carlo (MCMC) method. This method performs an high value of runs of the model with different sets of randomly chosen parameters with the goal of obtaining a series of simulations with elevated performance among which the best ones are extracted. The evaluation of the performance of the simulations has been calculated with the Nash-Sutcliffe efficiency.

Since the model under exam is supposed to run in continuous, the objective of the calibration is the best simulation of the discharge obtained at the closure section compared to the discharge measured at the hydrometer of Castelfranco Veneto for a long period of time, including the evaluation and duration of the peaks and the behavior of the discharge during the recession curve and dry periods.

For the calibration it has been chosen the period of time between September 1, 2010 and December 31, 2010. Such period is long enough and includes many rainfall events. Longer calibration periods have been tested but the discarded because the model was constrained too much during droughts periods. The set of parameters obtained during the calibration is reported below:

- coefficient for the evaluation of the saturated hydraulic conductivity $K_c = 616, 12$;
- coefficient for the partitioning of the water that infiltrates in the soil between the rapid and slow component of the runoff $\alpha = 0, 24$;
- root zone depth $Z_r = 563, 62 \text{ mm}$;
- Clapp-Hornberger coefficient $c = 24, 60$;
- coefficient for the partitioning of the deep leaching term in the slow runoff component and a part that recharges the groundwater $\beta = 0, 68$;
- coefficient for the partitioning of the urban runoff component in a part that generates discharge and a part that exits the system $\gamma = 0, 28$;
- maximum discharge leaked from the bottom of the river $Q_d^* = 15, 97 \text{ m}^3/\text{s}$;
- coefficient that defines the dependence of the discharge leaked from channels $k = 0, 04$;
- mean residence time in urban areas $t_{urb} = 1, 23 \text{ h}$;
- mean residence time for the rapid subsurface response $t_{rap} = 3, 42 \text{ h}$;
- mean residence time for the slow subsurface response $t_{slow} = 521, 11 \text{ h}$.

Other parameters were considered to be fixed:

- porosity $n = 0, 3$;
- flood-wave celerity $a = 3, 5 \text{ m/s}$;
- dispersion coefficient $D_h = 1000 \text{ m}^2/\text{s}$;
- water content at field capacity $\theta_{FC} = 0, 4$;
- water content at wilting point $\theta_{WP} = 0, 1$.

The initial soil water content for the event was considered equal to 0,2 and not calibrated but the effect of this assumption disappears in few weeks and the computational effort did not justify the inclusion of an additional parameter to be calibrated.

The model performances during the calibration period are shown in Figure 4.1 and Figure 4.2. The first graph (Figure 4.1) shows the comparison between the measured discharge at Castelfranco Veneto with the total modeled discharge, while in the second graph (Figure 4.2) the modeled discharge is decomposed in the three components generated by the model. It is appreciable the ability of the model to simulate the discharge both in peaks, duration and maximum value, and in the recession curve. Some problems can be noticed in the first month of simulation where the model is not able to evaluate properly the measured discharge but this can be due to a misestimate of the initial soil water content $s(t = 0)$. Starting from October 1, the model performances increase and, in the last part of the

year, when the rainfall events are more frequent, the prediction of the discharge is really good also considering that these events are different in terms of peak values, duration and volume of water. This part of the year is the most important since it includes the major floods and the capacity of the model to properly reproduce the observed discharge is the very goal of the study itself. Concerning the separation of the components of discharge (Figure 4.2) is appreciable the fact that the *slow* contribution sustains the base flow in the dry periods while the *rapid* and *urban* contributions contribute to the peaks of discharge in response of the rainfall events.

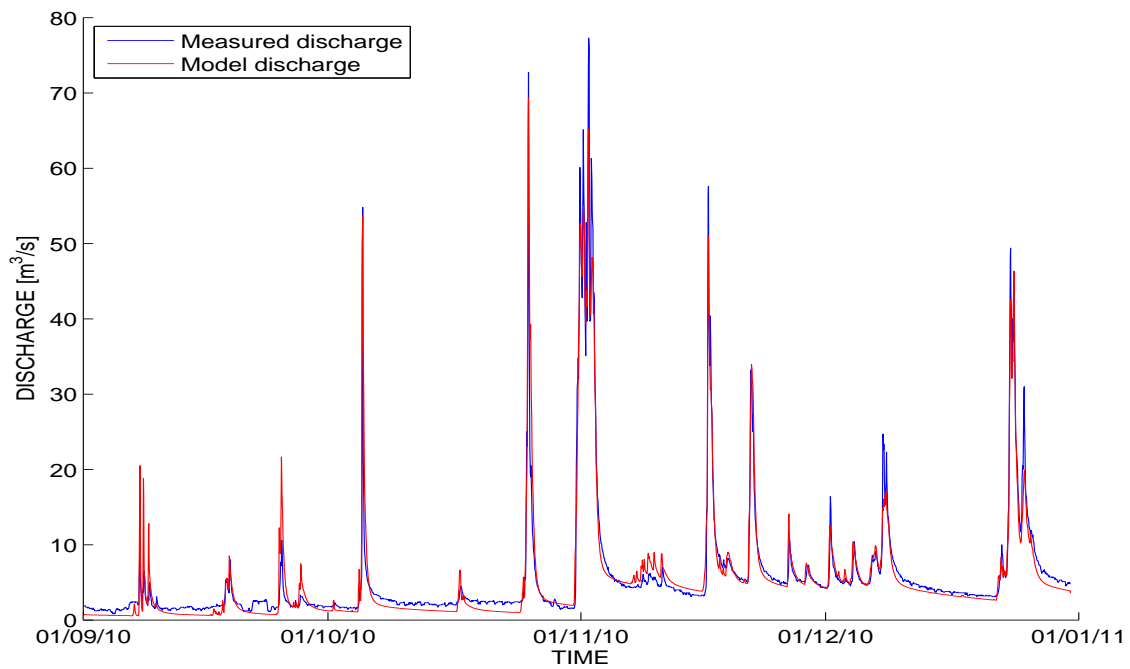


Figure 4.1: Calibration results for the period between 01-09-2010 and 31-12-2010

Figure 4.3 shows the calibration results focusing on the series of events occurred between the October 24 and November 5. The performance of the hydrologic model is remarkable in reproducing the sequence of peaks (despite an underestimation of the peak values of the second series of high discharges), the recession curves and also the recession period between the two events. In terms of runoff volumes, there is a small overestimation of volume discharged for the event observed around October 26.

4.2 Validation

The developed hydrologic model is validated applying the set of calibrated parameters obtained in Section 4.1 to the period of years from 2004 to 2013. The modeled discharge is compared to the discharge measured at Castelfranco Veneto and the results are discussed year by year at hourly, daily and weekly time-scales. The main events of the period of

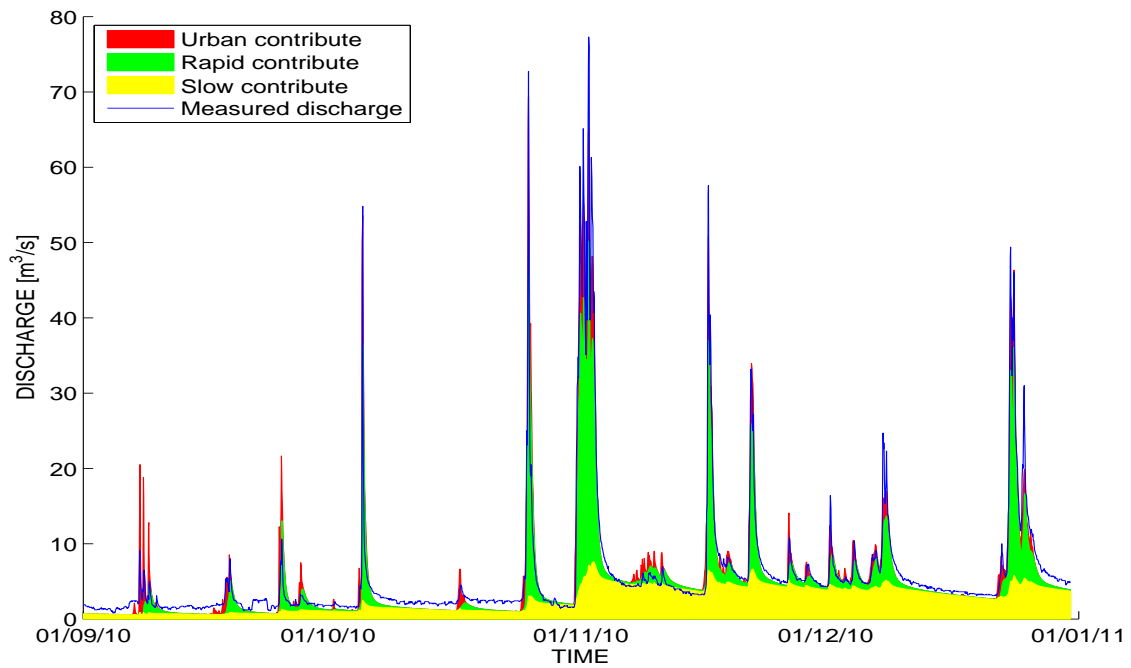


Figure 4.2: Calibration results for the period between 01-09-2010 and 31-12-2010 decomposed in the three different runoff components

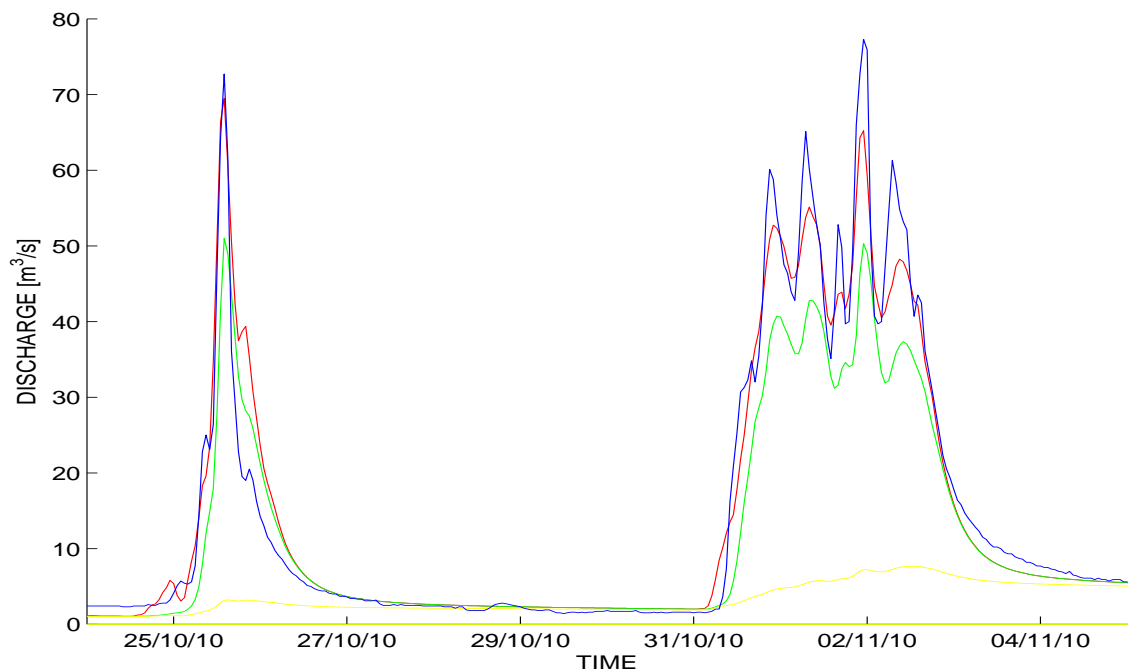


Figure 4.3: Calibration results for the events between 24/10/2010 and 05/11/2010 decomposed in the three different runoff components

study are then evaluated to better understand the ability of the model to simulate high discharge values.

For the year 2004 an initial soil water content $s = 0,2$ has been taken, while, for the other years, the initial conditions of the soil have been extracted from the last data of the previous year.

Year 2004

Figure 4.4 and Figure 4.5 report the comparison of the measured and modeled discharges at hourly time-scale. These graphs show a good correspondence between observed and modeled discharges either for the timing of the peaks and for the values of maximum discharge for each peak. Some events are characterized by an underestimation of the maximum discharge, mainly during the summer period. The main problem seems to be an underestimation of the low discharges but the error is comprised between 1 and $2\text{ m}^3/\text{s}$. This underestimation, small in terms of discharge, is emphasized in Figure 4.6 and Figure 4.7 where the volumes per day and per week are plotted. In terms of weekly discharge, indeed, the small error of less than $2\text{ m}^3/\text{s}$ produced an underestimation of 1 million of m^3/week . During the wet periods instead the measured and modeled volumes are very similar.

Figure 4.8 represents a zoom for the event occurred between October 28 and November 3, 2004, that is the most relevant event of the year, characterized by a discharge peak value of $60,5\text{ m}^3/\text{s}$. The model is able to simulate the peak, both in term of duration and maximum discharge (with a small error of $3\text{ m}^3/\text{s}$) but the modeled recession curve is a bit gentler than the observations.

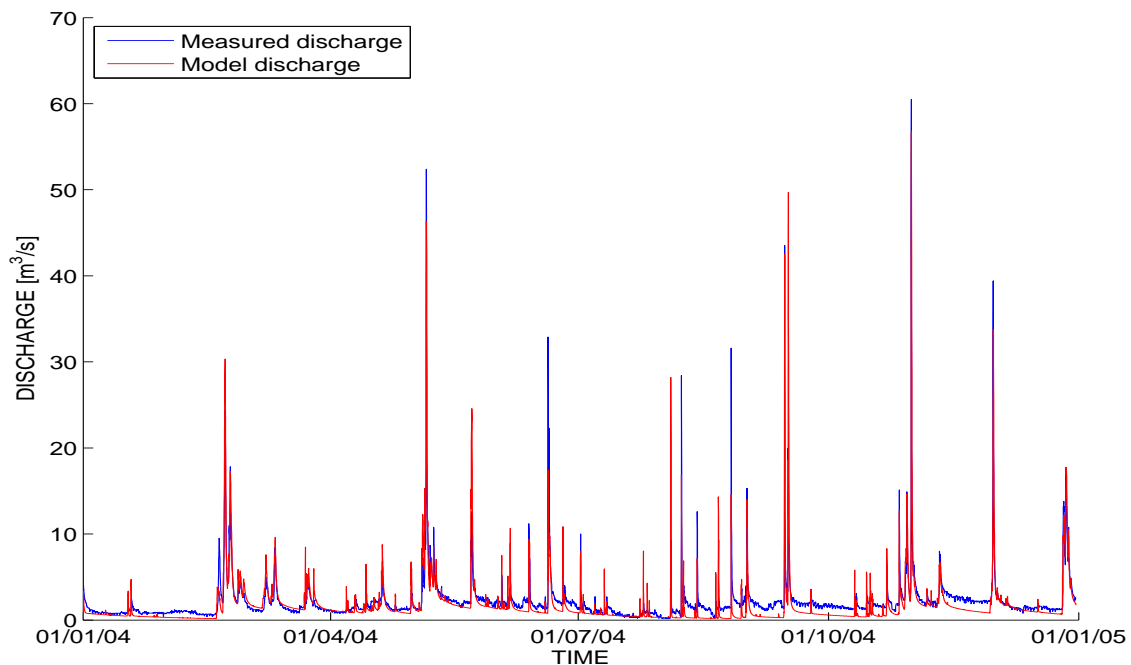


Figure 4.4: Comparison between measured and modeled discharge for the year 2004

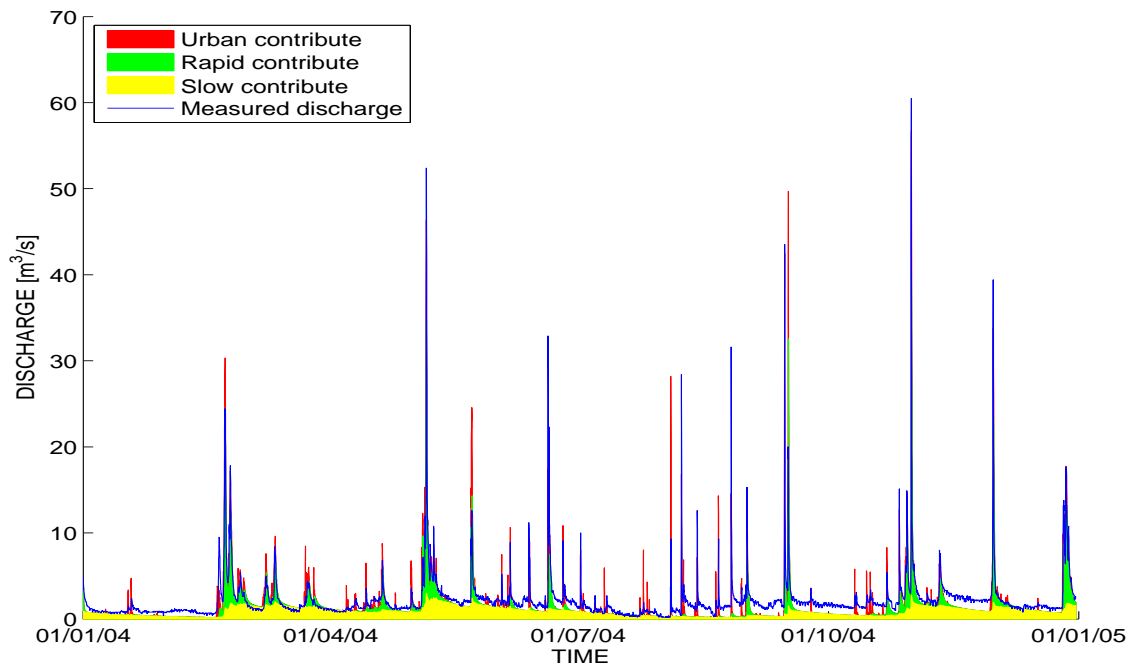


Figure 4.5: Comparison between measured and modeled discharge for the year 2004 decomposed in the three different runoff components

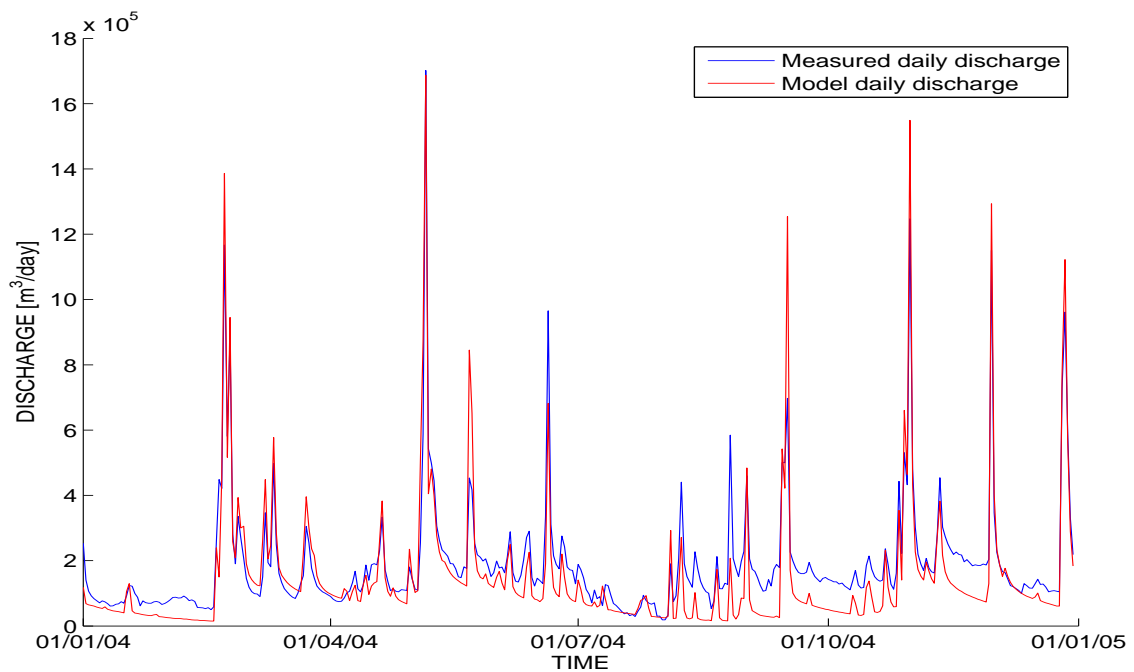


Figure 4.6: Comparison between daily measured discharge and daily modeled discharge for the year 2004

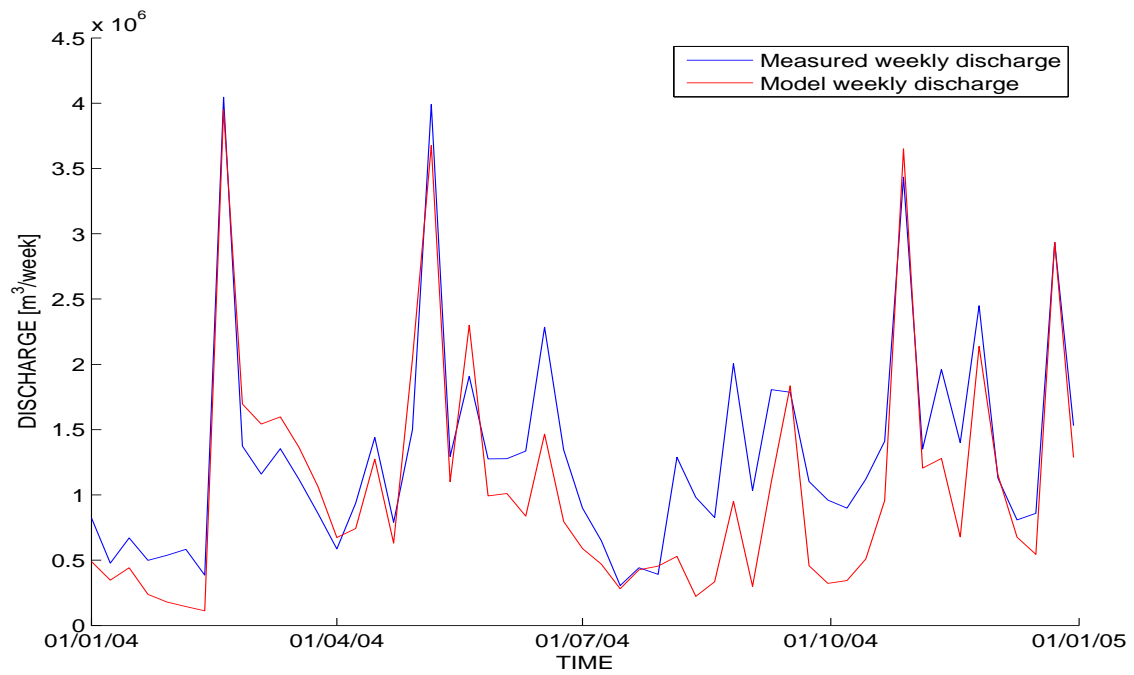


Figure 4.7: Comparison between weekly measured discharge and weekly modeled discharge for the year 2004

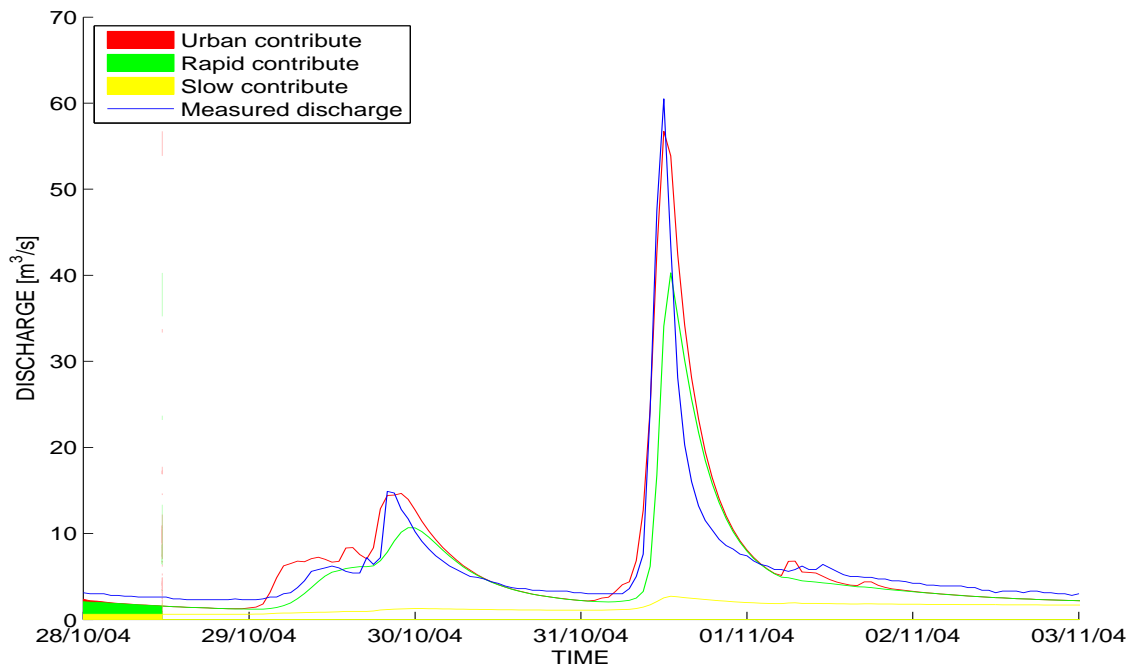


Figure 4.8: Comparison between measured and modeled discharge for the event between 28/10/2004 and 03/11/2004

Year 2005

The results for the year 2005 at the hourly time-scale, are reported in Figure 4.9 and Figure 4.10. In this case the model performances are poor compared to the ones obtained for the year 2004. The year 2005 was characterized by low precipitation and low discharge (mean discharge $Q_{mean} = 1,5 m^3/s$, instead of $2,2 m^3/s$ which is the long-term mean for the entire period of study) and this fact seems to influence the response of the catchment. The precipitations create high discharges with an overestimation of the peaks, maybe due to the poor ability of the model to simulate the drainage from dry soils. Nevertheless the lowest discharges are simulated in a good way. Figure 4.11 and Figure 4.12 evidence an underestimation of the water volumes released in the first period of the year, and a large overestimation during the rainfall events (differently from the year 2004 where the opposite trend is observed).

Figure 4.13 represents the event occurred between the October 1 and October 7, 2005, that is the one characterized by the highest measured discharge (but not the event with the highest modeled discharge). There is indeed an event at the beginning of September, caused by intense rainfall in the mountain area of the catchment, that does not produce any relevant discharge at Castelfranco Veneto. The tendency of the model to overestimate discharges is also shown by Figure 4.13. For a measured discharge of $62,2 m^3/s$ on October 4, a simulated discharge of around $100 m^3/s$ is obtained. The shape of the peak both in the growth phase and in the recession limb of the hydrograph is correctly reproduced by the model.

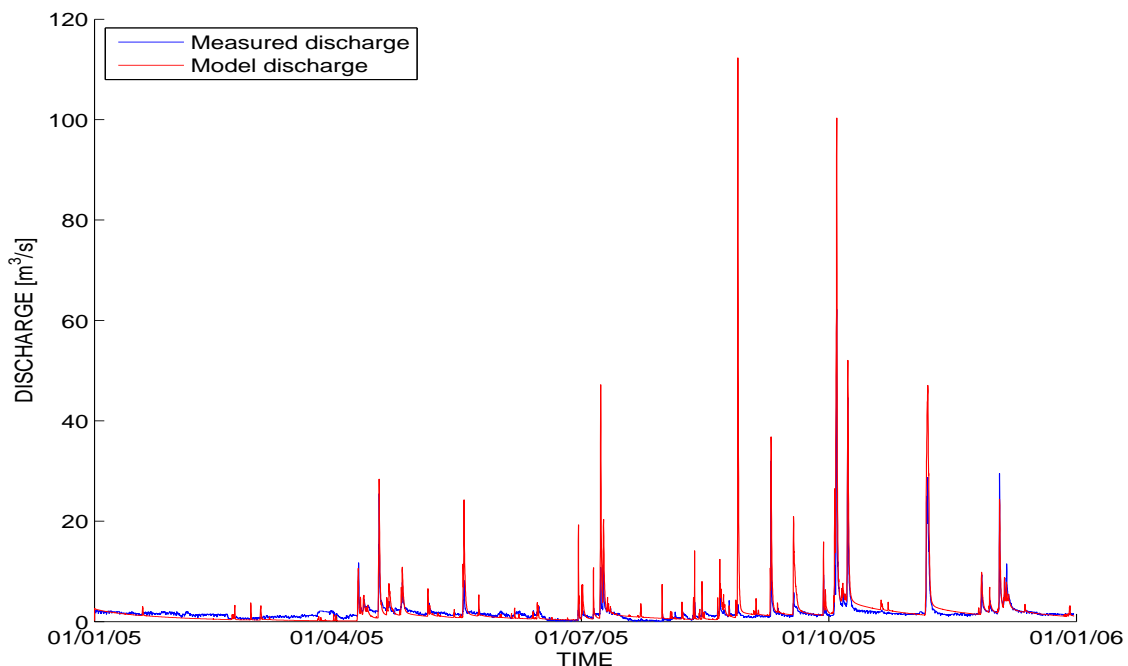


Figure 4.9: Comparison between measured and modeled discharge for the year 2005

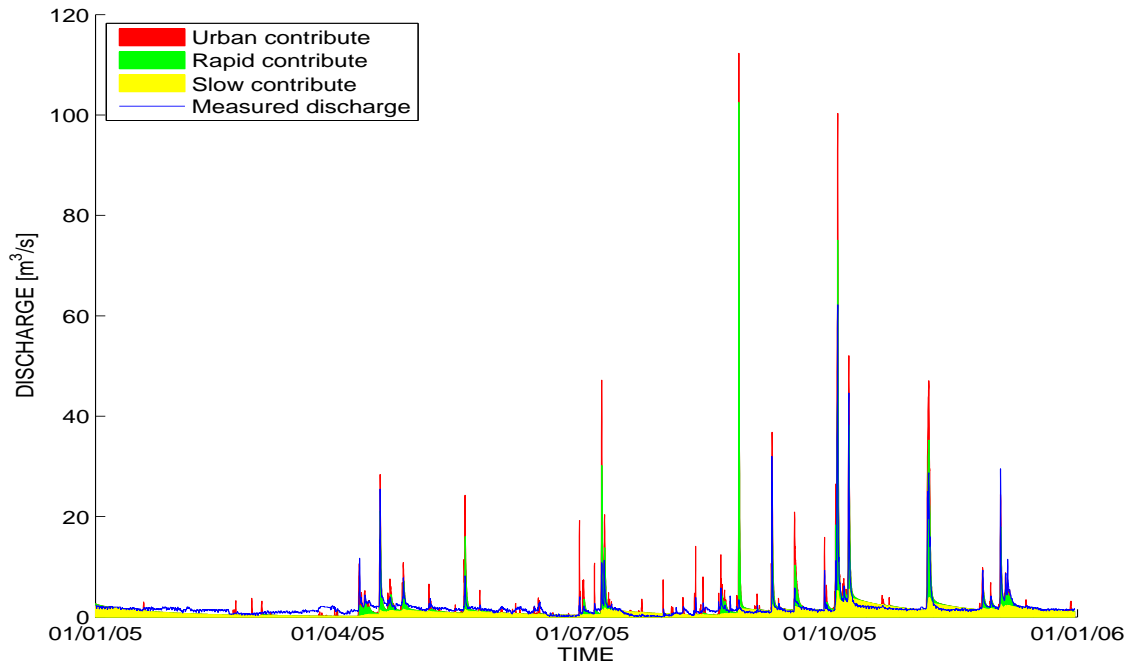


Figure 4.10: Comparison between measured and modeled discharge for the year 2005 decomposed in the three different runoff components

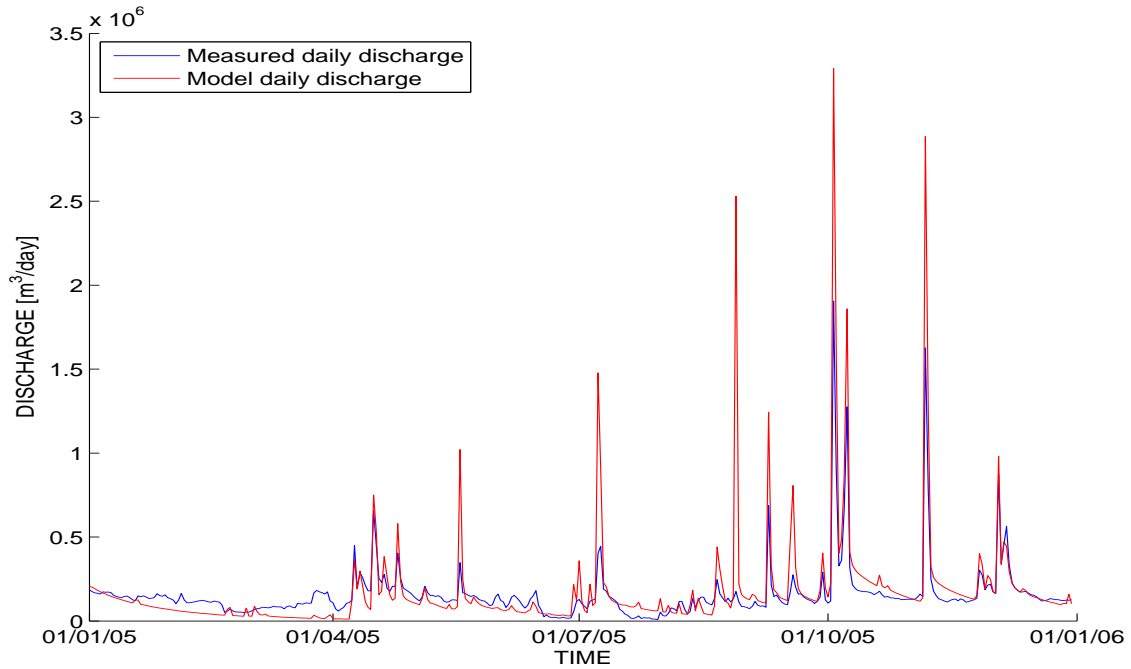


Figure 4.11: Comparison between daily measured discharge and daily modeled discharge for the year 2005

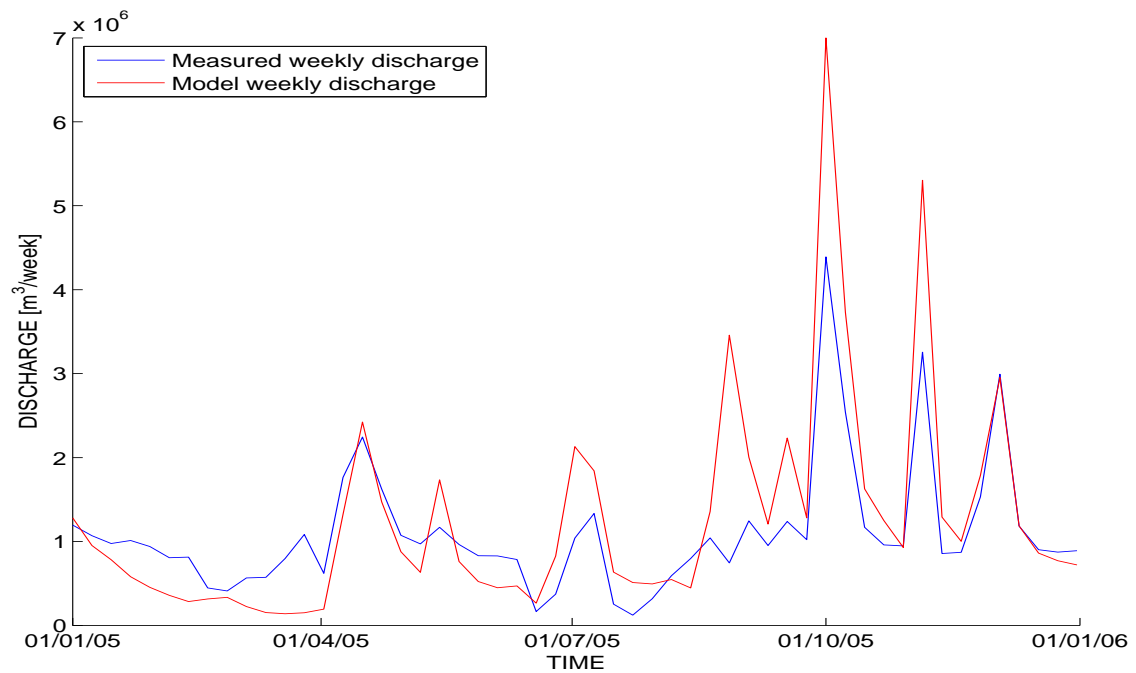


Figure 4.12: Comparison between weekly measured discharge and weekly modeled discharge for the year 2005

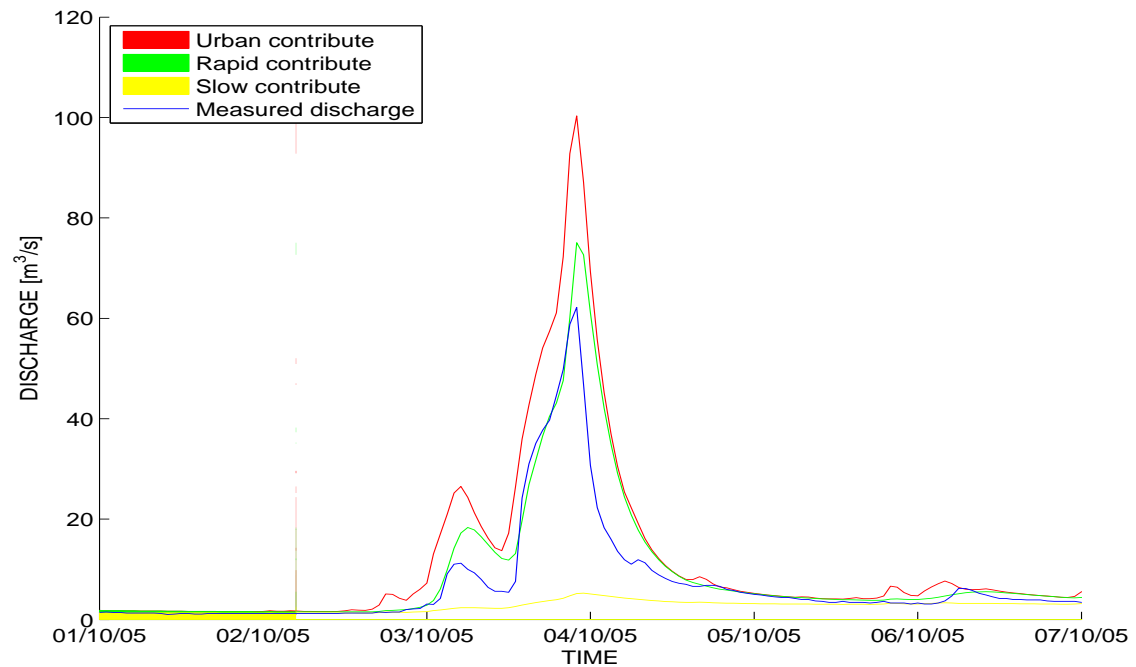


Figure 4.13: Comparison between measured and modeled discharge for the event between 01/10/2005 and 07/10/2005

Year 2006

The hydrologic behavior of the Muson dei Sassi during the year 2006 is really similar to that observed during the year 2005, with low precipitation and low discharges. However the performance of the model is better with respect to the year 2005, providing good results both during rainfall events, during recessions and low discharge (Figure 4.14 and Figure 4.15). There is a week overestimation of the peaks, except than during the event that occurs at the end of September, where the observed peak ($35 m^3/s$) is largely overestimated by the model ($70 m^3/s$).

During the entire year the observed peaks are not significant, with only three events characterized by around $30 m^3/s$. In terms of exiting volumes (Figure 4.17) the model simulate in a good way the entire year with the exception of the event described before and the dry period after it, that means that the water is kept within the volume for a longer period.

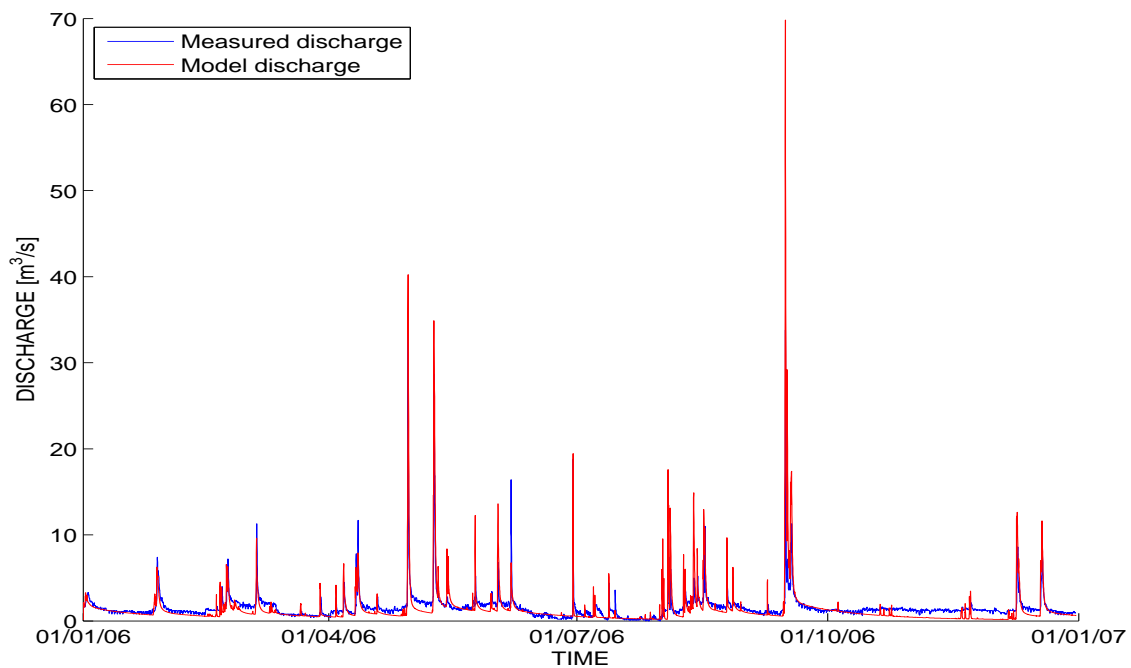


Figure 4.14: Comparison between measured and modeled discharge for the year 2006

Year 2007

Similarly to the two previous years, the year 2007 is really dry ($Q_{mean} = 1,4 m^3/s$) and characterized by low discharges and rainfall events. Figure 4.19 shows that the model tends to overestimate the small peaks of the hydrologic response during the month of May, June and October but there are no big differences in discharge during the dry periods. This fact is confirmed also by Figure 4.21 where the modeled weekly fluxes leaving the catchment are shown to be similar to the measured ones with some exceptions during the summer period.

Figure 4.22 shows a zoom for the only relevant event of the year with a peak value of

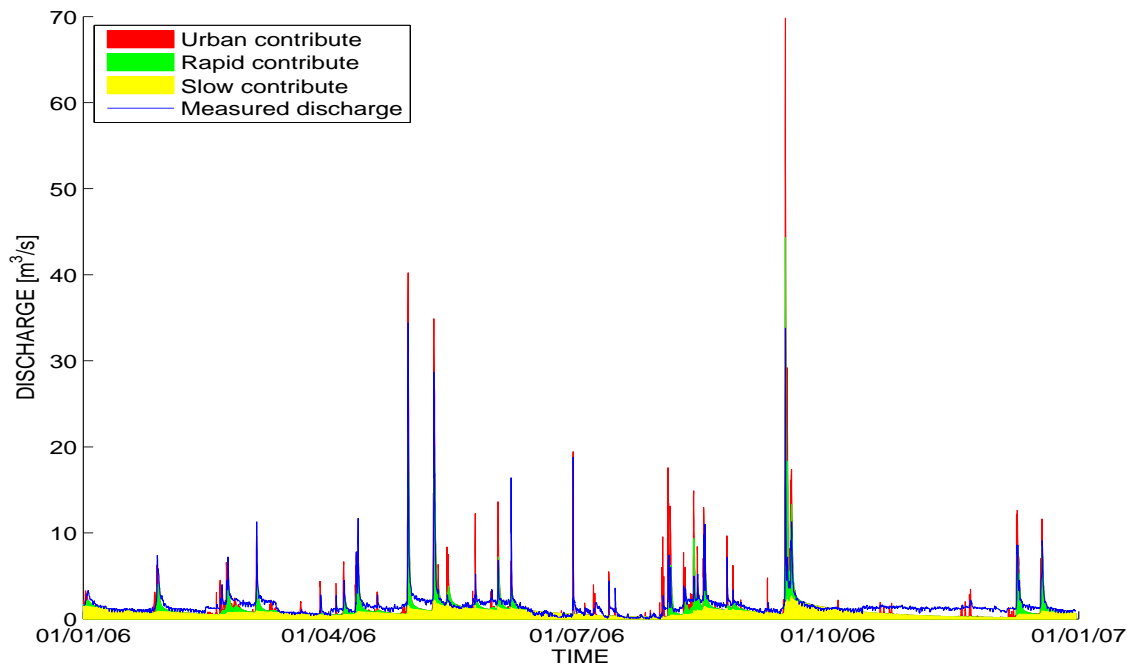


Figure 4.15: Comparison between measured and modeled discharge for the year 2006 decomposed in the three different runoff components

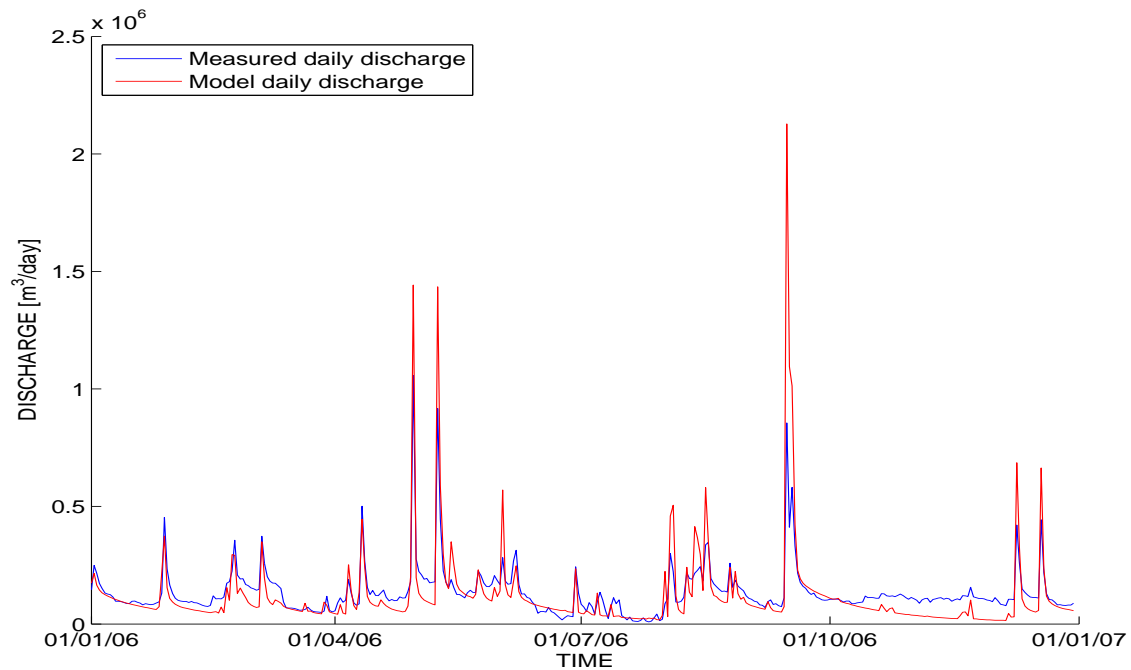


Figure 4.16: Comparison between daily measured discharge and daily modeled discharge for the year 2006

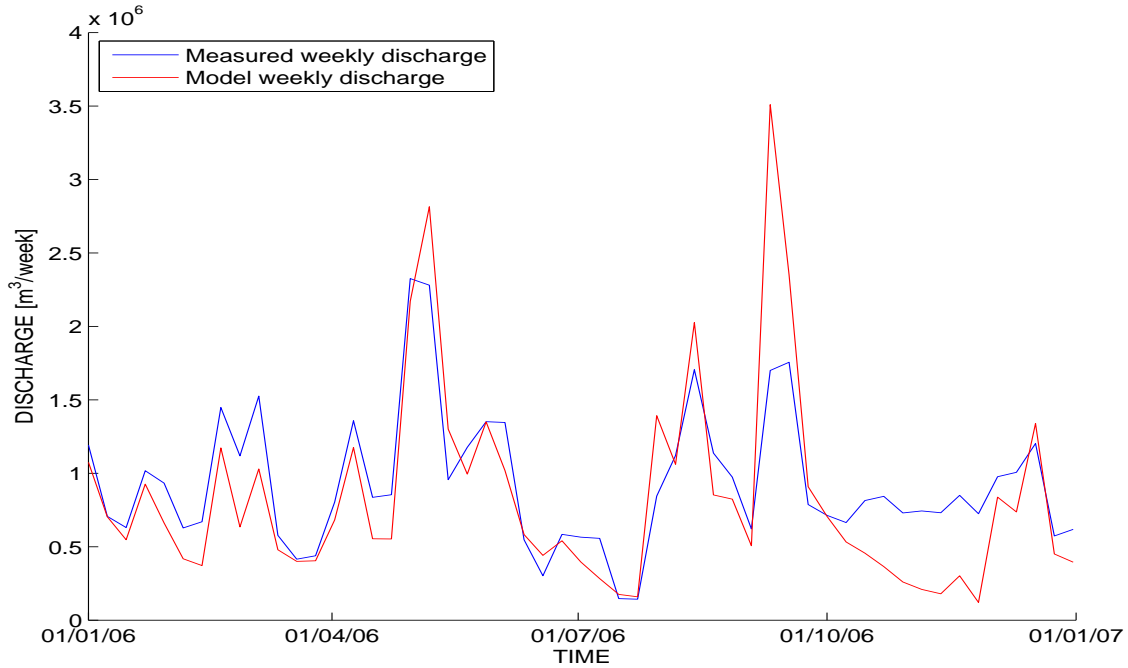


Figure 4.17: *Comparison between weekly measured discharge and weekly modeled discharge for the year 2006*

$64,7 m^3/s$. The modeled maximum discharge weakly underestimates the observed discharge and the recession curve is gentler. As a result, the simulated released volumes during the event are larger than the observed volumes. Considering the uncertainties involved, the model gives a good representation of the event under examination.

Year 2008

The hydrologic model developed gives remarkable result for the year 2008. Figure 4.23 and Figure 4.24 report the comparison of the observed and modeled discharges at hourly time-scale. It can be noticed that the entire year is characterized by an high number of rainfall events and the response in term of timing and peak value is appreciable. The main problems occurs during the summer period, where for every precipitation corresponds a peak in discharge that are not measured in the reality. All these peaks are given by the urban component of the runoff and it can be due to the fact that the evaporation term from the urban area (if considered to be included in the term γ described in the Section 3.4) does not vary during the year, and it is important during the warm periods. Figure 4.25 and Figure 4.26 shows the ability of the model to reproduce the daily and weekly discharge. Except for the uncertainties related to the summer peaks, the modeled and observed released volumes are almost the same.

During the year 2008 there are not particular high levels of discharge and the main events occurs in the month of December. The series of event registered in the final part of the year is perfectly reproduced by the model.

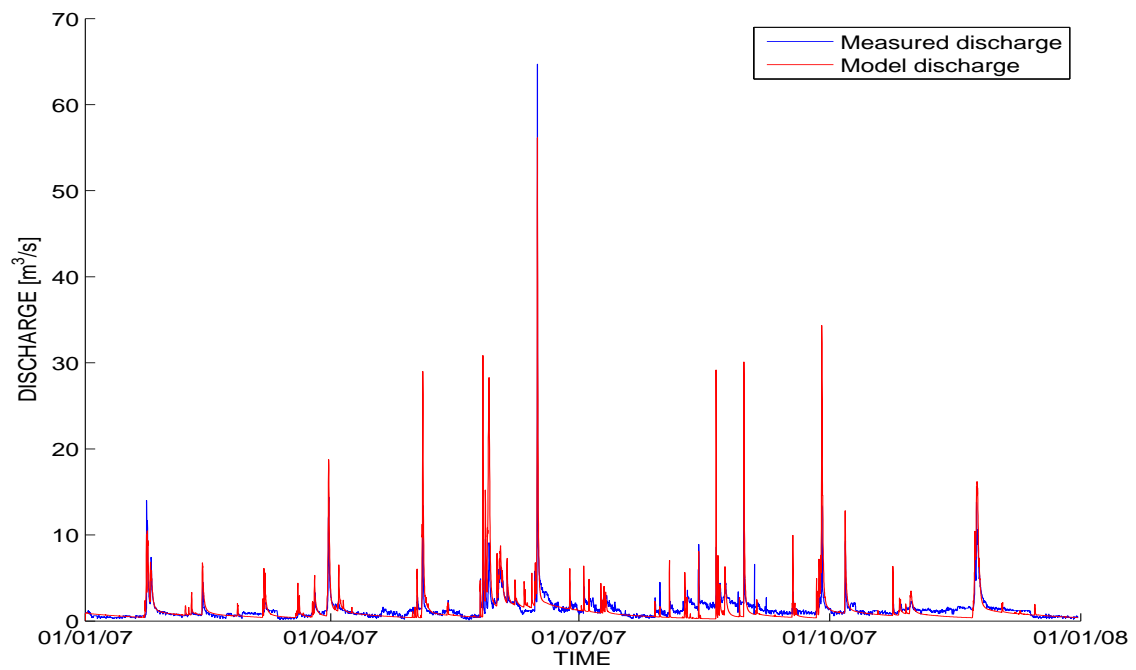


Figure 4.18: Comparison between measured and modeled discharge for the year 2007

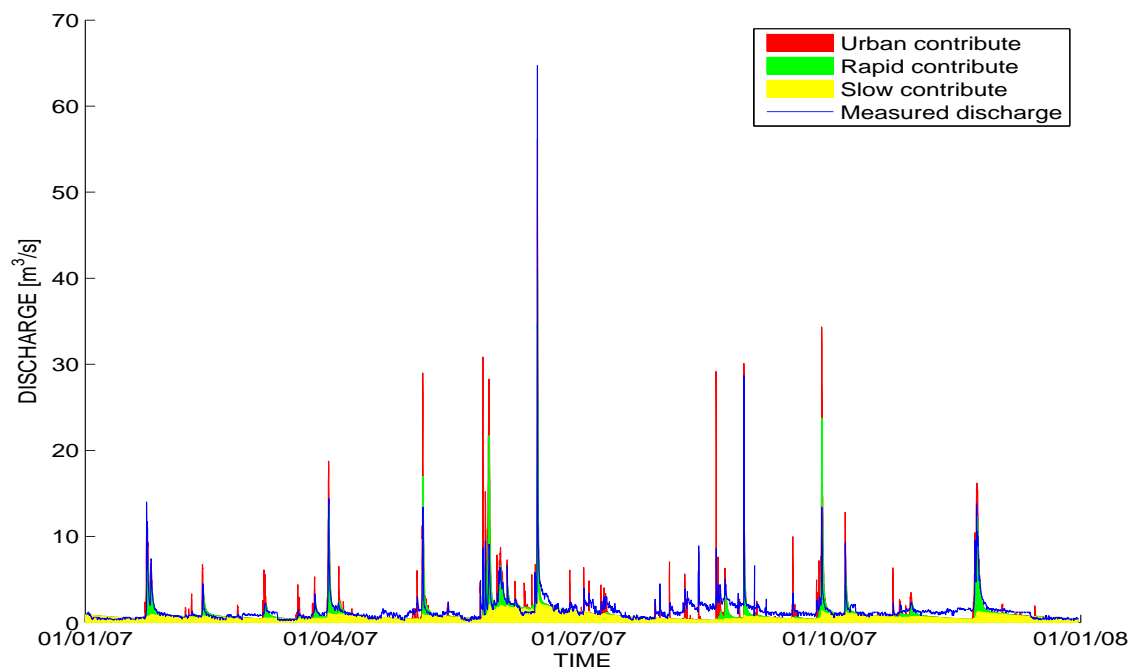


Figure 4.19: Comparison between measured and modeled discharge for the year 2007 decomposed in the three different runoff components

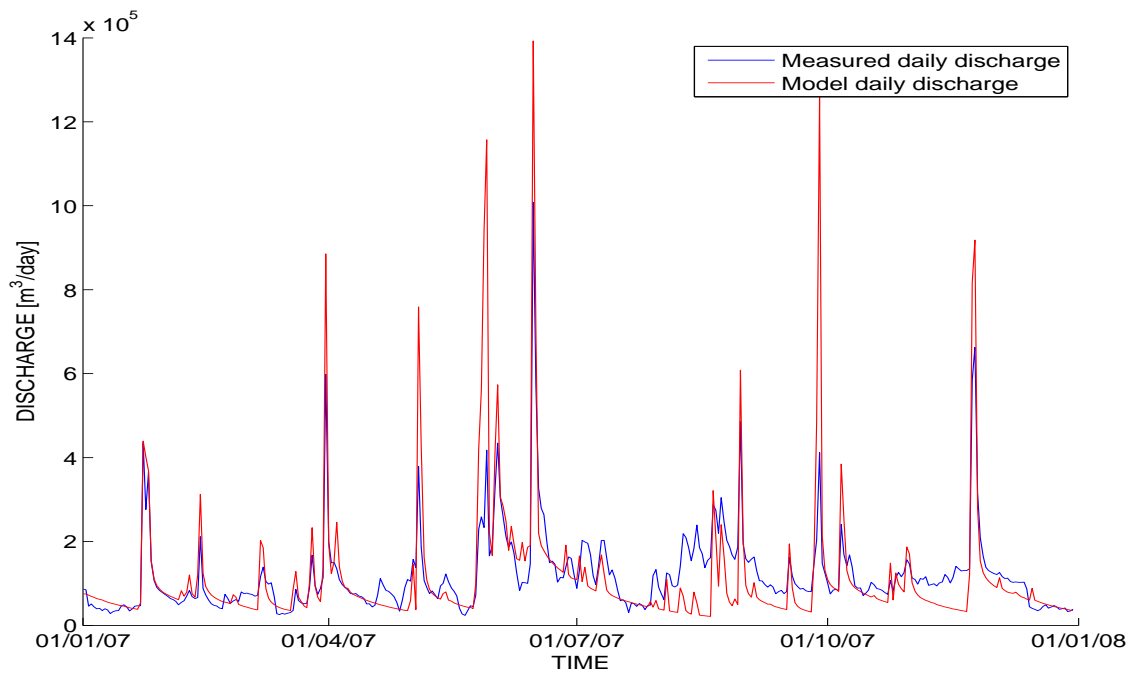


Figure 4.20: Comparison between daily measured discharge and daily modeled discharge for the year 2007

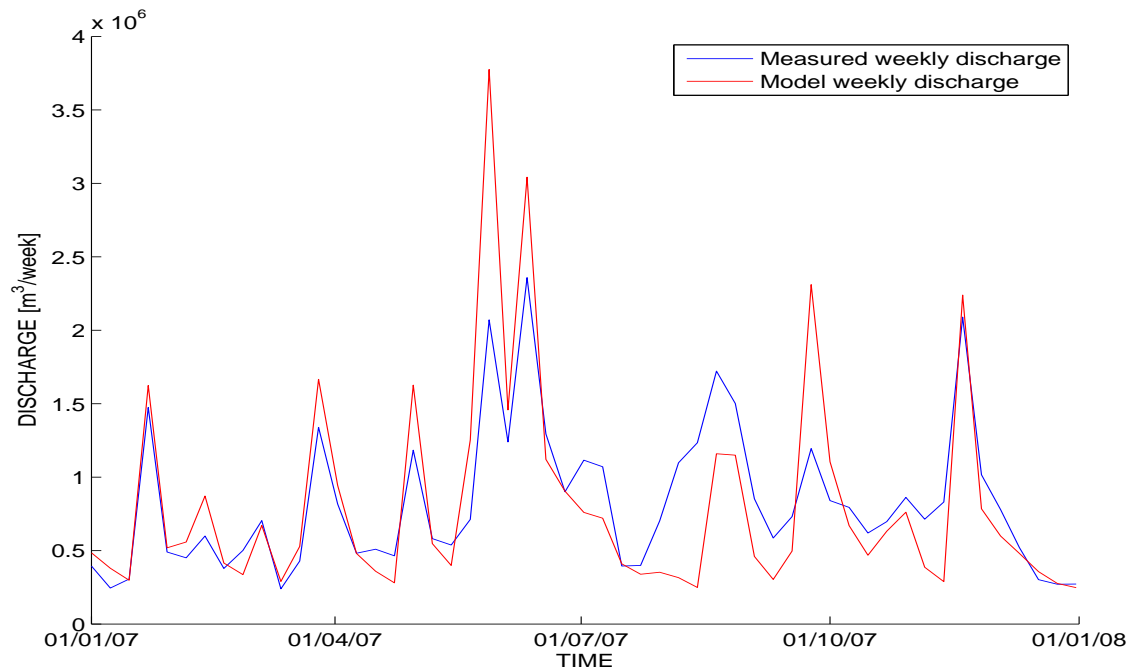


Figure 4.21: Comparison between weekly measured discharge and weekly modeled discharge for the year 2007

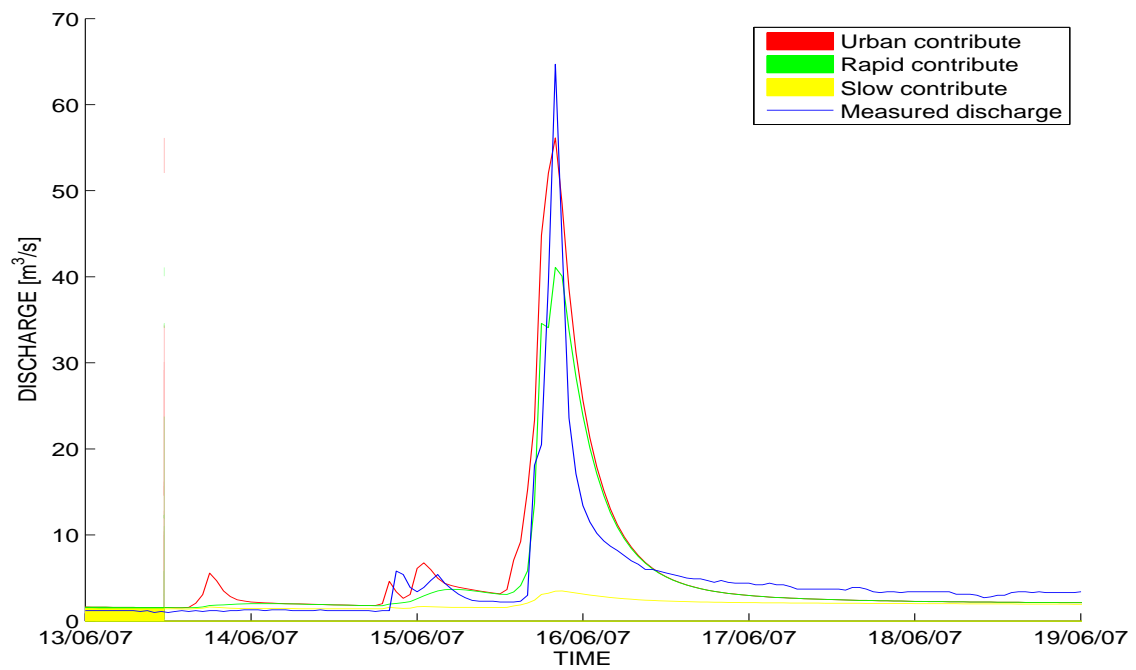


Figure 4.22: Comparison between measured and modeled discharge for the event between 13/06/2007 and 19/06/2007

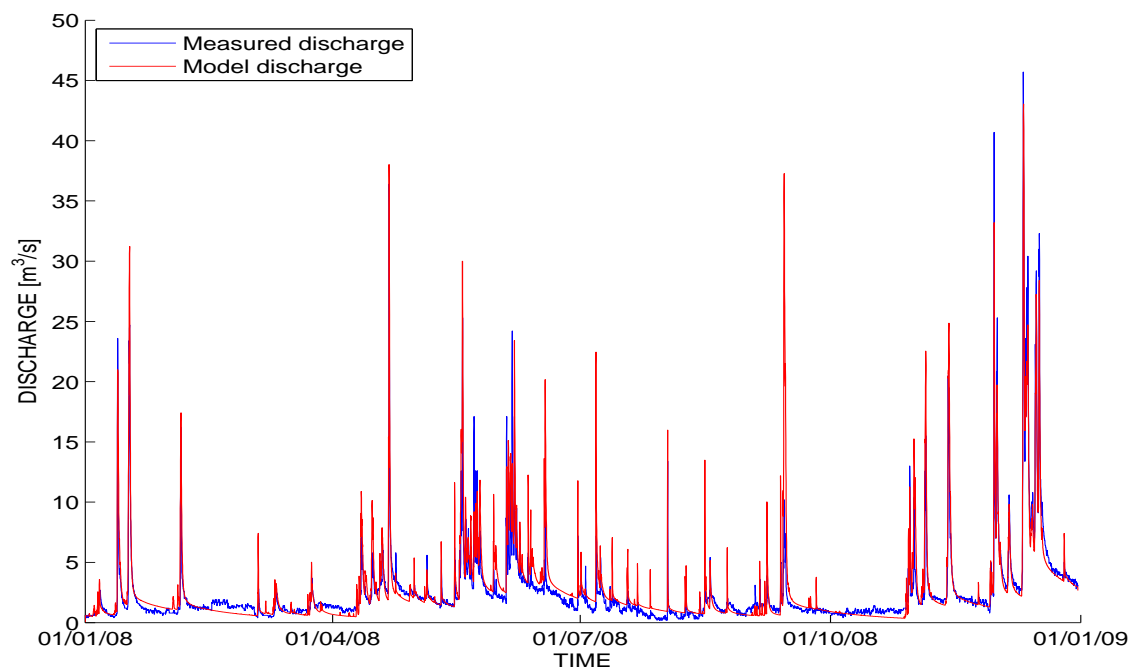


Figure 4.23: Comparison between measured and modeled discharge for the year 2008

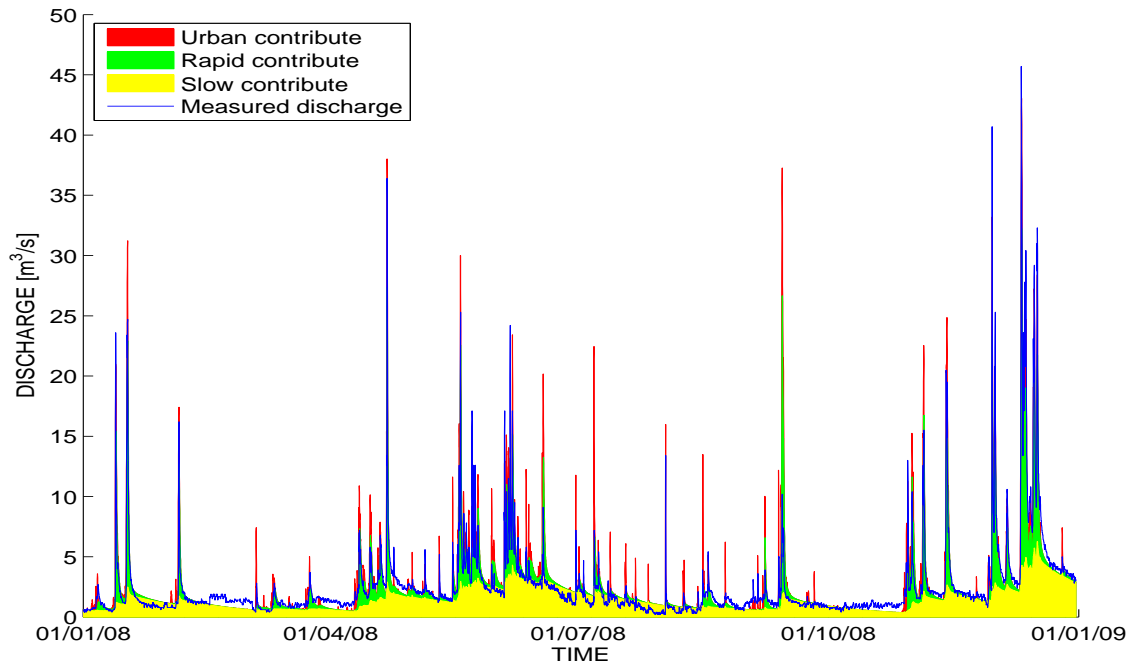


Figure 4.24: Comparison between measured and modeled discharge for the year 2008 decomposed in the three different runoff components

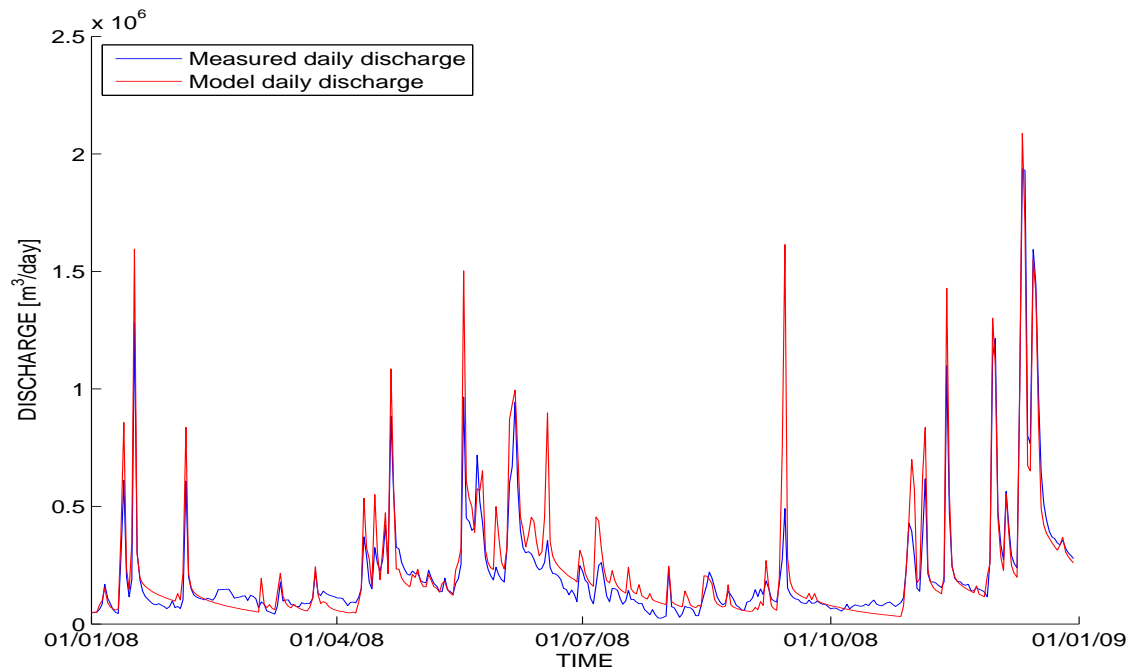


Figure 4.25: Comparison between daily measured discharge and daily modeled discharge for the year 2008

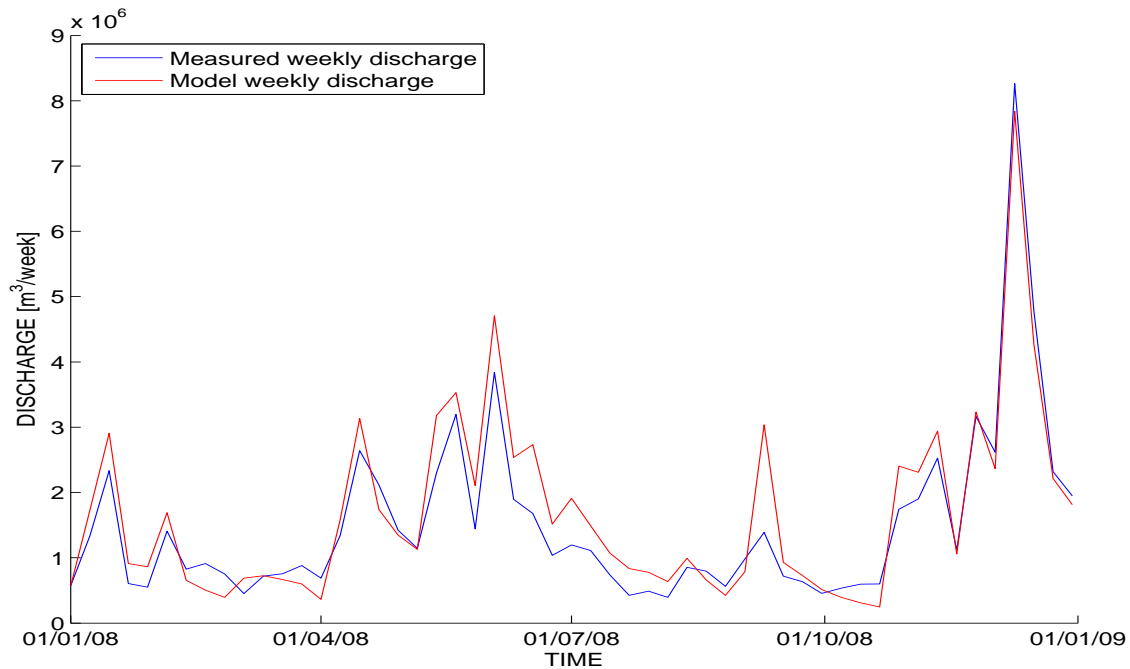


Figure 4.26: Comparison between weekly measured discharge and weekly modeled discharge for the year 2008

Year 2009

Figure 4.27 and Figure 4.28 show the ability of the model to reproduce the discharge for the year 2009. Mainly the results obtained are good even if some comments have to be done. The low discharges are properly simulated for the entire year, even though there are some errors in the simulation of the peaks. As reported for the year 2008, during the summer the model tends to overestimate the peaks and it is principally due to the urban contribution, while, for the remaining part of the year the peak values are slightly underestimated. This trend is confirmed also by Figure 4.29 and Figure 4.30 where daily and weekly discharge are plotted. In the first and last part of the year the results coincide with the observed discharge while starting from May until mid-October the model underestimates the low discharges and overestimates the peak of September.

Figure 4.31 shows a zoom on the event between September 14 and September 20, 2009. A strange behavior of the response of the model is reported. The event, characterized by a maximum discharge of $79,2 m^3/s$, is composed by two consecutive peaks, a first small followed by the mean peak. The model on the contrary generates first a large peak with a discharge comparable to the maximum measured discharge and then a small peak. Also the volumes of water involved are different being higher the volume released for the modeled curve. This large error should be due to a problem in the spatio-temporal distribution of the precipitation since the time shift between the observed and modeled peak (11 h) is much larger than the mean residence time in the *urban* and *rapid* states (respectively 1, 23 and 3, 42 hours).

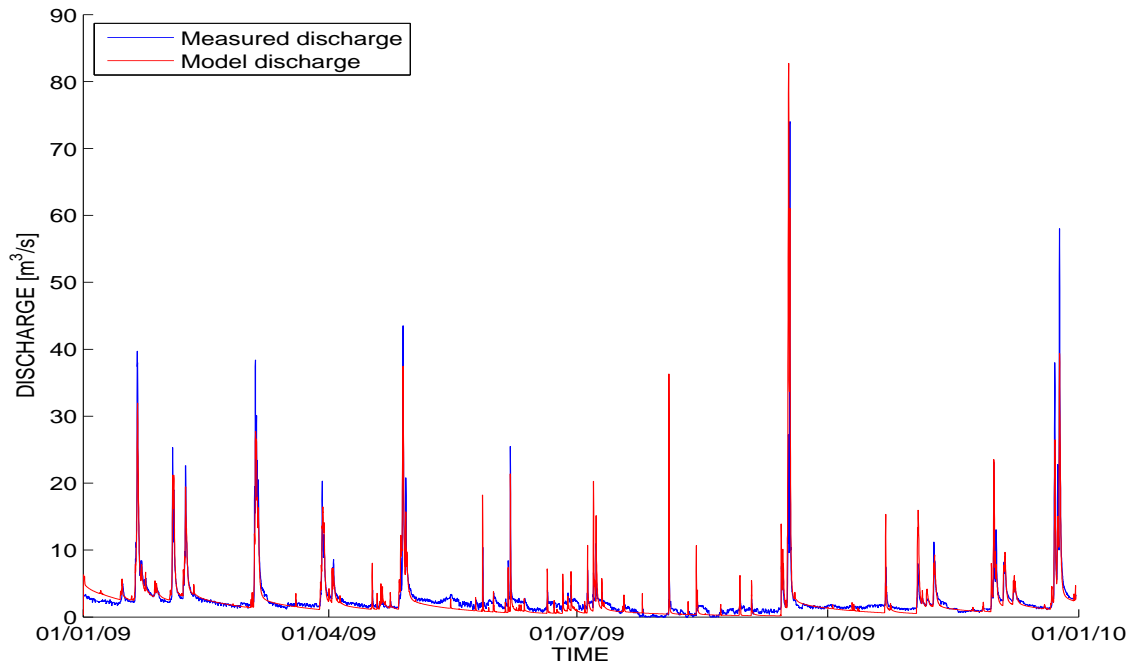


Figure 4.27: Comparison between measured and modeled discharge for the year 2009

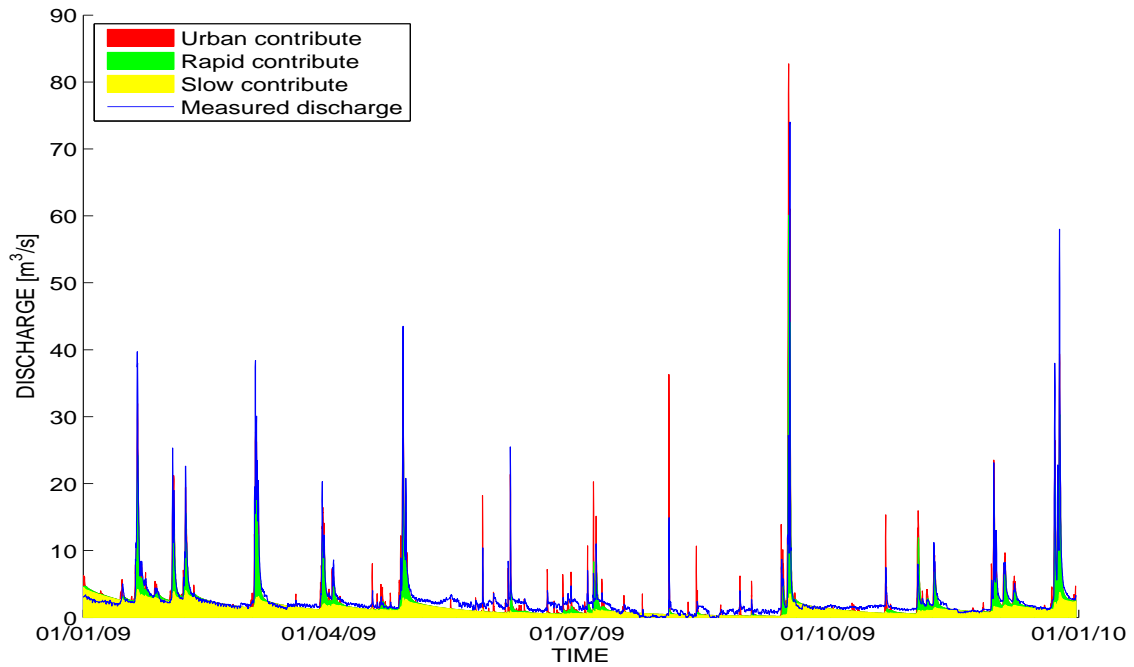


Figure 4.28: Comparison between measured and modeled discharge for the year 2009 decomposed in the three different runoff components

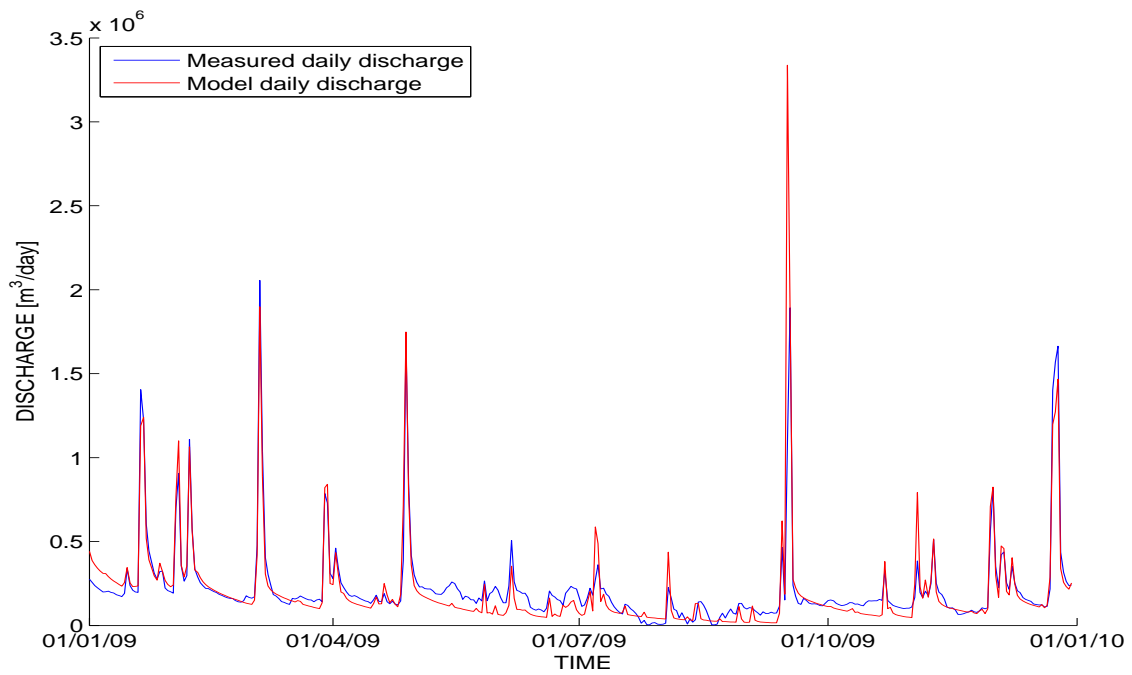


Figure 4.29: Comparison between daily measured discharge and daily modeled discharge for the year 2009

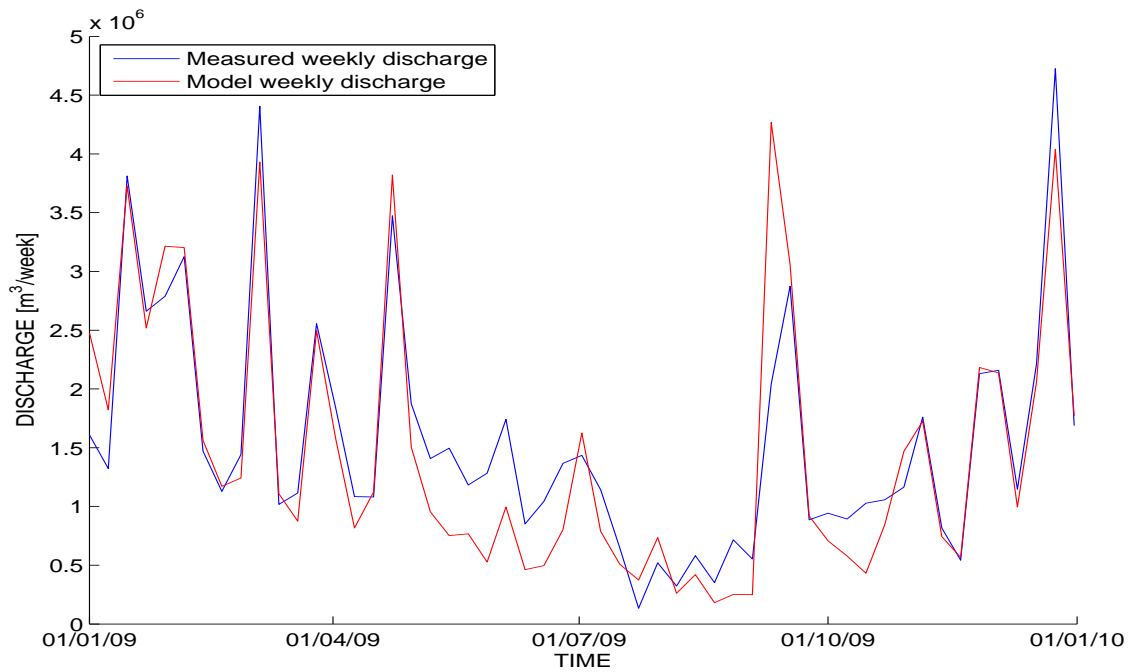


Figure 4.30: Comparison between weekly measured discharge and weekly modeled discharge for the year 2009

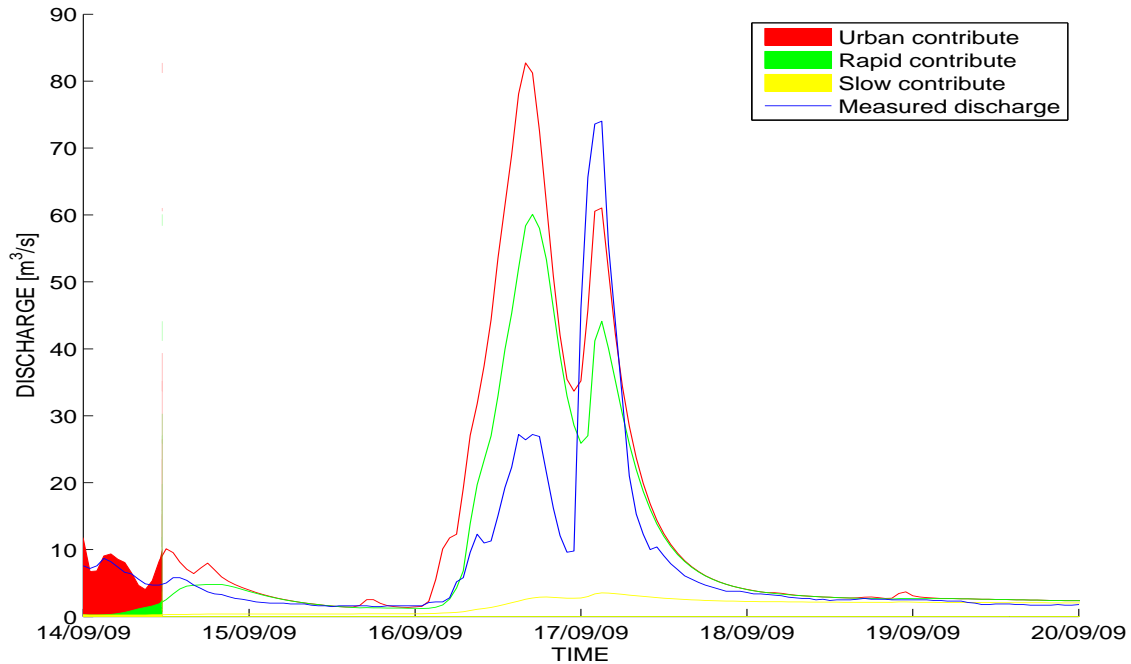


Figure 4.31: Comparison between measured and modeled discharge for the event between 14/09/2009 and 20/09/2009

Year 2010

The year 2010 was the year partially used for the calibration and thus the final part of the year and the main event, that are described in Section 4.1, are not commented here. The results reported in Figures 4.32 and 4.32 show the good capability of the model to simulate the catchment behavior during the whole year, which is characterized by the highest mean discharge during the period-of-record ($Q_{mean} = 3,7 m^3/s$). As for the previous year the peaks during winter, spring and autumn are almost perfectly simulated while during summer the model overestimates the peaks, due to the large contribution provided by the urban runoff component. Low discharges are systematically underestimated by the model. This feature is shown in Figures 4.34 and 4.35, even though the differences between the two curves in each plot are really limited, implying that the model properly estimates daily and weekly volumes. The main event of the year (Figure 4.3) is described in Section 4.1.

Year 2011

The hydrological model applied to the year 2011 gives satisfying results depicted in Figures 4.36 and 4.37. The few peaks present during the year are properly simulated, with a little exception for the small urban peaks during the summer period, and the low discharges are weakly underestimated. Figure 4.38 and 4.39 (daily and weekly discharges) show the same problem (i.e. the underestimation for dry periods). In addition an overestimation of the released volumes for three of the four events of the year is depicted. Figure 4.40 shows a zoom on the peak occurred on October 26, characterized by a maxi-

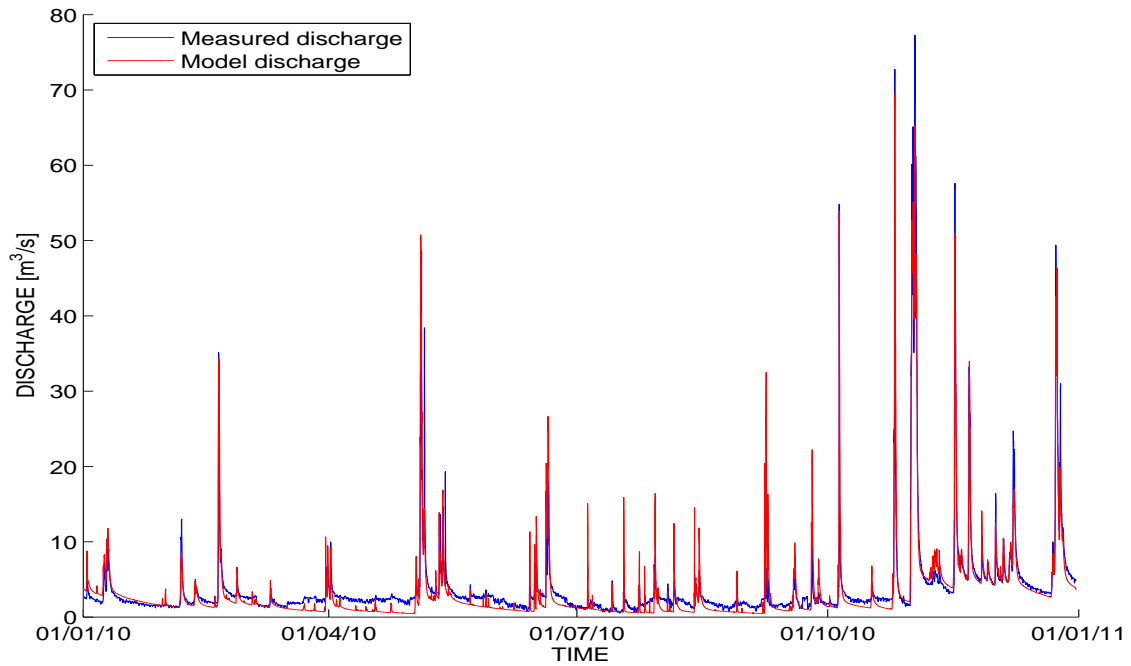


Figure 4.32: Comparison between measured and modeled discharge for the year 2010

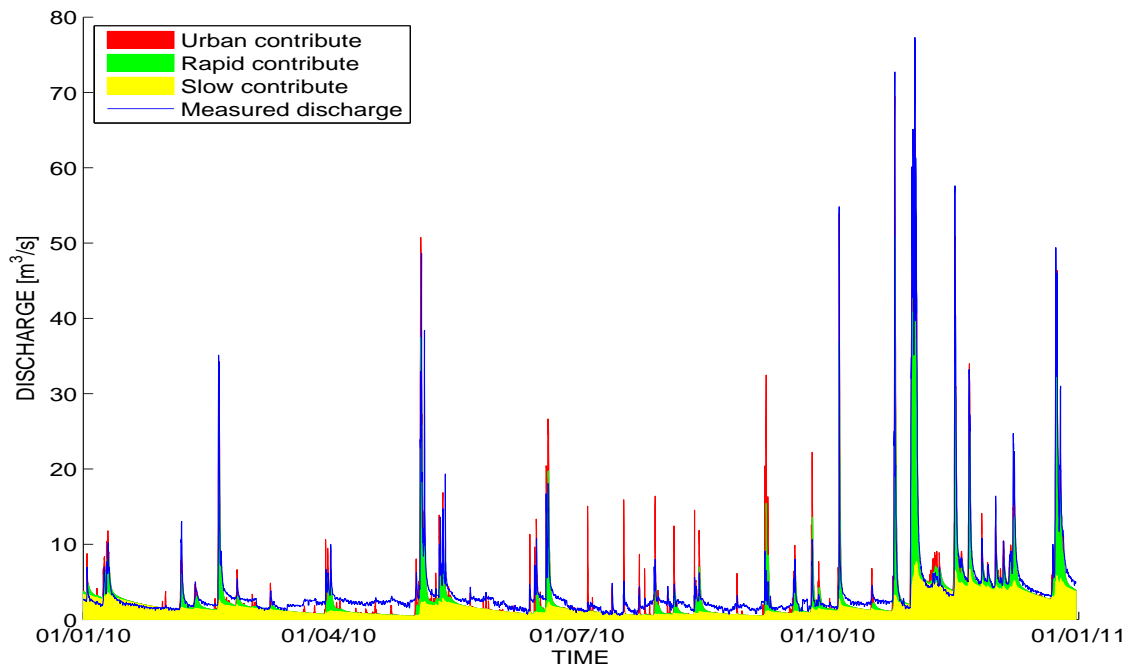


Figure 4.33: Comparison between measured and modeled discharge for the year 2010 decomposed in the three different runoff components

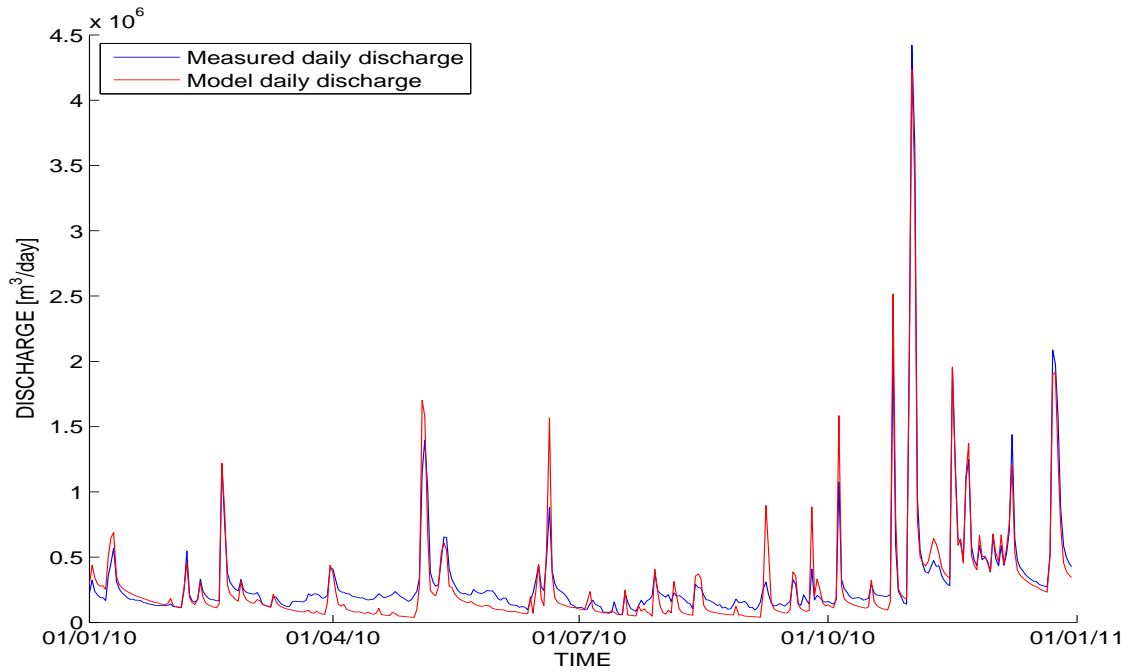


Figure 4.34: Comparison between daily measured discharge and daily modeled discharge for the year 2010

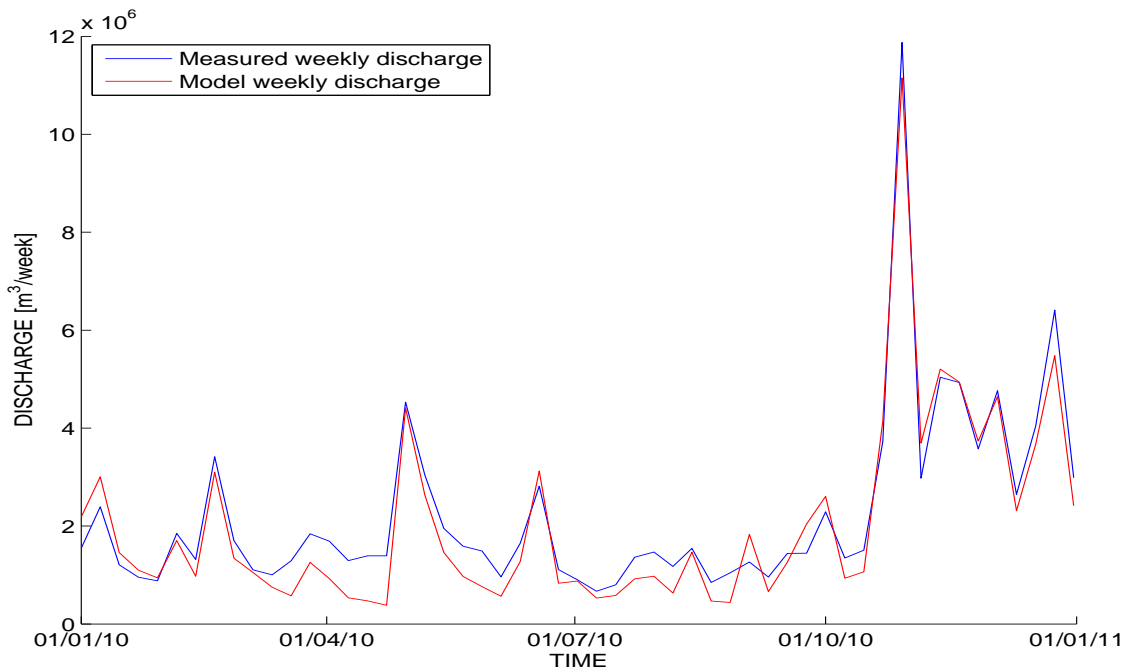


Figure 4.35: Comparison between weekly measured discharge and weekly modeled discharge for the year 2010

imum discharge of $63,9 \text{ m}^3/\text{s}$. The peculiarity of the model of overestimating the maximum discharge is confirmed. For the event of study also the behavior of the modeled curve is different from the observed one, being composed by two peaks instead of only one. Moreover the water volume of the event is higher than the observed volume.

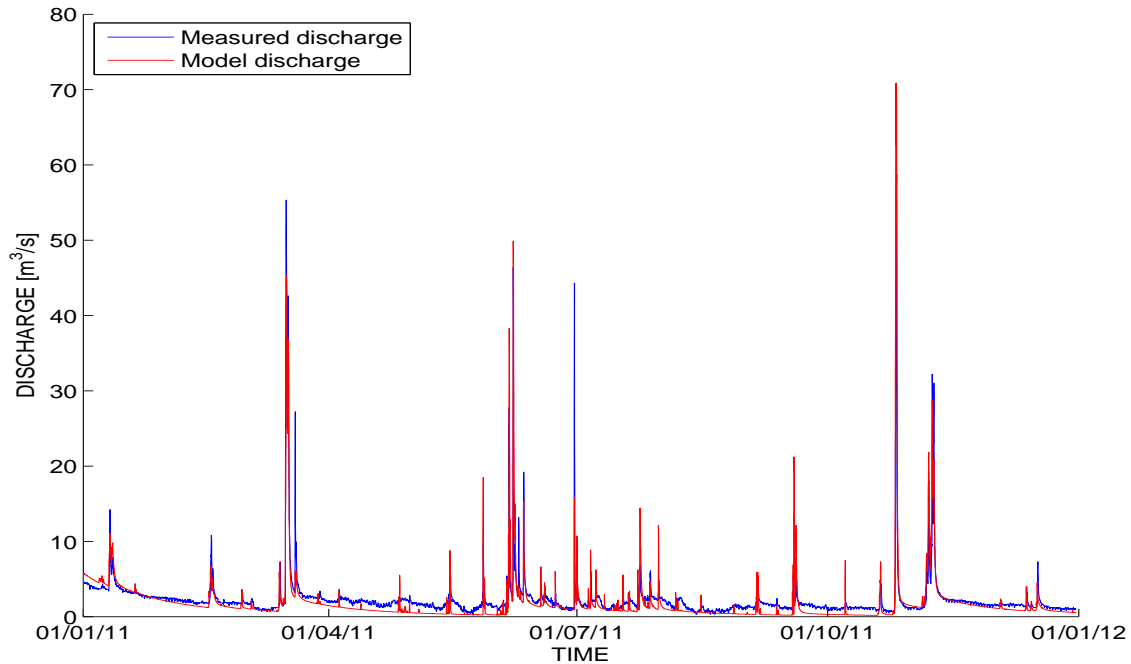


Figure 4.36: Comparison between measured and modeled discharge for the year 2011

Year 2012

The year 2012 summarize, better than the other years considered, the erratic flow regime of the Muson dei Sassi river. Figures 4.41 and 4.42 show that during the entire year the base flow is really low, with long periods characterized by less than $0,5 \text{ m}^3/\text{s}$, except from a couple of huge peaks in the autumn season. The response of the model is almost perfect in both the phases even if the summer peaks are again weakly overestimated due to the urban runoff component. Figure 4.43 and Figure 4.44 show the results for the year 2012 in terms of daily and weekly discharges. Those are the best obtained for the period of study. The model has remarkable performances at all the different time-scale considered.

Figure 4.45 shows a zoom on the event occurred between the November 11 and November 13, where it is appreciable the good simulation offered by the model. This event, characterized by a maximum measured discharge of $106,9 \text{ m}^3/\text{s}$, is the largest event occurred during the entire period of study going from January 1, 2004, and December 31, 2013. The huge storm, that caused the before-written discharge, was estimated having a return period in terms of rainfall of 50 years for the considered area and it caused floods in different points of the catchment before the closure section at Castelfranco Veneto. Considering the importance of the event the results obtained are almost perfect both in term of duration,

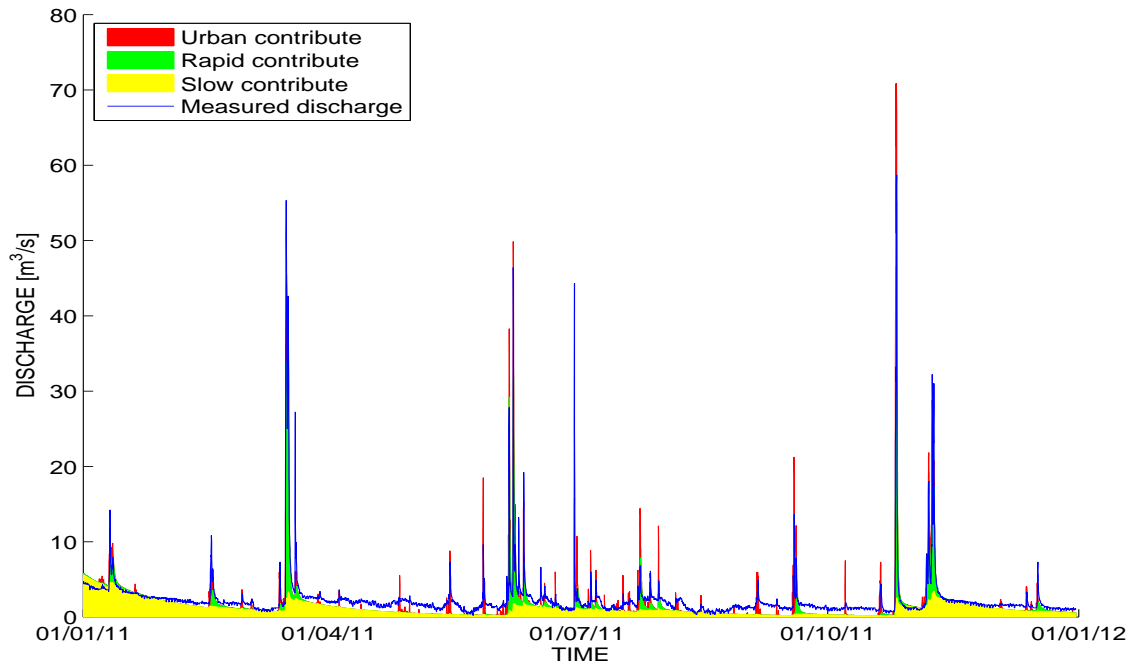


Figure 4.37: Comparison between measured and modeled discharge for the year 2011 decomposed in the three different runoff components

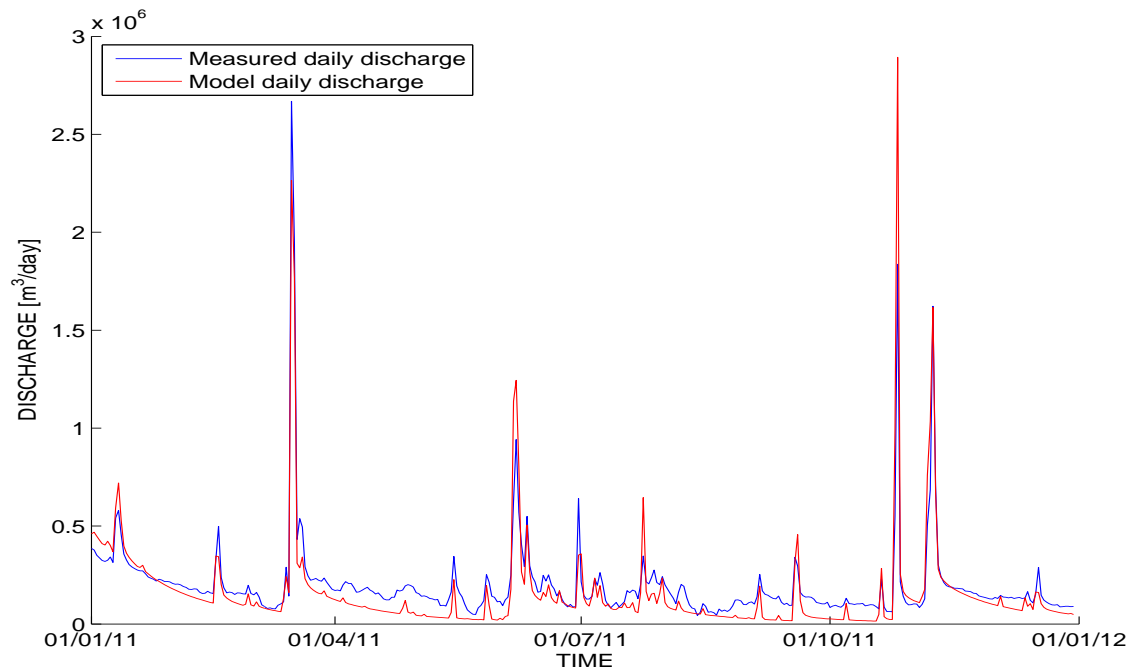


Figure 4.38: Comparison between daily measured discharge and daily modeled discharge for the year 2011

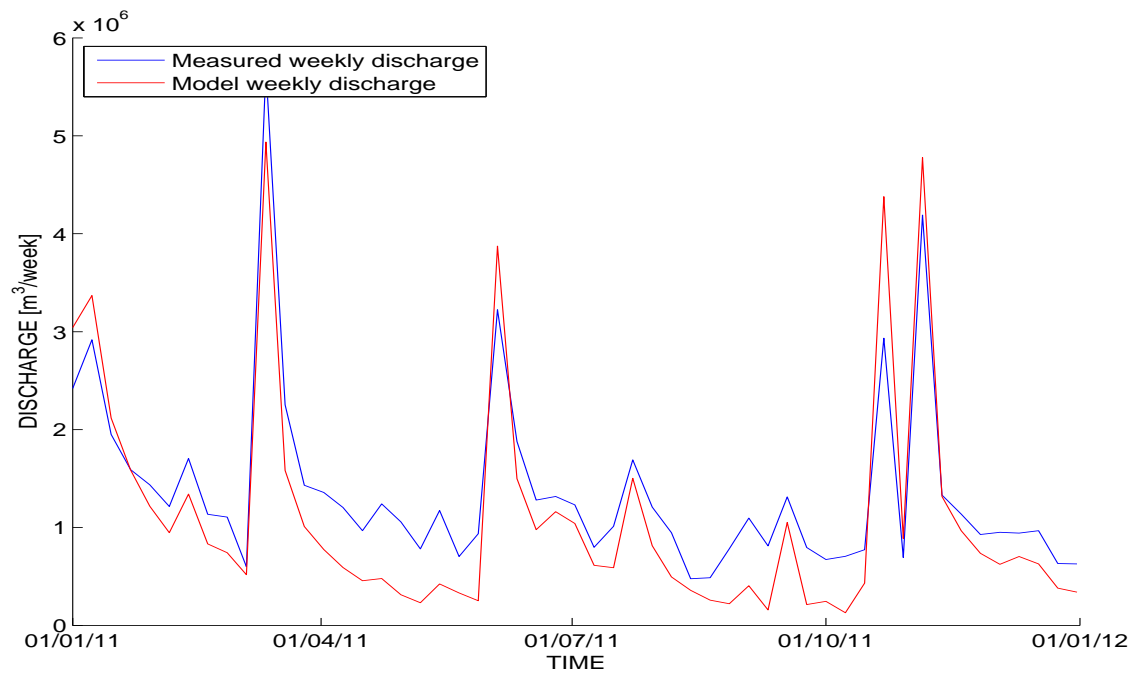


Figure 4.39: Comparison between weekly measured discharge and weekly modeled discharge for the year 2011

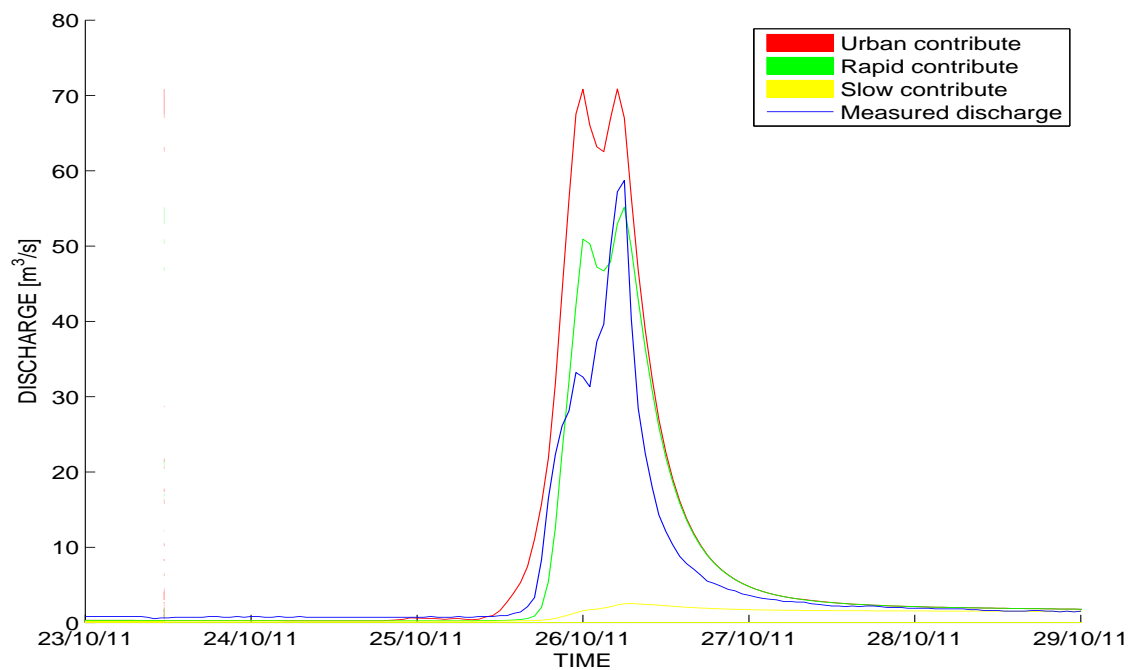


Figure 4.40: Comparison between measured and modeled discharge for the event between 23/10/2011 and 29/10/2011

peaks and recessions. A small overestimation of the maximum discharge is present but it can be due to the water that overflows the banks before the closure section.

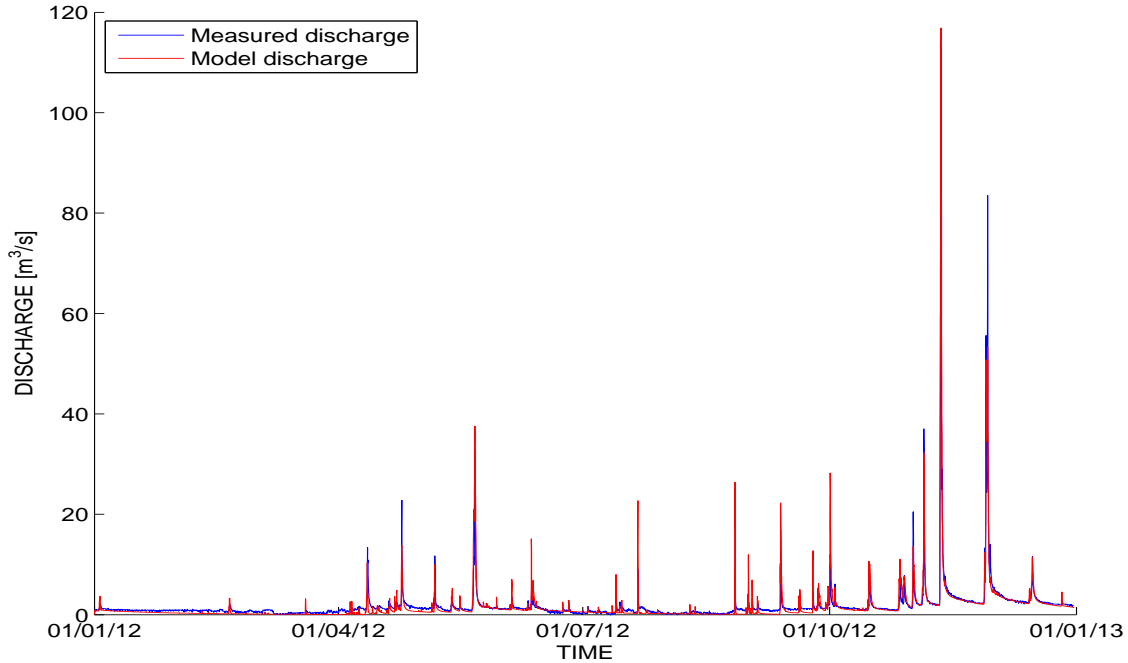


Figure 4.41: Comparison between measured and modeled discharge for the year 2012

Year 2013

Figure 4.46 and Figure 4.47 represent the comparison between the measured and modeled discharge for the year 2013. Differently from the previous year, the results obtained are poor for almost all the aspects analyzed, except the first months of simulation. In particular the low discharges are underestimated throughout the year of around $1 - 2 m^3/s$. The 2013 is characterized by an high frequency of precipitation, an high mean discharge $Q_{mean} = 3,2 m^3/s$ and a really high level of the groundwater table. This last aspect probably influence the infiltration capability of the soil, reducing the volume of water leaching in deeper layer of the soil, and can partially justify the lack of water during the entire year. Also looking to Figure 4.43 and 4.49 it is possible to notice the differences in volume discharged at daily and weekly time-scale.

Figure 4.50 shows a zoom on the series of peaks occurred between the May 16 and the May 25, 2013. The first two peaks are approximately well simulated, with a good response in terms of maximum value (even if a bit overestimated), volume of water and shape of the recession curve. The last peak ($Q_{max} = 81,1 m^3/s$) instead is totally missed by the model and the reason is explained below. There were only two meteorological gauges that registered a big amount of rainfall for that event ($21,2 mm/h$ at Bassano del Grappa and $19,6 mm/h$ at Pove del Grappa), while for the remaining station no rain was recorded. Hence the weight that this two stations have during the spatial interpolation of rainfall is not sufficient to produce a runoff volume comparable to the measured discharge amount.

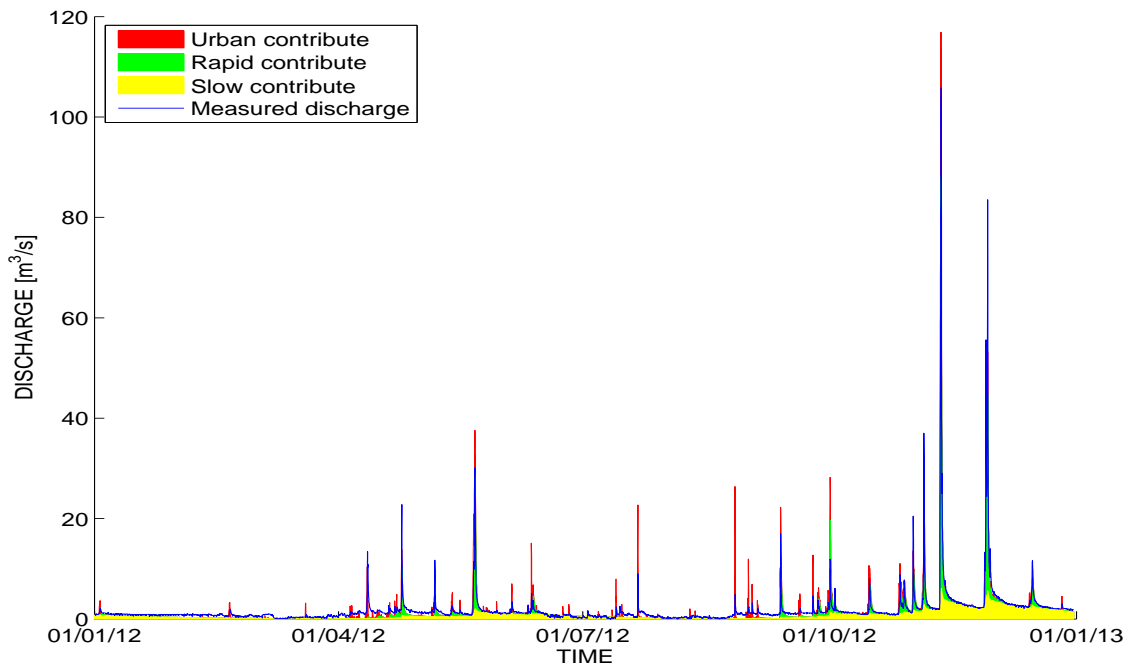


Figure 4.42: Comparison between measured and modeled discharge for the year 2012 decomposed in the three different runoff components

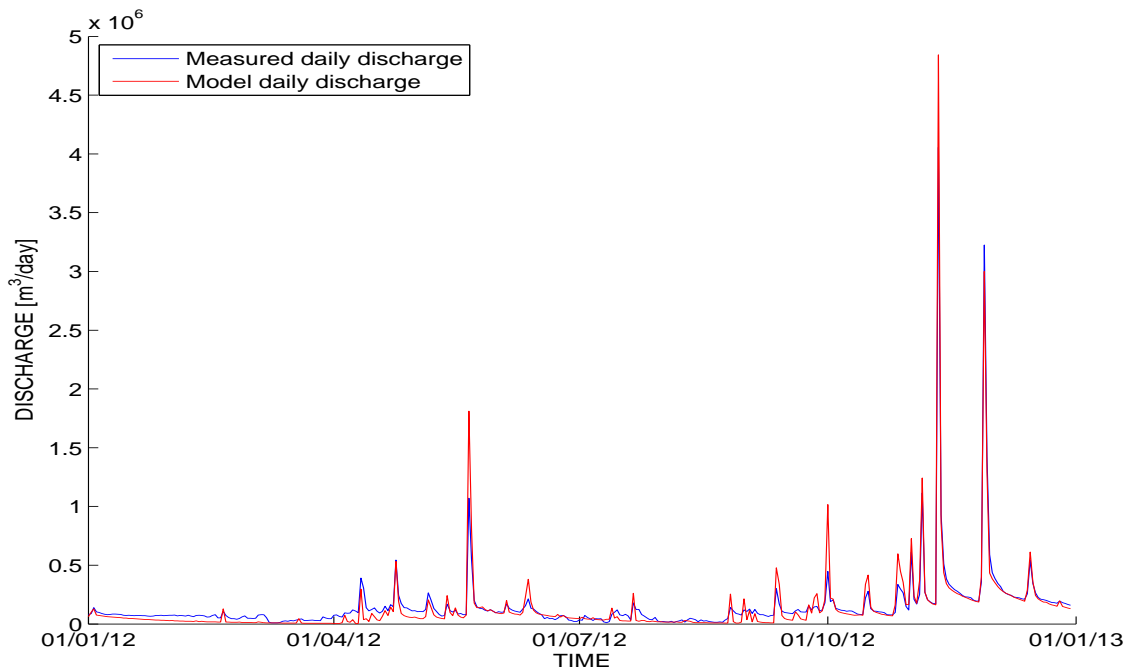


Figure 4.43: Comparison between daily measured discharge and daily modeled discharge for the year 2012

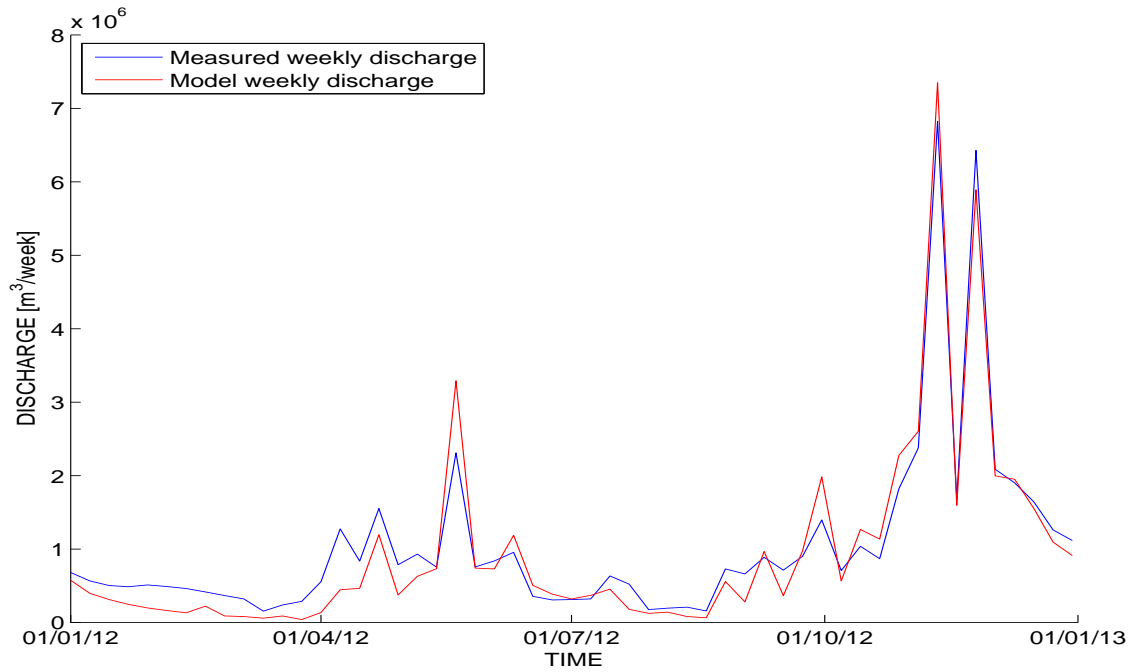


Figure 4.44: Comparison between weekly measured discharge and weekly modeled discharge for the year 2012

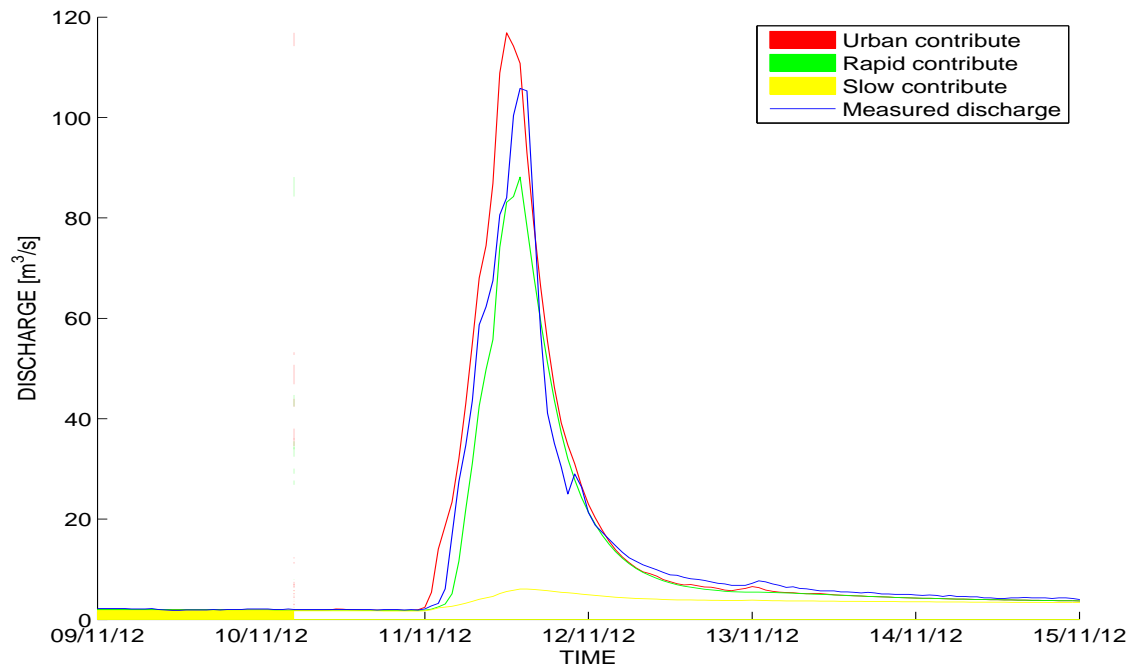


Figure 4.45: Comparison between measured and modeled discharge for the event between 09/11/2012 and 15/11/2012

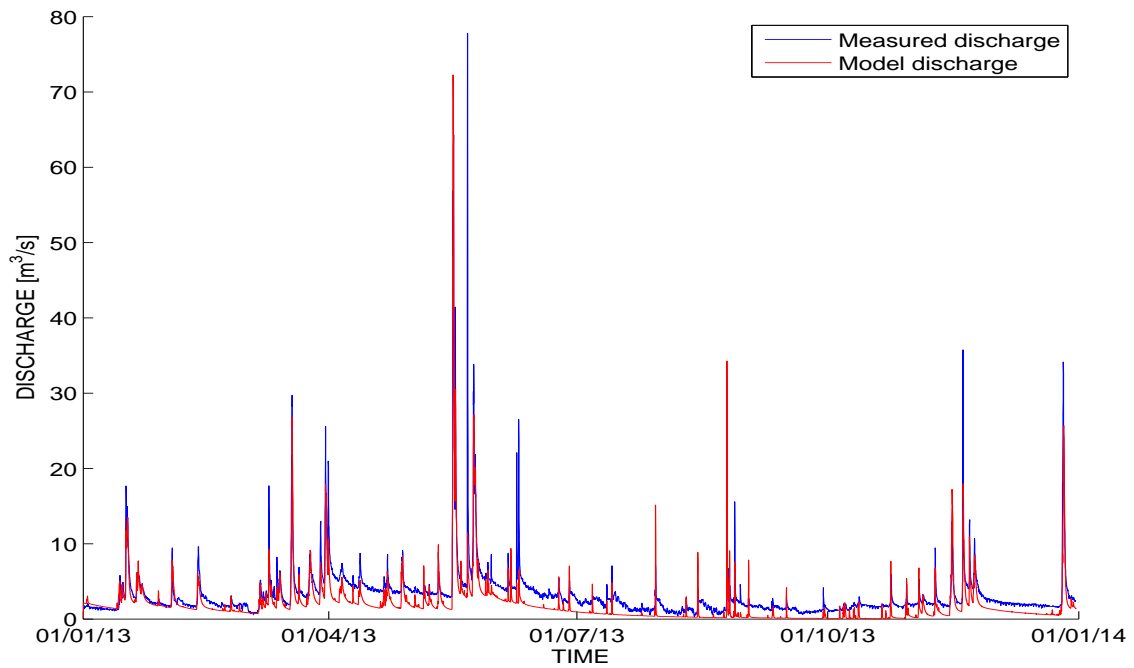


Figure 4.46: Comparison between measured and modeled discharge for the year 2013

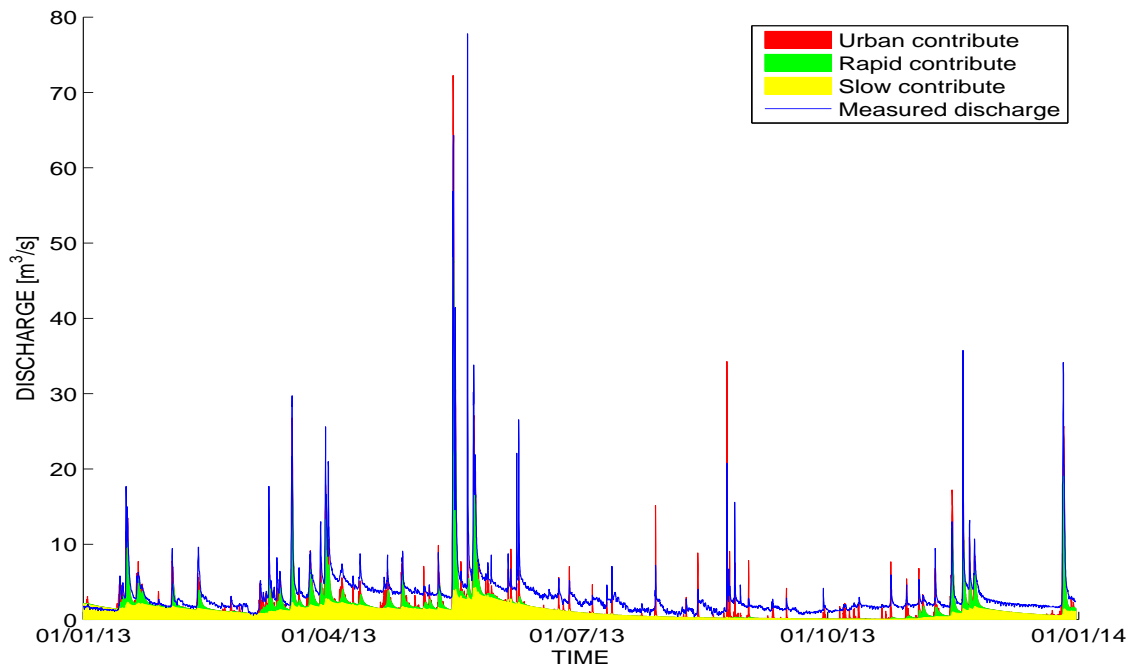


Figure 4.47: Comparison between measured and modeled discharge for the year 2013 decomposed in the three different runoff components

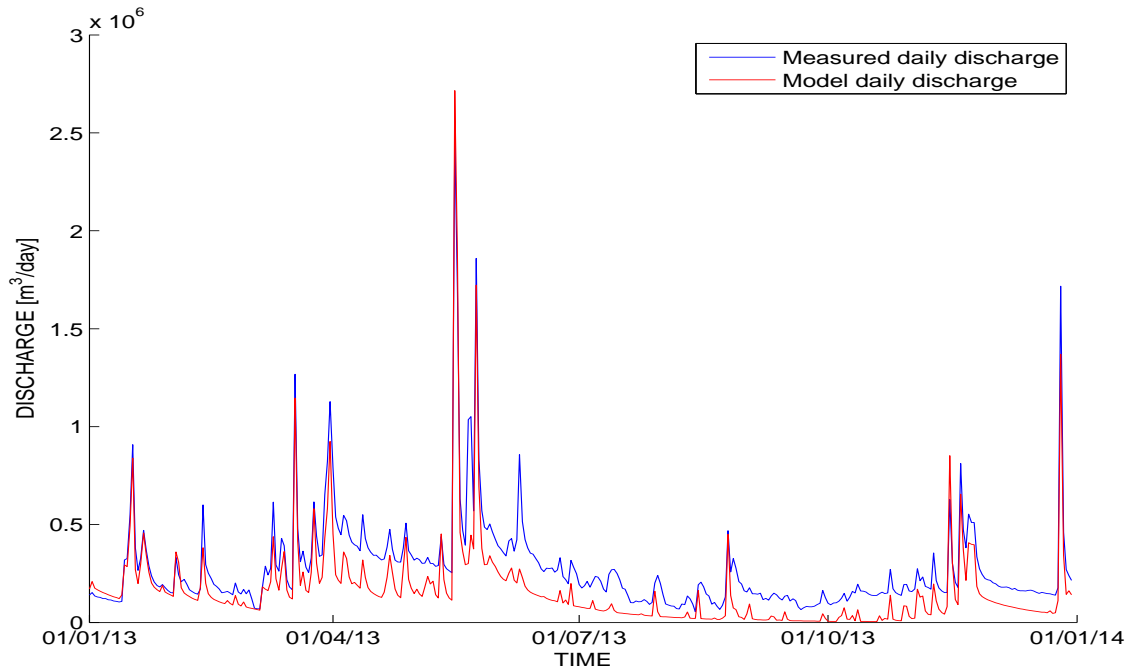


Figure 4.48: Comparison between daily measured discharge and daily modeled discharge for the year 2013

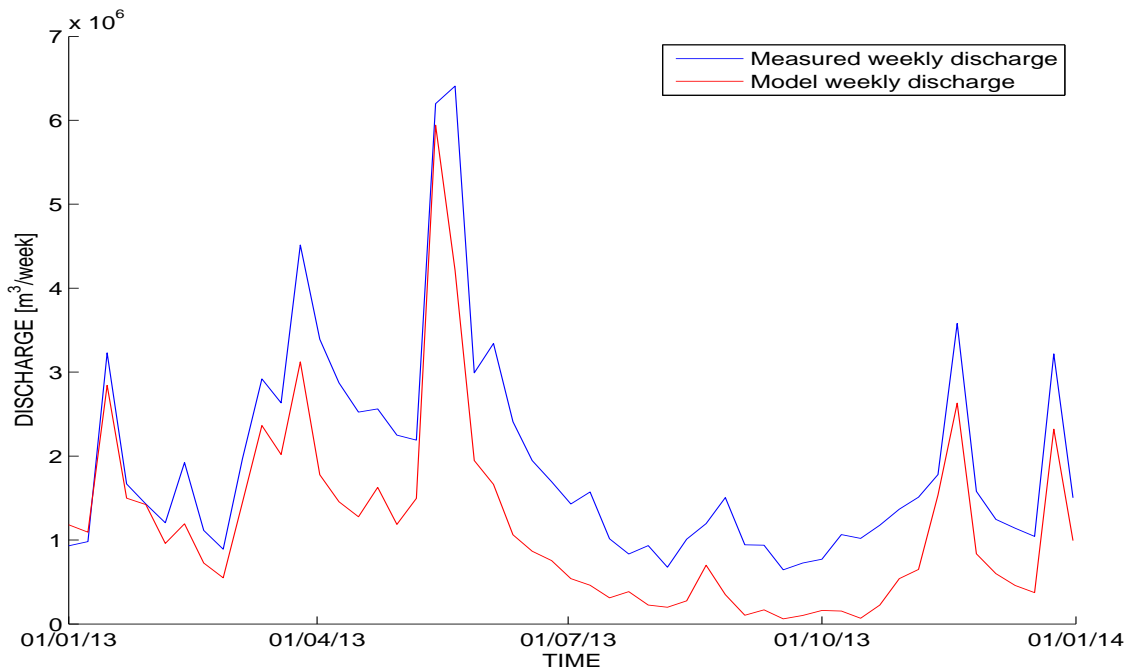


Figure 4.49: Comparison between weekly measured discharge and weekly modeled discharge for the year 2013

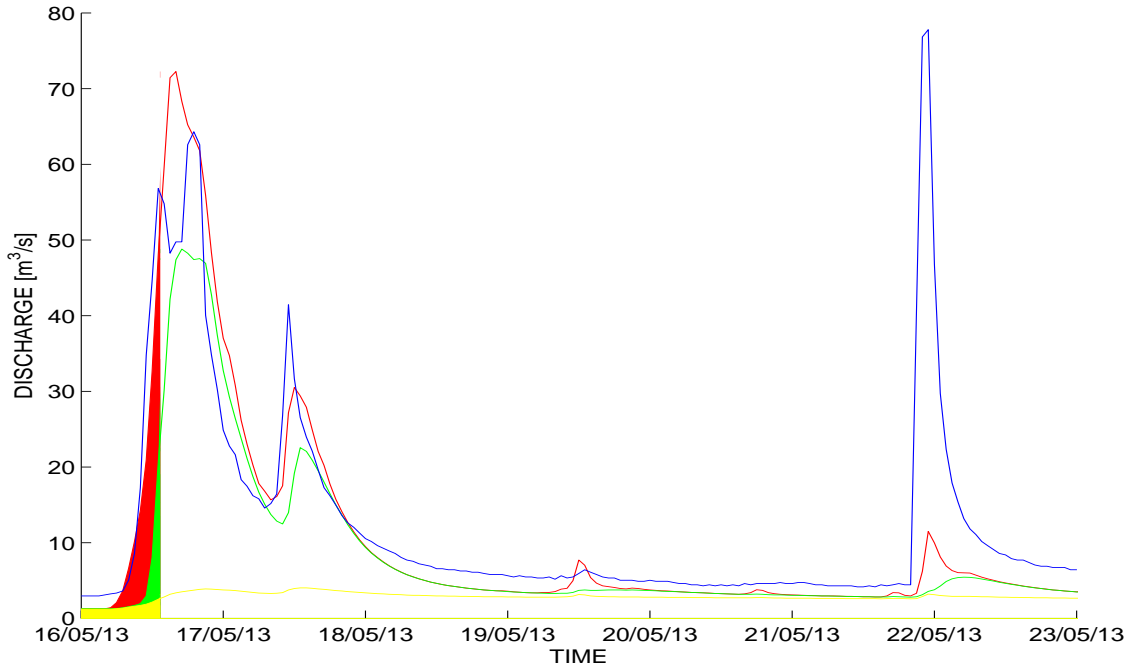


Figure 4.50: Comparison between measured and modeled discharge for the event between 16/05/2013 and 23/05/2013

4.3 Reviews of the results

The results reported in Section 4.2 shows that the model developed provides a good approximation of the observed hydrographs both in the long-term and for most of the major events recorded in the period 2004-2013. It should be noted that the different periods analyzed in this thesis have really different characteristics, a circumstance that makes particularly valuable the model ability to reproduce the observed patterns of discharge during different hydrologic conditions. The three years that give unsatisfactory results are the 2005, 2006 and 2013. The first two years (2005 and 2006) were really dry years and the model tends to systematically overestimate the peaks. The year 2013, instead, was a really rainy year, and the model underestimates low discharges during the entire period. Table 4.1 summarizes the results for the major events observed. In particular the percentage error of the peak discharge Q_{peak} , the percentage error of the runoff volume and the time shift between modeled and observed time to peak are reported. The + or the - means respectively that the model overestimate or underestimate the modeled feature. Looking in detail to the main events, that represent the most critical issue of this study, it can be concluded that the model developed simulates well most of the floods and in particular the event occurred in November 2012, the higher measured during the study period. Both the growth phase and the recession are properly captured by the model and the maximum discharge is always approximated with errors less than 15%. On the other hand, at event-scale, the model overestimates the released volume.

The main uncertainties found are related to the underestimation of the low discharges and

Event	Date of start	Q_{peak} [m^3/s]	Q_{peak} error [%]	Volume error [%]	Time shift [h]
1	31/10/2004	60,5	-6,3	+18	0
2	03/10/2005	62,2	+61,3	+73,3	0
3	15/06/2007	64,7	-13,2	+26,9	0
4	16/09/2009	79,2	+4,4	+74,6	-11
5	25/10/2010	72,7	-4,4	+24,9	0
6	31/10/2010	77,3	-15,6	-6,8	0
7	25/10/2011	63,9	+11,0	+62,4	0
8	11/11/2012	106,9	+9,3	+14,3	-1
9	16/05/2013	64,3	+12,3	+7,3	-3

Table 4.1: Results for the major events occurred in the period 2004-2013.

the overestimation of the peaks during the summer period. Those issues could be analyzed in forthcoming studies. To eliminate the systematic underestimation of low discharges the effect of irrigation during the growing season should be included. For irrigation water is mainly taken from the Brenta (in the western part of the catchment) and from the Piave river (in the eastern part). This amount of water is supplied to cultivated land during the entire summer and could sustain the low discharges and explain the underestimation of the base flow of $1 - 2 m^3/s$. To improve the model performances during the year 2013 instead, as suggested in Section 4.2, the water table fluctuations should be included in the model. The leaching terms and the discharge from the bottom of the river could be thus correlated to such fluctuations. The overestimation of the summer peaks due to the urban runoff component, as reported in Section 4.2 for the year 2008, could be caused by the absence of an evaporation process from the urban area, that could be potentially relevant during the summer months. The parameter γ that defines the portion of urban water that exits the system could be thus correlated to the meteorological condition as done for the evapotranspiration term. A more detailed study on the role played by the wastewater treatment plant and the fate of the urban runoff components would be also recommended.

Conclusion

The present thesis deals with the implementation, calibration and validation of a rainfall-runoff model for the Muson dei Sassi creek, based on the geomorphological theory of the hydrologic response.

The model is spatially explicit as many sub-catchments are separately considered, so as the discharge in different locations along the river network can be evaluated. This is an important feature to allow a proper connection with the hydro-dynamic model that uses a spatially distributed grid network for the calculation of discharges and stages in the transportation region.

The results obtained can be positively judged both in the long-term and for single events. In particular, the main events are approximated properly both in terms of shape and peak of the hydrograph.

The most difficult phase of the work was the definition of the different terms of effective rainfall and the decomposition of runoff in its main components (*urban*, *rapid* and *slow* component). The runoff coefficient at the closure section at Castelfranco Veneto is about 0,2, implying that only 20% of rainfall, in the long term, is released as runoff. To reproduce this experimental evidence four different terms of water losses were included in the model: leaching from the deep layer, dispersion from the channel bed, evapotranspiration and a spill from the water drained by urban areas.

The calibration phase posed serious difficulties since many calibration tests were performed to obtain the results showed in Chapter 4. In fact the time span considered in this study is characterized by heterogeneous rainfall patterns, wet-dry periods etc., and it was not easy to find the set of parameters that best simulate all these features for all the simulation period. Still, some uncertainties due to the seasonal variability of the hydrologic response remain, in terms of overestimation of the summer peaks and underestimation of the base flow, but they do not significantly influence the discharge forecasting during the floods. The presence of only one measure of discharge, located before the junction of the Muson with the Avenale stream, did not allow to define a set of parameters for the entire catchment.

Further improvements of this model are obviously feasible. Measurements of the dispersion from the channel bed and the correlation of deep leaching terms with ground water levels would be possibly beneficial for a more accurate description of the various loss terms. A suitable update of the land use map, and a more detailed study of the fate of flow components originated from urban areas would be desirable.

Bibliography

- [Allen et al., 1998] Allen, R.G., L.S. Pereira, D. Raes, and M. Smith (1998), Crop evapotranspiration - Guidelines for computing crop water requirements, *FAO Irrigation and drainage paper 56*, Roma.
- [ARPAV, 2005] ARPAV (2005), Carta dei suoli del Veneto.
- [ARPAV, 2008] ARPAV (2008), Considerazioni sulla scala di deflusso del fiume Muson dei Sassi a Castelfranco Veneto, Livelli e Portate Anni 2004-07, *Relazione n° 08/08*.
- [ARPAV, 2011] ARPAV (2011), Livelli e portate medie giornaliere del torrente Muson dei Sassi a Castelfranco Veneto negli anni 2008-10, *Relazione n° 07/11*.
- [Beven, 2001] Beven, K.J. (2001), Rainfall-Runoff Modelling, Wiley, Chichester.
- [Clapp and Hornberger, 1978] Clapp, R.B., and G.N. Hornberger (1978), Empirical equations for some soils hydraulic properties, *Water Resour. Res.*, 14(8), 601-604.
- [D'Alpaos, 2003] D'Alpaos, L. (2003), Studio idraulico mediante un modello matematico per la simulazione degli eventi di piena lungo le aste dei corsi d'acqua dell'area pedemontana in sinistra Brenta e confluenti nel Muson dei Sassi.
- [D'Alpaos, 2006] D'Alpaos, L. (2006), Propagazione delle onde di piena lungo l'asta del Muson dei Sassi mediante modello bidimensionale, Dipartimento IMAGE, Università di Padova.
- [Dietrich and Dunne, 1993] Dietrich, W.E., and T. Dunne (1993), The channel head, in *Channel Network Hydrology*, edited by K. Beven and M.J. Kirkby, pp. 176-219, John Wiley, New York.
- [Genio Civile, 2011] Genio Civile di Padova (2011), Studio idraulico dell'asta del torrente Muson dei Sassi nel tratto di competenza del Genio Civile di Padova da Castelfranco Veneto (TV) alla confluenza nel fiume Brenta.
- [Gupta et al., 1980] Gupta, V.K., E. Waymire and C.T. Wang (1980), A Representation of a Unit Hydrograph from Geomorphology, *Water Resources Research*, 16, 5, 855-862.
- [Marani, 2003] Marani, M. (2003), Processi e modelli dell'idrometeorologia, Dipartimento IMAGE, Università di Padova.

- [Marani et al.,2010] arani, M., S. Basso, F. Zambon, and G. Botter (2010), Modellazione matematica del bacino idrografico del fiume Brenta, relazione tecnica, Centro Internazionale di Idrologia.
- [Montgomery e Dietrich, 1989] Montgomery, D.R., and W.E. Dietrich (1989), Source areas, drainage density and channel initiation, *Water Resour. Res.*, 25, 1907-1918.
- [Rinaldo and Rodriguez-Iturbe, 1996] Rinaldo A., and I. Rodriguez-Iturbe (1996), Geomorphological theory of the hydrologic response, *Hydrol. Processes*, 10(6), 803-844.
- [Rinaldo et al., 2002] Rinaldo, A., A. Bellin, M. Ferri, M. Marani, R. Rigon, A. Fornasiero, and S. Silvestri (2002), Modellazione matematica del bacino idrografico del fiume Brenta, Dipartimento IMAGE, Università di Padova.
- [Rinaldo et al.,2006] Rinaldo, A., G. Botter, E. Bertuzzo, A. Uccelli, T. Settin and M. Marani (2006), Transport at basin scales: 1. Theoretical framework, *Hydrology and Earth System Sciences*, 10, 19-29, 2006.
- [Rodriguez-Iturbe e Valdes, 1979] Rodriguez-Iturbe I. and J.B. Valdes (1979), The geomorphologic structure of hydrologic response, *Water Resour. Res.*, 15(6), 1409-1420.
- [Rodriguez-Iturbe and Rinaldo, 1997] Rodriguez-Iturbe, I., and A. Rinaldo (1997), *Fractal River Basins*, Cambridge University Press.
- [Cimolino et al., 2011] Cimolino, A., A. Cisotto, I. Saccardo, A. Deana, and A. Marin (2011), Le campagne di misura per la valutazione delle dispersioni in alveo, chapter 6 of *Il progetto TRUST Life+*.